Microstructural Development

during

Welding of TRIP Steels

The research described in this thesis was performed in the department of Material Science and Engineering, Faculty of 3mE, Delft University of Technology, Mekelweg 2, 2628CD, Delft, The Netherlands.

This research was carried out as part of the innovation program of the Materials innovation institute (M2i) (formerly, the Netherlands Institute for Metals Research) on “Development of microstructure in welded TRIP and DP steels”, project number MC8.04188 (www.m2i.nl).

Microstructural Development

during

Welding of TRIP Steels

PROEFSCHRIFT

ter verkrijging van de graad van doctor
aan de Technische Universiteit Delft,
op gezag van de Rector Magnificus prof.ir. K.C.A.M. Luyben,
voorzitter van het College voor Promoties,
in het openbaar te verdedigen op maandag 25 oktober 2010 om 10.00 uur

door

Murugaiyan AMIRTHALINGAM

Master of Science in Metallurgical and Materials Engineering
Indian Institute of Technology - Madras, Chennai, India
Geboren te Erode, Tamilnadu, India

Dit proefschrift is goedgekeurd door de promotor:
Prof.dr. I.M. Richardson

Samenstelling promotiecommissie:

Rector Magnificus,	voorzitter
Prof.dr. I.M. Richardson,	Technische Universiteit, Delft, promotor
Dr.ir. M.J.M. Hermans,	Technische Universiteit, Delft
Prof.dr.ir. J. Sietsma,	Technische Universiteit, Delft
Prof.dr. M.A. Gutierrez De La Merced,	Technische Universiteit, Delft
Dr.ir. T. van der Veldt,	Tata Steel - Corus, RD&T, IJmuiden
Prof.dr. R. Boom,	Technische Universiteit, Delft
Prof.dr. B.J. Thijsse,	Technische Universiteit, Delft, reservelid

Dr.ir. M.J.M. Hermans heeft als promotiebegeleider in belangrijke mate aan de totstandkoming van dit proefschrift bijgedragen.

Microstructural Development during Welding of TRIP steels
M. Amirthalingam
PhD thesis of Delft University of Technology - with summary in Dutch
ISBN 978-90-77172-99-5

Key words: TRIP steels, Welding, Retained austenite, Microstructural evolution, Phase transformations

Printed in The Netherlands.

Contents

Nomenclature

Symbol	Description	Unit
a	Thickness of the test piece in Erichsen cupping test	m
a_α	Lattice parameter of ferrite	m
a_γ	Lattice parameter of austenite	m
A_{c_1}	Austenite nucleation temperature during heating	^{o}C
A_{c_3}	Temperature at which a sample becomes fully austenitic during heating	^{o}C
A_{e_1}	Austenite nucleation temperature under equilibrium condition	^{o}C
A_{e_3}	Temperature separating the $\alpha + \gamma$ and γ fields	^{o}C
A_{r_3}	Temperature at which an austenitic sample begins to transform to ferrite during cooling	^{o}C
b	Width of the test piece in Erichsen cupping test	m
B	Magnetic flux density	Tesla
d_0	Spacing between the planes in the atomic lattice under stress free condition	m
d_1	Diameter of the spherical end of the punch in Erichsen cupping test	m
d_2	Bore diameter of the die in Erichsen cupping test	m
d_3	Bore diameter of the blank holder in Erichsen cupping test	m
d_4	Outside diameter of the die in Erichsen cupping test	m
d_5	Outside diameter of the blank holder in Erichsen cupping test	m
f_γ or x_γ	Austenite fraction	-
h_1	Height of the inside rounded part of the die in Erichsen cupping test	m
h	Depth of the indentation during the Erichsen cupping test	m
I	Diffracted X-ray intensity	counts
IE	Erichsen cupping index	m
M	Mass magnetisation	A m^2 kg^{-1}

$M_{fcc-bcc}$	Austenite-ferrite interface mobility	M^4 (J s)$^{-1}$
M_o	Saturation magnetisation at -273 ^{o}C	A m^2 kg^{-1}
M^s	Saturation magnetisation	A m^2 kg^{-1}
M_s	Martensitic start temperature	^{o}C
Q	Activation energy	J mol^{-1}
R_1	Outside corner radius of the die, outside corner radius of the blank holder in Erichsen cupping test	m
R_2	Inside corner radius of the die Erichsen cupping test	m
T	Temperature	^{o}C
t	time	seconds
T_c	Curie temperature	^{o}C
v	Velocity	m s^{-1}
x_c	Carbon concentration of retained austenite	wt. %
x_{Mn}	Manganese concentration of retained austenite	wt. %
x_{Al}	Aluminium concentration of retained austenite	wt. %
α	Ferrite	-
α	Thermal expansion coefficient	^{o}C^{-1}
α'	Martensite	-
α_β	Bainite	-
γ	Austenite	-
γ_{RA}	Retained austenite content	%
ϵ	Iron carbide ($Fe_{2.4}C$)	-
$\eta(\epsilon')$	Iron carbide (Fe_2C)	-
θ	Diffraction angle	degrees
λ	Wavelength of the X-ray beam	m

Abbreviation	**Meaning**
2D	Two dimensional
3D	Three dimensional
3D-XRD	Three dimentional X-ray diffraction
AC	Alternating current
AHSS	Advanced high strength steels
BH	Bake hardening
CP	Complex phase
CW	Continuous wave
DC	Direct current
DP	Dual phase
DD	Deep drawing
EDD	Extra deep drawing
EDM	Electro discharge machining
EDS	Energy dispersive X-ray spectroscopy
ESRF	European synchrotron radiation facility

EPMA	Electron probe micro analysis
FEG	Field emission gun
FZ	Fusion zone
GTA	Gas tungsten arc
HAZ	Heat affected zone
HSLA	High strength low alloyed
HT	Heat treated
IA	Inter-critical annealing
IBT	Isothermal bainitic holding
IF	Interstitial free
LB	Laser beam
Nd-YAG	Neodymium-yttrium aluminium garnet
PFHT	Post forming heat treatable
RS	Resistance spot
TRIP	Transformation induced plasticity
TWIP	Twinning induced plasticity
SEM	Scanning electron microscopy
UTS	Ultimate tensile strength
VSM	Vibrating sample magnetometer
WCL	Weld centre line
WDS	Wavelength dispersive X-ray spectroscopy
YS	Yield strength

Chapter 1

Introduction

The development of modern automotive vehicles with improved environmental, safety and vehicle performance has driven the development of new steel grades that are lighter, safer, greener and more cost effective. As a result, conventional low carbon steels such as deep drawing (DD), extra deep drawing (EDD), bake hardening (BH), interstitial free (IF) steels and high strength steels such as carbon-manganese and high strength low alloyed (HSLA) steels are increasingly being replaced with advanced high strength steels (AHSS) due to their better combination of strength and ductility (figure 1.1). Transformation Induced Plasticity (TRIP) steel is one of the materials that

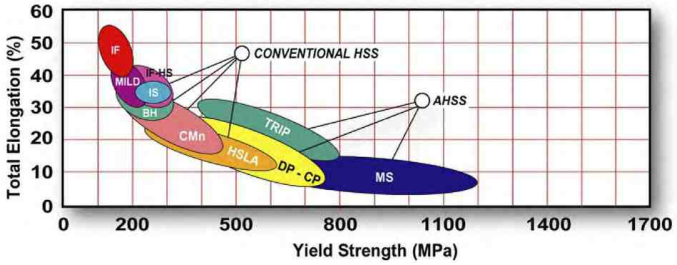

Figure 1.1: *A comparison of relationship between ultimate tensile strength to total elongation of various steels [1].*

offers a high strength and toughness combination with excellent uniform elongation compared with conventional high strength low alloyed (HSLA) steel and other AHSS such as dual phase (DP) steels (figure 1.2). Along with these properties, TRIP steels also have an ability to absorb more energy during crash due to the delayed transformation of retained austenite to martensite upon deformation. The superior combination of strength, ductility and formability of the TRIP steels compared to conventional steels is achieved by carefully designing the microstructure. A typical microstructure of a TRIP steel consists of ferrite (α), bainite (α_β) and retained austenite (γ_{RA}),

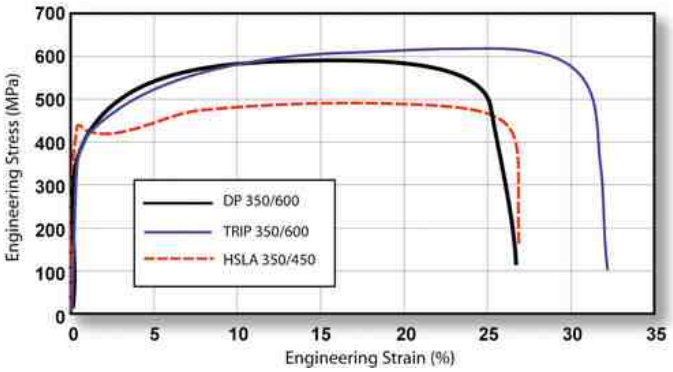

Figure 1.2: *TRIP steel showing a higher uniform and total elongation with a similar strength level as dual phase (DP) and conventional high strength low alloyed (HSLA) steels [1].*

(usually about 5 to 10 %) distributed in the matrix as shown in figure 1.3. The size, shape, chemical composition and volume fraction of the microstructural constituents, especially retained austenite, are critical in tailoring the mechanical properties of the TRIP steels.

In automotive manufacturing processes, fusion welding is an important process employed for the joining of steel parts and components (figure 1.4). However, the thermal cycle of a welding process destroys the carefully designed microstructure. The mechanical properties of a welded TRIP steel are therefore affected by weld thermal cycles, which limit their commercial applicability. In order to improve the commercial applicability, it is necessary to understand the evolution of the microstructure during welding, by studying the welding behaviour with emphasis on specific welding processes and their thermal cycles. The effect of alloying additions, the development of residual stresses and the influence of specific heat treatments in the weld, heat affected zones and base metal are also of particular relevance.

The aim of this work is to improve our understanding of the response of the material to welding by (i) studying the microstructural evolution during weld thermal cycles of specific joining processes generally employed in automotive manufacturing, (ii) the use of specific heat treatments and (iii) the influence of thermal cycles on the final properties of the welded material.

1.1 Research approach and outline of the thesis

The transformation induced plasticity steels posses a typical microstructure containing retained austenite. This microstructure is generated by a heat treatment, involving isothermal holding in the inter-critical ($\alpha + \gamma$) region and during bainitic transformation. The size, shape, distribution and composition of the retained austen-

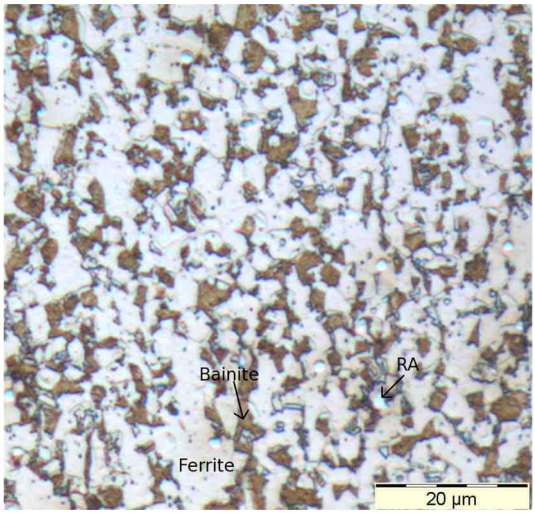

Figure 1.3: *A typical microstructure of a TRIP steel, showing the presence of retained austenite (RA) in bright white and bainite in brown in a ferrite matrix.*

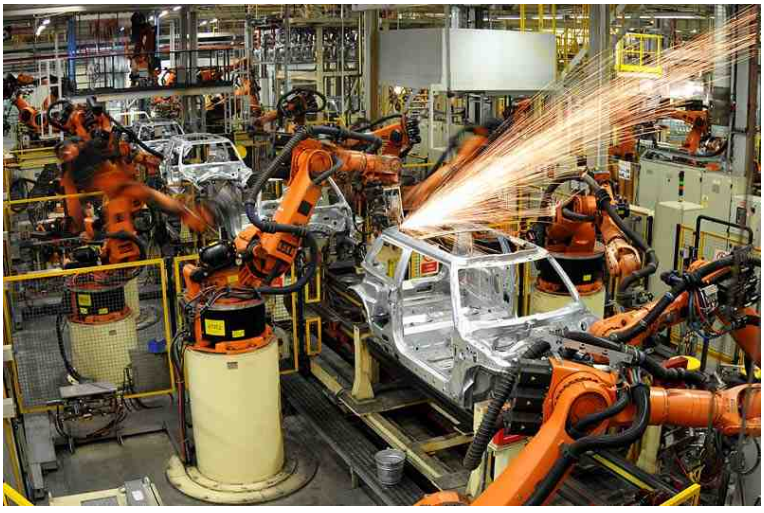

Figure 1.4: *Fusion welding of body components in an automobile manufacturing assembly line.*

ite is dependant on heat treatment parameters, such as temperature and isothermal holding duration. Chapter 2 provides an overview of advanced high strength steels (AHSS), their microstructural features and mechanical properties. A review of work done in the field on the welding of AHSS is given with special emphasis on the welding of dual phase (DP), complex phase (CP) and TRIP steels. After a short introduction to the welding processes generally used to weld TRIP steels, work so far reported on the weldability of TRIP steels is reviewed. The experimental techniques available to quantify the retained austenite in the steel microstrcutures are discussed and compared to highlight the merits and limitations of each technique.

The research work begins with an assessment of the effect of heat treatment parameters on the retained austenite content in the microstructure. Various microstructures with different retained austenite contents were generated by setting appropriate heat treatment parameters. Chapter 3 begins with an introduction to TRIP steels including composition, microstructure and the heat treatment used to generate the microstructure. The results of the experiments carried out to understand the effect of heat treatment parameters on the retained austenite contents is presented and analysed in order to generate a base microstructure for the welding experiments. In this chapter, an introduction to various microstructural characterisation techniques used in this work is provided together with an analysis of experimental accuracy.

Selected base metal microstructures have been welded with gas tungsten arc (GTA), laser beam (LB) and resistance spot (RS) techniques to study the phase transformations during the thermal cycles imposed by these welding processes. The behaviour of alloying elements and their effect on the microstructural constituents such as non-metallic inclusions and retained austenite are presented in chapter 4. The role of aluminium and silicon, important alloying additions in TRIP steels, on the formation of non-metallic inclusions in the welded steels is analysed, and their effect on the partitioning behaviour of other alloying elements during solidification of the weld pool is examined. The effect of solidification and phase transformation induced chemical heterogeneity in the stabilisation of ferrite and retained austenite is discussed in this chapter.

The thermal stability of retained austenite after imposing weld thermal cycles on TRIP steel plates is studied by means of magnetic saturation and synchrotron X-ray diffraction. Chapter 5 deals with the quantitative measurements of retained austenite in welded TRIP steel microstructures. The effect of weld thermal cycles on the distribution of retained austenite across the welded TRIP steel plates is reported and correlated with the peak temperatures reached across the heat affected and fusion zones during welding.

The phase transformation behaviour of TRIP steels has also been studied by *in-situ* synchrotron X-ray diffraction while imposing simulated weld thermal cycles in order to understand (i) the kinetics of phase transformations, (ii) lattice parameter and thermal expansion behaviour of co-existing phases, and (iii) stabilisation and decomposition mechanisms of retained austenite during welding. The results of these studies are presented in chapter 6. Along with these results, evidence of possible decomposition of austenite at room temperature is also provided.

Mechanical characterisation of welded TRIP steels has been carried out to correlate the weld microstructure with mechanical properties and to examine the effect of possible room temperature decomposition of austenite on the mechanical properties of the welded TRIP steels, and results are presented in chapter 7. The variation of micro-hardness across the weld zones and the tensile properties of welded TRIP steels are provided and compared with the base metal properties. The formability behaviour of welded TRIP steel is studied by means of Erichsen cupping tests and presented in this chapter. The possible effect of room temperature transformation of austenite on the mechanical properties of welded TRIP steel is explained with reference to the Erichsen cupping test results conducted at various time intervals after welding.

Each chapter has its own discussions and conclusions; in addition a general discussion based on the results of the previous chapters is provided (chapter 8) and the conclusions derived from the entire work are presented in the chapter 9. Based on the conclusions, recommendations to the welding industry and suggestions for future work are also presented.

Throughout the thesis, all the units and dimensions are specified in SI units other than in some specifically mentioned cases. The temperature is presented in '^oC' throughout the thesis. References to the published literature are given at the end of each chapter.

Reference

[1] S.Keeler, 'Advanced high strength steels (ahss) guidelines', Tech. Rep. Version 4.1, World auto steel, World steel association, 2009.

Chapter 2

Background

In this chapter, an introduction to advanced high strength steels (AHSS) and the welding processes that are generally used for fusion joining for these steels is provided. The welding behaviour of AHSS in general is discussed and compared with the reported work on the weldability of TRIP steels. The general material response to a typical thermal cycle is discussed in order to understand the phase transformation behaviour and microstructural evolution during welding. Along with this, the work published to date on the welding of TRIP steels and quantification of retained austenite in TRIP steels are reviewed.

2.1 Introduction to advanced high strength steels and their weldability

The use of AHSS in modern automobiles is increasingly preferred due to their improved crash energy management and high strength-ductility combinations. These steels are classified based on the microstructure and forming mechanisms, and the welding behaviour of each steels is affected by the thermal cycle of the welding process used to make in construction. The following sections provide an introduction to the classification of AHSS and the welding processes used for fusion joining.

2.2 Classification of steels

The world steel association classifies advanced high strength steels (AHSS) based on their metallurgical designation as [1],

- Dual phase (DP) steels,
- Complex phase (CP) steels,
- Martensitic steels (MS),

Table 2.1: *The mechanical properties of advanced high strength steels.*

Steel grade	YS, MPa	UTS, MPa	Tot. El, %
HSLA 350/450	350	450	23-27
DP 300/500	300	500	30-34
DP 350/600	350	600	24-30
TRIP 450/800	450	800	26-32
DP 500/800	500	800	14-20
CP 700/800	700	800	10-15
DP 700/1000	700	1000	12-17
MS 1250/1520	1250	1520	4-6

- Ferritic-Bainitic steels,
- Transformation induced plasticity (TRIP) steels,
- Quench and Partitioning (Q&P) steels,
- Twinning-Induced Plasticity (TWIP) steels,
- Boron-based hot formed steels and
- Post-Forming Heat-Treatable (PFHT) steels.

In these steel grades, the Q&P steel, the TWIP steel, boron-based hot formed steels and PFHT steels are newly developed grades and the commercial development of these steels is still under investigations. Among the steels used commercially, the TRIP steels offer high strength, high formability and high dynamic energy absorption during high strain rate deformation due to deformation induced transformation of austenite to martensite. Table 2.1 shows the mechanical properties of some commercially available AHSS, where it can be seen that TRIP steels offer a good combination of strength and ductility compared to the other steels [1].

2.3 Welding processes

In a commercial automotive manufacturing, the majority of advanced high strength steel parts are fusion welded using laser beam (LB) or resistance spot (RS) welding [1]. Along with these two processes, gas tungsten arc (GTA) welding can be employed to extend the range of thermal cycles with varying heating and cooling rates, typically $\geq 10\ ^{o}\mathrm{C\ s^{-1}}$, $\geq 10^{2}\ ^{o}\mathrm{C\ s^{-1}}$ and $\geq 10^{3}\ ^{o}\mathrm{C\ s^{-1}}$ for GTA, LB and RS welding respectively. These can be simulated to study microstructural evolution during the welding of TRIP steels.

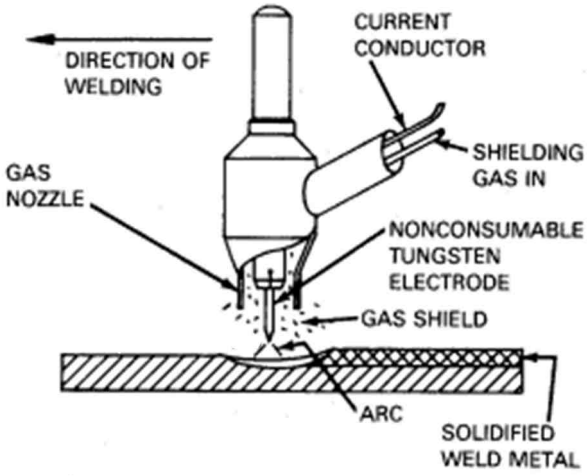

Figure 2.1: *Schematic illustration of gas tungsten arc (GTA) welding.*

2.3.1 Gas tungsten arc (GTA) welding

Gas tungsten arc (GTA) welding, sometimes referred as tungsten inert gas (TIG) welding uses an arc as a heat source for the fusion process. An electric arc is ignited between a non-consumable tungsten electrode and the work-piece to be welded. The work-piece is heated by the electrical energy generated by the welding arc, resulting in local melting and the formation of a weld pool. Figure 2.1 schematically depicts the GTA welding process. The tungsten electrode used in this process is often doped with lanthanum oxide (La_2O_3) to increase electron emission and to improve the stability of arc as well as to improve arc ignition and to decrease electrode erosion [2]. The electrode and the weld pool are shielded from the atmosphere using an inert gas, usually argon and sometimes helium or a mixture of both. The shielding gas is passed around the electrode and weld pool by a nozzle which is placed around the electrode (figure 2.1). For steels generally direct current is used to generate the arc. An automatic voltage control algorithm can be employed to maintain a constant arc voltage by altering the arc length during welding.

2.3.2 Laser beam welding

Laser welding is a technique widely used to join materials. The laser is focussed onto a substrate material creating a concentrated heat source in order to melt and fuse the material. Depending on the medium, lasers are classified as solid-state or gas lasers. In solid-state lasers, a solid matrix such as glass, Al_2O_3 or yttrium aluminium garnet (YAG, $Y_3Al_5O_{12}$) doped with neodymium (Nd:YAG) is used as a lasing medium. In gas lasers, an active gas, such as CO_2 forms the lasing medium. In gas lasers the

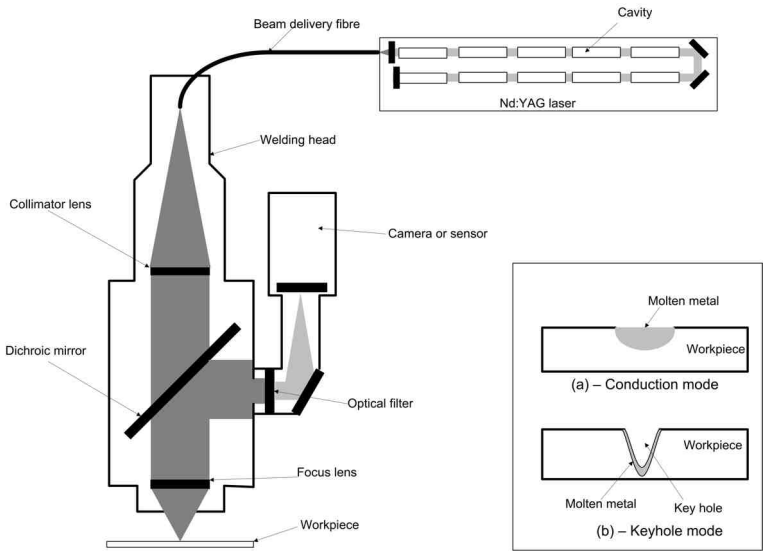

Figure 2.2: *Schematic illustration of laser beam welding set-up. The insert describes the (a) conduction and (b) keyhole mode of welding [2, 3].*

medium is generally activated by a glow discharge.

A special type of laser known as "fibre laser" is increasingly used nowadays for high-power welding applications (up to 50 kW). In this laser, the active gain medium is an optical fibre doped with rare-earth elements such as erbium, ytterbium, neodymium, dysprosium, praseodymium or thulium.

Laser welding can be performed with a relatively small heat input compared to arc welding, due to the high energy density of the laser beam. As a result, a weld with narrow heat affected zone with little shrinkage can be obtained. During welding, when the energy density is low, the beam energy is absorbed by the metal and conducted as thermal energy from the surface to the surrounding material, resulting in a semi-spherical weld pool. This situation is known as welding in the conduction mode. When the energy density is increased above a critical threshold, metal vaporisation starts to occur during welding. As a result, the laser beam is able to open a through thickness hole (keyhole) along the beam in the metal. Under these conditions, the beam energy can be absorbed by multiple reflection inside the keyhole and absorption efficiency can be increased; welding therefore occurs in the keyhole mode [2]. A schematic description of a laser beam welding arrangement with operational modes is shown in figure 2.2.

2.3.3 Resistance spot welding

In resistance spot welding, the metal parts to be fusion joined are pushed together mechanically by the electrodes and an electric current is passed through the faying interfaces. Joule heat is generated in the interface based on the current, resistance of the interface and the time of current flow. The metal parts around the interface are heated due to this heat generation, resulting in melting and the formation of a weld pool. When the current flow is switched off, the temperature starts to decrease, the weld pool solidifies and a joint (weld nugget) is produced. During welding, the electrodes are water cooled to reduce the heat generated from the electrode-workpiece interface and to avoid fusion at these interfaces. Figure 2.3 shows a schematic overview of resistance spot welding equipment [2, 4].

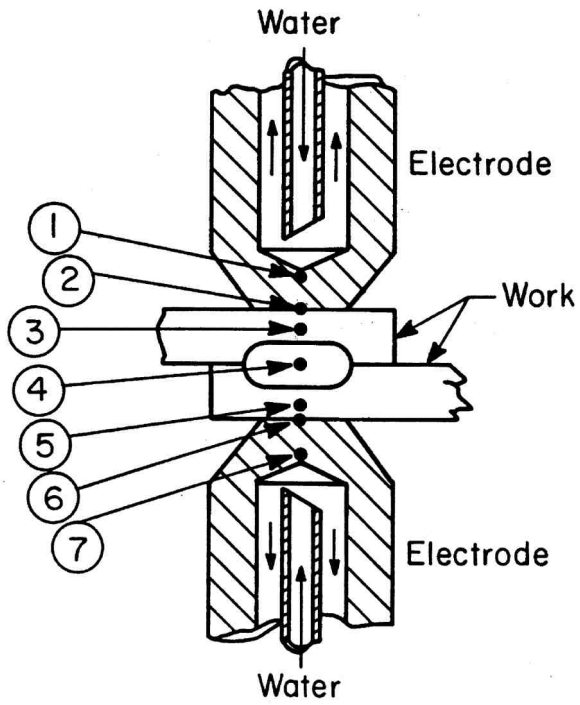

Figure 2.3: *Schematic illustration of resistance spot (RS) welding, where, (1) and (7) are electrodes, (3) and (5) are work pieces to be welded, (4) is the weld nugget, (2) and (6) are faying interfaces. The electrodes are water cooled [4].*

2.4 Response of advanced high strength steels to welding

During welding, the steel is subjected to a typical thermal cycle consisting of continuous heating and cooling. During heating, the peak temperature locally exceeds the melting point in the fusion zone and the un-molten material in the heat affected zone reaches a peak temperature dependent on the distance from the fusion boundary. The molten weld pool solidifies during cooling, forming a columnar structure with solidification induced chemical heterogeneity and non-metallic inclusions (due to the presence of oxidising alloying elements such as aluminium) [5, 6]. Along the fusion boundary, partial melting takes place in a region known as the mushy zone. In the un-molten heat affected zone, grain coarsening, grain refining, complete or partial phase transformation or tempering can occur during cooling dependent on the peak temperature reached during heating. Thus, a typical weld thermal cycle generates a microstructure in the weld zone with constituents which generally affect the mechanical properties of the advanced high strength steels. Moreover, these microstructural constituents contain residual stresses emanating from the thermal dilatation of the welded material under constrained weld conditions and specific volume changes occurring during the solid state phase transformation [7].

2.4.1 Influence of welding on dual and complex phase steel microstructure

Dual and complex phase steels are generally regarded as being weldable [8–13], with weld and HAZ strengths exceeding those of the parent material for steels with ultimate tensile strengths below about 690 MPa. Some softening in the heat affected zone was reported as a result of martensite tempering at higher strengths or when heat input due to welding is excessive [12, 13]. In these steels, the fusion zones of the welds are predominantly martensitic, due the relatively high cooling rates involved during welding [8]. In the heat affected zone of the arc and resistance spot welded dual phase steels, both the coarse-grained and fine-grained zones consist mainly of martensite with allotriomorphic ferrite; the volume fraction of ferrite increases with distance from the fusion line. In the heat affected zone where the peak temperature during welding reaches the inter-critical ($\alpha + \gamma$) temperature region, a mixture of allotriomorphic ferrite with martensite and bainite is observed. The heat affected zone of DP steel laser welds extends about 0.2 mm from the fusion boundary and consists mainly of martensite with allotriomorphic ferrite. In DP1000 steels, close to the transition between the heat affected zone and the base metal a tempered zone exists, showing a similar microstructure to the base metal but with partly tempered martensite. The presence of tempered martensite in this zone is reported to reduced the hardness of by $Hv_{0.3}$ compared to the base metal after laser welding [8, 12].

2.4.2 Weldability of TRIP steels

A typical microstructure of TRIP steels consists of austenite grains, retained at room temperature after the steel processing thermal treatment, embedded in a primary ferrite matrix. In addition to retained austenite and ferrite, varying amounts of bainite and/or martensite are present. This microstructure is generated by adding alloying elements such as silicon and aluminium and then preforming a controlled thermal treatment involving an intermediate isothermal holding to produce some bainite (see section 3.2 for description of this heat treatment). The improved strength and ductility in TRIP steels is mainly due to the presence of retained austenite in the microstructure. During deformation, the retained austenite transforms to high strength and high carbon martensite (referred to as the TRIP effect) with a volume expansion. Both effects suppress plastic instability and extend the range of uniform elongation. The mechanical stability of the retained austenite during deformation is influenced by its size, shape, chemical composition (especially carbon) and the stress state [14]. As can be expected, the thermal cycle of a fusion joining process destroys the carefully designed microstructure of the steel, especially affecting the retained austenite in the microstructure, which results in a deterioration of the mechanical properties in the weld region compared with the base metal.

A few attempts have been made in the past to improve the mechanical properties of welded TRIP steels by modifying weld thermal cycles. Cretteur *et al.* [15] attempted to improve the weldability of four TRIP steels by *in-situ* pre and post weld heat treatment during spot welding. They modified the conventional spot welding cycle by adding pre-heating and post-heating with reduced holding time and showed that the TRIP steels are sensitive to interfacial cracking and that the carbon content of the steel largely influences the weldability. Kim *et al.* [16] tried to optimize the spot welding parameters by conducting several experiments by varying welding current, time and force. They reported the effect of these welding parameters on the required weld metal properties. This work resulted in optimum welding conditions required to achieve the stipulated weld properties and improved the mechanical properties of the welded steel.

The CO_2 laser welding of a 800 MPa grade TRIP steel showed the formation of surface and internal porosity at low welding speeds. After welding it was found that the tensile properties of the welded steel were similar to the base metal. Under tensile loading parallel to the weld axis, both yield and tensile strength is proportional to the welding speed, whereas the elongation was inversely proportional; however, there were no metallurgical reasons reported for this behaviour [17, 18].

The press formability of TRIP/DP steels tailor welded blanks was investigated by Nagasaka *et al.* [19]. They used an Nd:YAG laser with pulse energy of 6 J per pulse, pulse width of 3.8 ms with 45 Hz frequency and welding speed of 500 mm min^{-1}, using N_2 as a shielding gas (25 l min^{-1}) and conducted hardness, tensile and stretch forming tests on the tailor welded blanks concluding that a high level of stretch formability can be achieved using high-strength tailored blanked steels. They also quoted that the deep drawability of high-strength tailored blanks deteriorated with increasing carbon

equivalence.

Although the research work referred in this section deals with the welding of high strength DP and TRIP steels, these works commonly lack microstructure-property correlations. The effect of specific welding processes and their thermal cycles, the effect of alloying additions, development of residual stresses and the influence of specific heat treatments on the evolution of weld microstructure in the weld zone are not reported in any of the published literature to date. In TRIP steels, the retained austenite (γ_{RA}) present in the microstructure plays a major role as it transforms to martensite during deformation, extends the total elongation and delays the onset of necking. Thus, it is important to study the γ_{RA} volume fraction, its carbon concentration, grain size and the stress state in the heat affected and fusion zones to correlate the mechanical properties of the welded steel to the microstructure.

2.4.3 Quantification of retained austenite

X-ray diffraction is widely used for the measurement of carbon content and volume fraction of austenite present in multiphase microstructures [20–22]. It can be seen from the published literature that the accuracy of measurements is largely influenced by a number of factors such as texture, residual stresses present in the material, experimental and calculation factors [23]. These shortcomings have led to the use of high energy synchrotron X-ray diffraction for quantitative volume fraction and carbon content measurement of retained austenite. Moreover, the possibilities of *in-situ* synchrotron X-ray diffraction techniques during controlled thermo/thermo-mechanical cycling of TRIP steels offer significant opportunities in quantitative characterisation of multiphase microstructures. Van der Zwaag *et al.* used synchrotron X-ray diffraction as well as conventional X-ray diffraction to study the *in-situ* mechanical stability of retained austenite in a TRIP steel [24]. Kruijver *et al.* adapted a similar experimental procedure to study the mechanical stability of retained austenite using synchrotron X-ray diffraction [25] . Van Dijk *et al.* studied the thermal stability of retained austenite by synchrotron X-ray diffraction while cooling it from room temperature to 100 K [26].

The limitations in quantitative measurements in conventional and synchrotron X-ray diffraction measurements have led to the use of other techniques such as magnetic saturation, thermal diffusivity and ultrasonic measurements. The magnetic saturation method is based on the difference in saturation magnetization of specimens with and without austenite and is directly related to the volume fraction of non-ferromagnetic retained austenite. This is due to the fact that ferrite, as well as martensite and cementite, is ferromagnetic at temperatures below the Curie temperature while the austenite is paramagnetic. Zhao *et al.* used the magnetic saturation method to measure the retained austenite in two Al based TRIP steels [21]. They compared the results obtained by magnetic saturation measurements with conventional X-ray diffraction measurements and concluded that magnetic saturation measurements yielded more reliable and sensitive results than the X-ray diffraction. Van der Zwaag *et al.* also used this method to measure the retained austenite contents in TRIP steels and

compared the results with conventional and synchrotron X-ray diffraction measurements under various thermal and mechanical conditions [24]. However, the accuracy of this measurement is highly dependent on the empirical equations used to translate the measured magnetic signal into the volume fraction of austenite [27]. The measurement of retained austenite by thermal diffusivity is reported in some literature and is based on the large difference of thermal conductivity of austenite and ferrite [27]. However, this technique requires a relatively large number of samples and several assumptions have to be made to measure the retained austenite contents. The use of ultrasonic waves for the measurement of retained austenite is reported by Jacques *et al.* [27]. In this method, the longitudinal velocity of ultrasonic waves generated by the impingement of a laser beam on a steel sample is related to the amount of retained austenite present in the steel by empirical relationships. However, the relationship between the retained austenite content and the ultrasonic velocity is still questionable and needs further systematic work. A few examples from the literature explored the possibilities of measuring retained austenite content in the steels using Mossbauer spectroscopy [27–29]. However, this measurement can only be done in thin foils (25 to 50 μm), resulting in difficulties during preparation of samples for the measurements. There is no literature available on the quantification of retained austenite in welded TRIP steels except for a recent work by Zhao *et al.* [30]. In this work, the magnetic saturation technique was used to quantify the retained austenite fraction across the weld zone of a welded TRIP steel.

2.5 Summary

Conventional low carbon automotive grade steels are being replaced with advanced high strength steels (AHSS) which offer a better combination of mechanical properties. The weldability of the TRIP steels is reported to be poor due to their high alloying content and the decomposition of retained austenite during welding. These steels are generally welded with laser beam or resistance spot welding during commercial automobile manufacturing. Several attempts have been reported to improve the mechanical properties of welded TRIP steels but these works lack understanding of the microstructural evolution during welding and correlation of weld microstructure with mechanical properties. The role of retained austenite in the microstructure and its effects on mechanical properties of welded TRIP steels is still not known. Investigating these relationships form the basis of the current work.

References

[1] S.Keeler, 'Advanced high strength steels (ahss) guidelines', Tech. Rep. Version 4.1, World auto steel, World steel association, 2009.

[2] G.den Ouden and M.J.M.Hermans, Welding technology, VSSD, Delft, The Netherlands, 2009.

[3] B.Aalderink, Sensing, monitoring and control of laser based welding of aluminium sheets, Ph.D. thesis, University of Twente, 2007.

[4] A.J.Murphy, K.S.Yeung and P.H.Thornton, 'Transient thermal analysis of spot welding electrodes', *Welding research supplement*, (January), 1s – 6s, 1999.

[5] S.S.Babu, S.A.David, J.M.Vitek, K.Mundra and T.DebRoy, 'Development of macro- and microstructure of carbon-manganese low alloy steel welds:inclusion formation', *Material Science and Technology*, 11(2), 186–199, 1995.

[6] S.S.Babu and S.A.David, 'Inclusion formation and microstructure evolution in low alloy steel welds', *ISIJ international*, 42(12), 1344–1353, 2002.

[7] P.J.Withers and H.K.D.H.Bhadesia, 'Overview: Residual stress, part 2 - nature and origin', *Materials Science and Technology*, April, 366 – 375, 2001.

[8] I.M.Richardson, M.Amirthalingam, M.J.M.Hermans and N.Den Uijl, 'The influence of welding on advanced high strength trip and dp steels', *Mathematical modelling of weld phenomena*, vol. 9, Technical University Graz, 2010.

[9] Cs.Orosz, B.Palotas and J.Dobranszky, 'The effect of coatings on the resistance spot welding behavior of 780 MPa dual-phase steels', *Welding Journal*, 86(6), 161s–169s, 2007.

[10] M.Xia, E.Biro, Z.L.Tian and Y.N.Zhou, 'Effects of heat input and martensite on HAZ softening in laser welding of dual phase steels', *ISIJ International*, 48(6), 809–814, 2008.

[11] M.Marya and X.Q.Gayden, 'Development of requirements for resistance spot welding dual-phase (DP600) steels - Part 1 - the causes of interfacial fracture', *Welding jounral*, 84(11), 172s–182s, 2005.

[12] M.K.Wibowo and I.M.Richardson, 'Investigation on the influence of welding processes on the microstructure and mechanical properties of DP 600 and DP 1000 steels', in '5th Asian Pacific IIW International Congress, Sydney', 2007.

[13] S.K.Panda, M.L.Kuntz and Y.Zhou, 'Finite element analysis of effects of soft zones on formability of laser welded advanced high strength steels', *Science and Technology of Welding and Joining*, 14(1), 52–61, 2009.

[14] B.C.De Cooman, 'Structure-properties relationship in TRIP steels containing carbide-free bainite', *Current Opinion in Solid State and Material Science*, 8, 285–303, 2004.

[15] L.Cretteur and A.I.Koruk, 'Heat treatments to improve weldability of new multiphase high strength steels', *Materials science forum,*, 426-432, 1225–1230, 2003.

[16] S.J.Kim, C.G.Lee, I.Choi and S.Lee, 'Effects of heat treatment and alloying elements on the microstructures and mechanical properties of 0.15 wt. % C transformation induced plasticity aided cold rolled steel sheets', *Metallurgical and Material Transactions A*, 32A, 505–514, 2001.

[17] T.K.Han, K.H.Kim, B.I.Kim, C.Y.Kang, I.S.Woo and J.B.Lee, 'Characteristics of CO_2 laser welded 800 MPa grade TRIP steels', *Materials forum*, 449-452, 409–412, 2004.

[18] T.K.Han, S.S.Park, K.H.Kim, C.Y.Kang, I.S.Woo and J.B.Lee, 'CO_2 laser welding characteristics of 800 MPa class TRIP steels', *ISIJ International*, 45(1), 60–65, 2005.

[19] A.Nagasaka, K.I.Sugimoto, M.Kobayashi, K.Makil and S.Ikeda, 'Press formability YAG laser welded TRIP/DP tailored blanks', *Journal of Physics IV France*, 115, 251–258, 2004.

[20] E.Girault, P.Jacques, P.Ratchev, J.van Humbeeck and B.Verlinden, 'Study of the temperature dependence of the bainitic transformation rate in a multiphase TRIP-assisted steel', *Material Science and Engineering A*, A273-275, 471–474, 1999.

[21] L.Zhao, N.H.van Dijk, E.Bruck, J.Sietsma and S.van der Zwaag, 'Magnetic and X-ray diffraction measurements for the determination of retained austenite in TRIP stees', *Material Science and Engineering A*, A313, 145–152, 2001.

[22] E.Girault, P.Jacques, Ph.Harlet, K.Mols, van Humbeeck, J., E.Aernoudt and F.Delannay, 'Metallographic methods for revealing the multiphase microstructure of TRIP-Assisted steels', *Materials characterization*, 40, 111–118, 1998.

[23] C.K.Lowe-Ma, W.T.Donlon and W.E.Dowling, 'Comments on determining X-ray diffraction-based volume fractions of retained austenite in steels', *Powder diffraction*, 16(4), 198–204, 2001.

[24] S.van der Zwaag, L.Zhao, S.O.Kruijver and J.Sietsma, 'Thermal and mechanical stability of retained austenite in aluminum-containing multiphase TRIP steels', *ISIJ International*, 42(12), 15651570, 2002.

[25] S.O.Kruijver, L.Zhao, J.Sietsma, S.E.Offerman, N.H.van Dijk, E.M.Lauridsen, L.Margulies, S.Griguli, H.F.Poulsen and van der Zwaag, S., 'In-situ observations on the mechanical stability of austenite in TRIP-steel', *Journal of Physics IV France*, 104, 499–502, 2003.

[26] N.H.van Dijk, A.M.Butt, L.Zhao, J.Sietsma, S.E.Offerman, J.P.Wright and S.van der Zwaag, 'Thermal stability of retained austenite in TRIP steels studied by synchrotron X-ray diffraction during cooling', *Acta Materialia*, 53, 5439–5447, 2005.

[27] P.J.Jacques et al., 'On measurement of retained austenite in multiphase TRIP steels results of blind round robin test involving six different techniques', *Materials Science and Technology*, 25(5), 567–574, 2009.

[28] P.Jacques, F.Delannay, X.Cornet, Ph.Harlet and J.Ladriere, 'Enhancement of the mechanical properties of a low-carbon, low-silicon steel by formation of a multiphased microstructure containing retained austenite', *Metallurgical and Material Transactions A*, 29A, 2383 – 2393, 1998.

[29] J.H.Ladriere and X.J.He, 'Mässbauer study on retained austenite in an FeMnC dual-phase steels', *Materials Science and Engineering*, 77, 133–138, 1986.

[30] L.Zhao, M.K.Wibowo, M.J.M.Hermans and S.M.C.van Bohemen, 'Retention of austenite in the welded microstructure of 0.16C-1.6Mn-1.5Si(wt.%) TRIP steels', *Journal of Materials Processing Technology*, 209, 5286 – 5292, 2009.

Chapter 3

Characterisation of TRIP steel base metals

The demanding mechanical properties of TRIP steel are sensitive to the multi-phase microstructure containing retained austenite (γ_{RA}) in a ferrite (α) and bainite (α_β) matrix. A combination of alloying elements with a complex heat treatment generates a microstructure with the required amount, size and distribution of retained austenite. The alloying elements used in TRIP steels and their role in phase transformation behaviour, especially in the stabilisation of retained austenite (γ_{RA}) are discussed in this chapter. The various stages in the commercially used heat treatment procedure to generate the TRIP steel microstructure and the influence of heat treatment parameters on the microstructural constituents are explained. The experimental procedures used in this thesis for the qualitative and quantitative microstructural characterisation of welded TRIP steels are also employed for the analysis of TRIP steel base metal microstructures prior to welding.

3.1 Composition of TRIP steels

Commercially produced cold rolled and galvanised TRIP steels with 700 MPa yield strength contain about 3.5 wt. % of alloying elements. Carbon remains the prime alloying addition with a concentration varying from 0.12 to 0.55 wt. % along with manganese (from 0.2 to 2.5 wt. %) and silicon (from 0.4 to 1.9 wt. %) in the conventional TRIP steels [1, 2]. These elements are substituted or added with aluminium, phosphorous, chromium and molybdenum to achieve the required microstructure and mechanical properties of the steel, and to ease commercial production. The importance of these alloying elements on the phase transformation behaviour of TRIP steels during the processing and their influence on the required mechanical properties are summarised as follows [3]:

1. **Carbon**
   Carbon plays a major role in stabilising austenite in the room temperature microstructure of TRIP steels. Although conventional and laboratory TRIP steels can contain about 0.12 to 0.55 wt. % carbon, novel steels have about 0.15 to 0.25 wt. % carbon to improve the weldability. Carbon determines the amount of austenite formed during inter-critical annealing. It partitions to austenite during the heat treatment and enriches it thereby reducing the Martensitic start (M_s) temperature to below room temperature. As a result, the required amount of austenite is retained in the microstructure to achieve the TRIP properties.

2. **Manganese**
   TRIP steels generally contain about 1.5 to 1.8 wt. % of manganese. Manganese is a strong austenite stabiliser, which reduces the cementite precipitation temperature and thereby increases the carbon concentration of austenite. However, high amounts of manganese (about 2.5 wt. %) in steel lead to banding and excessive stabilisation of retained austenite [4]. These may lead to inferior mechanical properties in TRIP steels.

3. **Silicon**
   Silicon is the prime alloying element in conventional TRIP steels with amounts varying from 1.5 to 1.9 wt. %. Silicon increases the temperature at which cementite starts to precipitate in ferrite. It also hinders cementite formation during the austempering stage of the TRIP heat treatment due to its low solubility in cementite (explained in detail in the following section 3.2). This results in enrichment of carbon in untransformed austenite during the austempering stage and the remaining austenite is retained at room temperature after the TRIP heat treatment. However, use of high amounts of silicon in steel leads to oxide film formation at the surface of the steels. This oxide film prevents the wetting of liquid zinc during hot dip galvanising, compromising the quality of the galvanising, which leads to inferior corrosion protection of the steel during commercial applications [5]. The formation of an oxide film also makes the zinc coated steel difficult to spot weld. For this reason, commercially applied conventional TRIP steels are primarily electro-galvanised.

4. **Aluminium**
   Aluminium partially replaces silicon in modern TRIP steels due to the latter's surface oxide forming characteristics. Both aluminium and silicon are insoluble in cementite and retard its formation. Aluminium may replace about 1 wt. % of silicon added to the steel, thereby leading to the possibility of hot-dip galvanising of TRIP steels. Unlike silicon, aluminium is found to increase the kinetics of bainite formation [6], thus its presence leads to a reduced austempering time. However, due to the limited solid solution strengthening of aluminium compared to silicon in steels, use of strong solid solution strengthening elements such as phosphorous is desirable when replacing silicon by aluminium.

5. **Phosphorous**
   About 0.05 to 0.1 wt. % of phosphorous is added in aluminium containing TRIP steels mainly as a solid solution strengthener to achieve the required mechanical properties. Phosphorous is also known to suppress the formation of cementite and the addition of a small amount of phosphorus increases the amount of austenite retained at room temperature [7]. Thus, the addition of 0.05 to 0.1 wt. % phosphorous may reduce both the amount of silicon and of aluminium in the steel. The use of a higher amount of phosphorous (>0.25 wt. %) leads to the formation of iron phosphide (Fe_3P), which is detrimental to the mechanical properties [8].

6. **Molybdenum**
   About 0.2 wt. % of molybdenum is added in galvannealed TRIP steels. During galvannealing, the galvanised steel plate is heated to a temperature of about 500 to 520 ^oC, and addition of molybdenum hinders the formation of pearlite during this heating stage, thus making it possible to form a TRIP microstructure.

Apart from these elements, chromium, and micro-alloying additions such as titanium, niobium and vanadium are sometimes added to produce TRIP steels with higher strength (>800 MPa).

Table 3.1 shows the compositions of the TRIP steels used in this work. The total content of alloying elements is about 3.5 wt. %. In the High-Si steel the silicon content is 1.47 wt. % and in the High-Al steel the aluminum content is 1.1 wt. %. Apart from aluminium, the High-Al steel contains 0.089 wt. % phosphorous which is slightly higher than the phosphorous content of the High-Si steel. All the steels have dissolved oxygen contents of about 0.002 wt. %. The carbon and manganese contents in High-Si and High-Al steels are almost identical. These two steels were extensively used to study microstructural evolution during TRIP heat treatments and welding to compare the effect of silicon and aluminium on the phase transformation behaviour.

Table 3.1: *Composition of the TRIP steels used in this work.*

Elements, wt. %	C	Mn	Si	Cr	Al	S	P	O
High-Si	0.19	1.67	1.47	0.21	0.04	0.005	0.080	0.002
High-Al	0.19	1.63	0.35	0.019	1.1	0.005	0.089	0.002

3.1.1 Pseudo binary phase diagrams of the TRIP steels

The phase transformation behaviour of the TRIP steels used in this work differ significantly in terms of their transformation temperatures and the phase fields mainly due to the variation in silicon and aluminium content in these steels (see figure 3.1, calculated using TCFE2 database of ThermoCalc®). The A_{e_3} temperature of the

High-Si is about 885 ^{o}C, whereas High-Al steel shows a higher temperature (1036 ^{o}C). In High-Al steel, due to the addition of aluminium, δ-ferrite is found to be stabilised to the inter-critical temperature region at lower carbon levels ($<$ 0.1 wt. %).

3.2 Introduction to TRIP heat treatment

A typical heat treatment cycle during the commercial processing of TRIP steel via the cold-rolling and annealing route consists of five stages. Figure 3.2 schematically shows the thermal cycle involved in these stages. Steel is heated to a temperature at which ferrite and austenite co-exist (inter-critical α+γ region) in the first stage. In the second stage, the steel is held at a temperature in the inter-critical region to form austenite with a sufficient enrichment of alloying elements. After this isothermal holding, the steel is rapidly cooled (third stage) to a temperature ranging from 350 to 490 ^{o}C. In the forth stage, traditionally known as the austempering stage, the steel is held at a constant temperature to form carbide free bainite from the austenite. After the isothermal holding, the steel is cooled to room temperature in the final stage. The metallurgical changes that occur in each stage of the heat treatment process are explained briefly in the following subsections.

Stage-1: Heating

During this stage, the cold rolled steel recrystallises, cementite dissolves and austenite nucleates once the temperature exceeds the A_{c_1} temperature. The heating rate during commercial production generally varies from 5 to 20 ^{o}C s^{-1}.

Stage-2: Inter-critical annealing

The main role of isothermal holding in the two phase ($\alpha + \gamma$) inter-critical region is to ensure the formation of austenite with sufficient enrichment of carbon and other alloying elements. Austenite attains its equilibrium carbon content, dictated by the A_{e_3} line of the Fe-C phase diagram at very short inter-critical holding times. However, during industrial processing, the substitutional alloying additions such as Mn and Si never attain equilibrium in austenite because of the sluggish diffusion of these elements at inter-critical annealing temperatures.

Stage-3: Rapid cooling

After inter-critical annealing, the steel is cooled to the isothermal bainitic holding temperature at a rate of 10 to 50 ^{o}C s^{-1}. During cooling, new ferrite grains are often found to form epitaxially on the existing inter-critical ferrite [9] and the transformation of austenite to pearlite is suppressed due to the fast cooling rates and the presence of alloying elements such as silicon and aluminium.

Stage-4: Isothermal bainitic holding

Isothermal bainitic holding or austempering, is strategically important in the processing of TRIP steels in several aspects. The size, volume fraction and carbon content of the austenite which is going to be retained after this stage is largely influenced by the isothermal bainitic holding temperature (IBT) and to some extent the holding time. During this holding, the bainitic transformation that takes place ceases, well before the complete consumption of the austenite that has formed during inter-critical

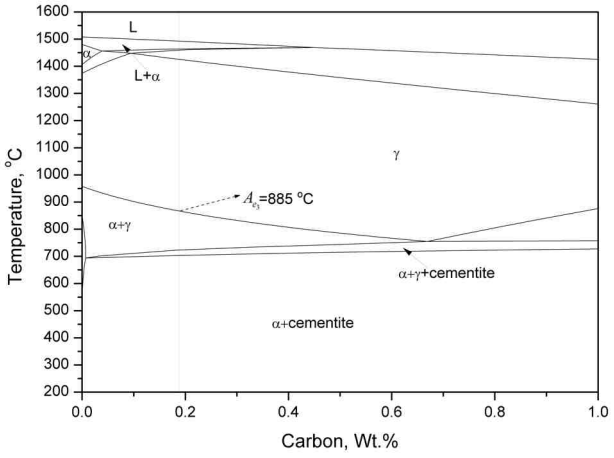

(a) *High-Si*

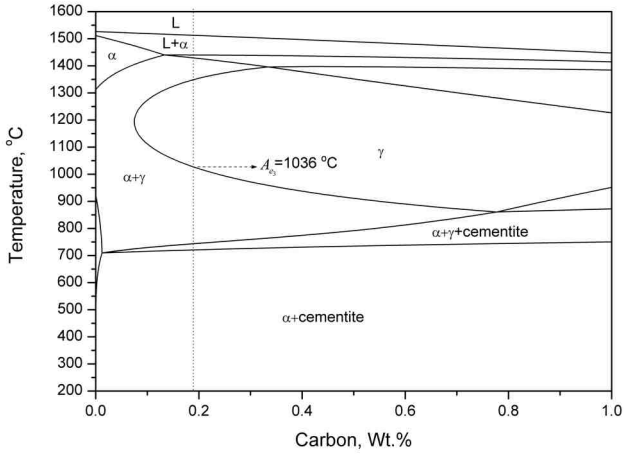

(b) *High-Al*

Figure 3.1: *Pseudo binary phase diagrams of the TRIP steels used in this research (the dotted lines indicate the bulk carbon content of the steels).*

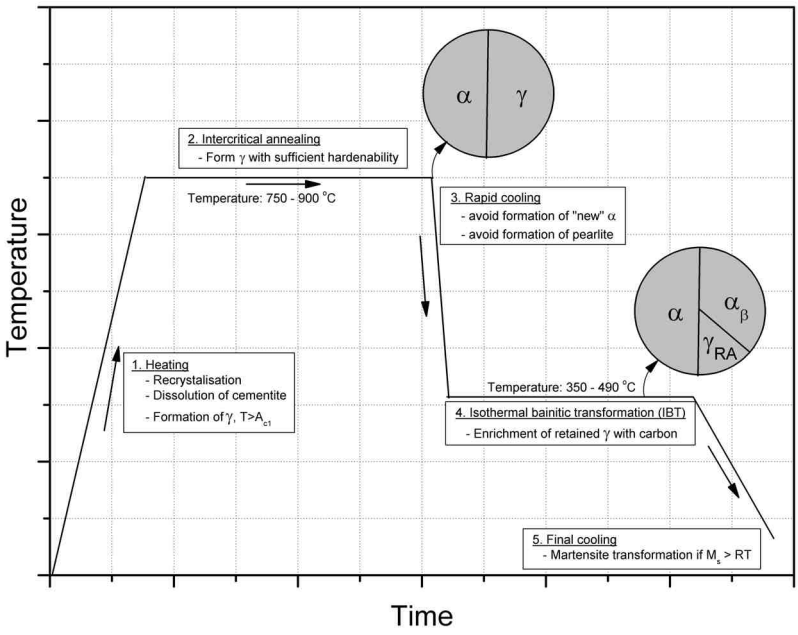

Figure 3.2: *Schematic illustration of the TRIP heat treatment to obtain a ferritic (α) and bainitic (α_β) microstructure with retained austenite (γ_{RA}).*

annealing, thereby exhibiting an incomplete reaction phenomenon [10]. Silicon and aluminium present in the steel retards the formation of cementite in bainite from austenite due to their incredibly low solubility in cementite. Cementite which forms during the isothermal bainitic holding (350 to 490 ^{o}C) by a para-equilibrium transformation mechanism (transformation in which the concentrations of substitutional solid solutions in the parent and product phases remain the same) and substitutional solute atoms such as silicon and aluminium are trapped in the cementite nuclei, when cementite starts to precipitate in bainite. However, due to the lower solubility of silicon and aluminium, para-equilibrium conditions retard further precipitation of cementite [11]. The formation of carbide free bainite leads to the enrichment of untransformed austenite with carbon during the holding, resulting in reduction of the temperature for martesnite transformation from the untransformed austenite in the subsequent fast cooling stage.

Stage-3: Final cooling

Isothermally held steel is further cooled to room temperature in the final stage of the heat treatment. Depending on the M_s temperature of the austenite left untrans-

formed after isothermal bainitic holding, martensite transformation takes place during cooling. In most cases, partial transformation of austenite to athermal martensite is found during final cooling to room temperature [3].

As a result of these treatment stages, the final microstructure of TRIP steel consists of 60 - 70 % ferrite (α), 20 - 30 % carbide free bainite (α_β), 5 - 15 % retained austenite (γ_{RA}) and a small fraction (<2 %) of martensite (α').

3.3 Effect of steel composition and heat treatment parameters on retained austenite

Apart from the composition of the steels, temperature and the duration of inter-critical annealing and isothermal bainitic holding stages in the TRIP heat treatment dictate the size, shape and distribution of retained austenite in the final microstructure. In order to generate base metal microstructures prior to welding with varying distributions of microstructural constituents, especially retained austenite, heat treatment parameters are altered for a given composition of TRIP steel. The objective of this experiment is to find heat treatment parameters that can generate different base metal microstructures for a given steel composition, with varying retained austenite contents for the welding experiments.

Commercial grade and industrially processed 1.25 mm thick cold rolled and annealed aluminium containing (High-Al) steel (Table 3.1) was used to study the effect of heat treatment parameters, such as inter-critical annealing and isothermal bainitic holding temperatures on the microstructural constituents. One of the heat treatment cycles was also used on a silicon containing (High-Si) TRIP steel in order to study the effect of composition on the microstructural constituents.

Steel samples were subjected to the TRIP heat treatment using salt bath furnaces. After the heat treatment, qualitative and quantitative microstructural characterisations were carried out on the heat treated samples by optical microscopy, scanning electron microscopy (SEM) coupled with Energy Dispersive X-ray Spectroscopy (EDS), Electron Probe Micro-Analysis (EPMA), vibrating sample magnetometry and 3D synchrotron X-ray Diffraction microscopy (3D-XRD). The following subsections describe the experimental procedures used for heat treatments and characterisation techniques. The characterisation techniques described were also used to analyse the microstructural constituents, especially retained austenite, after welding. This will be discussed in forthcoming chapters.

3.3.1 Heat treatment

Samples for TRIP heat treatment and subsequent welding experiments were cut from the steel plates and subjected to a heat treatment using salt baths. Plates with a length of 250 mm and a width of 100 mm were cut parallel to the rolling direction and immersed in the salt baths maintained at a required temperature. Inter-critical annealing was carried out using a commercial grade mixture of liquid alkali chlorides

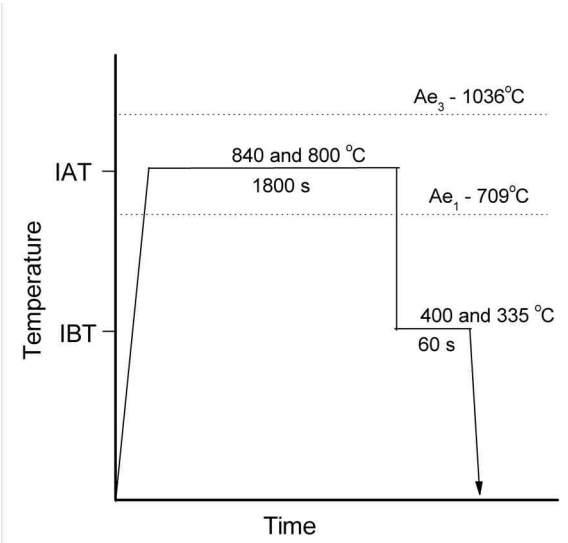

Condition	IAT, °C	IBT, °C
(a) HT840/400	840	400
(b) HT840/335	840	335
(c) HT800/400	800	400
(d) HT840/335	800	335

Figure 3.3: *Heat treatment parameters used to study the effect of inter-critical annealing temperature (IAT) and isothermal bainitic holding temperature (IBT) in High-Al TRIP steel. The heat treatment condition "c" was also used on High - Si steel plates to evaluate the effect of composition.*

(Durferrit™ - GS 600 salt bath). Isothermal bainitic holding was carried out by immersing the inter-critically annealed steel plates in a commercial grade sodium nitride bath (Durferrit™ - AS 140).

Two inter-critical annealing (800 and 840 ^{o}C) and isothermal bainitic holding (335 and 400 ^{o}C) temperatures were used to study the effect of heat treatment temperatures on the microstructural constituents and to generate the base metal microstructures for the welding experiments. Figure 3.3 schematically shows the heat treatment procedures along with the transformation temperatures of the High-Al TRIP steel used. Steel plates were immersed in the salt bath and maintained at the inter-critical annealing temperature for 1800 s. After inter-critical annealing, plates were transferred to another salt bath and kept at the isothermal bainitic holding temperatures for 60 s. Plates were subsequently quenched in water to room temperature. Throughout the experiments, the temperature of the salt baths were maintained with an accuracy of ± 5 ^{o}C.

To study the effect of composition, High-Si and High-Al steel plates were inter-critically annealed at 800 ^{o}C for 1800 s and subsequently cooled to 400 ^{o}C (isothermal bainitic holding temperature) and held there for 60 s (heat treatment (c) in figure 3.3).

3.3.2 Optical microscopy

The heat treated plates were cross sectioned in the transverse direction for metallography analysis of the base metal microstructures. Samples were polished and etched for optical and scanning electron microscopy studies. Three etching procedures were followed to clearly delineate the microstructural constituents present. In the first, samples were etched with a 4% Nital solution for 5 seconds. The second was carried out using a 10 % Picral solution for 90 seconds for better delineation of prior austenite grain boundaries. The third etching method was used to examine the presence of retained austenite in the microstructure. In this method, samples were etched for 15 seconds with 4 % Picral, followed by 30 seconds etching in 1 % sodium meta bisulphite solution in water. This etching procedure changes the colours of the retained austenite/martensite into bright whitish blue, bainite into brown and allotriomorphic ferrite into a tan colour [12, 13]. The samples were subsequently analysed using a Olympus BX60M™ optical microscope with a quantitative analysis software (analySIS™).

3.3.3 Scanning electron microscopy

Scanning electron microscopy (SEM) was performed on the metallographically polished samples using a JEOL JSM 6500F™ - field emission gun (FEG) scanning electron microscope in secondary and back scattered electron imaging modes. SEM coupled with an Energy Dispersive Spectroscopic (EDS) analysis was used for qualitative examination of the alloying elements present in the microstructural constituents. Quantitative elemental distribution among the various phases in the microstructures were measured by Electron Probe Micro Analysis (EPMA) using a JEOL JXA 8900R™ microprobe, and an electron beam with an energy of 15 keV and beam current of 50 nA employing Wavelength Dispersive Spectrometry (WDS). The counting error for aluminium, silicon, manganese and chromium in EPMA is 0.02, 0.02, 0.3 and 0.01 wt. % respectively.

3.3.4 Vibrating sample magnetometry

Vibrating sample magnetometry was one of the techniques used in this work to quantify the retained austenite in a TRIP steel microstructure. In this method, the saturation magnetisation of steel samples with and without austenite are measured from the magnetisation curves (mass magnetisation as a function of magnetic flux density). In steels, ferrite, martensite and cementite are ferromagnetic below their Curie temperature (T_c) while austenite and non-metallic inclusions are paramagnetic (for pure iron T_c is 770 ^{o}C and for cementite T_c is 210 ^{o}C). Thus, the difference in the saturation magnetisation is directly proportional to the amount of paramagnetic phases (retained austenite) in the TRIP steel samples [14, 15].

Cylindrical samples of 1.25 mm diameter were cut by means of electro-discharge-machining from the heat treated TRIP steel plates for the magnetic saturation measurements. The magnetisation measurements were performed in a LakeShore 7307 Vibration Sample Magnetometer (VSM) and were carried out by applying magnetic

fields starting from 2 Tesla to zero and then to -2 Tesla with a step size of 0.05 Tesla. This decreasing field measurement was made to ensure a well-defined field history for the magnetisation. Throughout the measurements, stability and accuracy were checked by periodic calibration of the equipment using a Nickel standard sample with a sensitivity of 1x10^{-11} A m^2. A high temperature oven (Model 73034) attached to the magnetometer was used for the thermo-magnetic measurements. The saturation magnetisation (M^s) of the steel samples was calculated from the mass magnetisation as a function of the magnetic flux density curves. A detailed description of these calculations can be found elsewhere [14, 16]. The accuracy in the volume percent of retained austenite measured by this technique is ±0.2 % [17].

3.3.5 3D synchrotron x-ray diffraction analysis

Synchrotron X-ray diffraction measurements were carried out on the heat treated samples at beam line ID11 at the European Synchrotron radiation facility, using a three-dimensional X-ray diffraction microscope (3DXRD). Cylindrical samples with a diameter of 1 mm and a length of 3 mm were electro-discharge machined from the TRIP heat treated plates with the cylindrical axis of the samples in the rolling direction. A monochromatic X-ray beam, with an energy of 71.64 keV (wavelength - 0.1732 Å) a horizontal size of 1.2 mm and a vertical size of 0.6 mm was used to illuminate the cylindrical samples. The diffracted intensities from the samples were recorded in transmission geometry using a FreLon 2D area detector. During the illumination, samples were continuously rotated around the sample axis over an angle of 10^o, starting from -90^o to +90^o. Based on the saturation intensity of the detector for a heat treated sample, various exposure times such as 4, 6 and 10 s in each 10^o rotation step were selected and the 2D diffraction rings from austenite and ferrite grains were recorded. The use of a large beam size and rotation over 180^o ensured that almost all the grains in the samples were illuminated. After subtracting detector background and distortion statistics, the 2D diffraction patterns were integrated using the *Fit2D* software. The volume fraction of austenite was calculated from the integrated intensities of $\gamma_{(200)}$, $\gamma_{(220)}$ and $\alpha_{(200)}$, $\alpha_{(211)}$ using the following equation [18];

$$f_\gamma = \frac{\frac{1}{N}\sum_{i=1}^{N}\left(\frac{I_{\gamma,i}}{R_{\gamma,i}}\right)}{\frac{1}{N}\sum_{i=1}^{N}\left(\frac{I_{\gamma,i}}{R_{\gamma,i}}\right) + \frac{1}{M}\sum_{i=1}^{M}\left(\frac{I_{\alpha,i}}{R_{\alpha,i}}\right)} \tag{3.1}$$

where N and M are the number of considered austenite and ferrite reflections, respectively. The index i refers to the {hkl} reflections of interest. R is the normalisation factor and is a function of incident photon flux, illuminated sample volume, sample transmission factor and theoretical diffraction intensity of the {hkl} reflections considered. The lattice parameters of austenite and ferrite were calculated from the experimental mean scattering angle (2θ) of the considered {hkl} diffractions. The accuracy in the volume percent of retained austenite measured by this technique is ±0.2 % and the lattice parameters of ferrite and austenite were measured with an accuracy of 0.002 Å.

3.3.6 Results

The four heat treatments applied on a High-Al TRIP steel plates give rise to microstructures with varying size and distribution of bainite and retained austenite grains. Optical microscopy analysis clearly indicates the presence of retained austenite after the heat treatments. The size of austenite grains in these microstructures are found to vary from 2 to 5 μm. The austenite content appears to be higher in the case of condition HT800/400, which is also found to contain coarser austenitic grains compared with the other conditions (figure 3.4). It can also be seen from this figure that the bainitic grains (shown as a dark colour) appear coarse and have a polygonal structure with clearly delineated grain boundaries in the case of higher inter-critical annealing conditions (HT840/400 and HT840/335). Conversely the grain boundaries are less well defined under lower inter-critical annealing conditions (HT800/400 and HT800/335).

The EPMA analysis indicates that ferritic grains are richer in aluminium than carbide free bainite or retained austenite in the microstructure of High - Al steel samples. Figure 3.5 shows results of line scans carried out on a HT800/400 High - Al steel sample. The aluminium content of ferrite grains is found to be more than the bulk content (1.1 wt. %), in some grains reaching about 1.4 wt. %. However, the manganese content in ferrite was less than the bulk manganese content which resulted in manganese enrichment (up to 2 wt. %) in co-existing carbide free bainite or retained austenite. Similar behaviour is also observed in High - Si steel samples, where the ferrite grains are richer in silicon and the manganese content of these grains is reduced compared with other phases present in the microstructure (figure 3.6). The EPMA analyses also show that the partitioning of silicon and aluminium in both steels does not reach a complete equilibrium during the TRIP heat treatment.

Figure 3.7 shows the magnetisation behaviour of the heat treated TRIP steel samples for the applied magnetic field. The saturation magnetisation (M^s) values were calculated from the high-flux density part of the magnetisation curves by fitting the equation [14];

$$M = M^s \left(1 - \frac{a}{B} - \frac{b}{B^2}\right) \tag{3.2}$$

where M is the mass magnetisation (A m^2 kg^{-1}) for the applied magnetic flux density B (Tesla) and, M^s is the saturation magnetisation, a and b are the fitting parameters. In order to measure the fraction of austenite present in the samples, one of the samples was heated to 600 ^{o}C and cooled to room temperature at a rate of 0.03 ^{o}C s^{-1} to transform the austenite present in the sample to a ferrite and cementite mixture [19]. The saturation magnetisation of the sample without austenite ($M^s(f)$) was measured at room temperature and the mass fraction of austenite present in the other samples is calculated using the relationship;

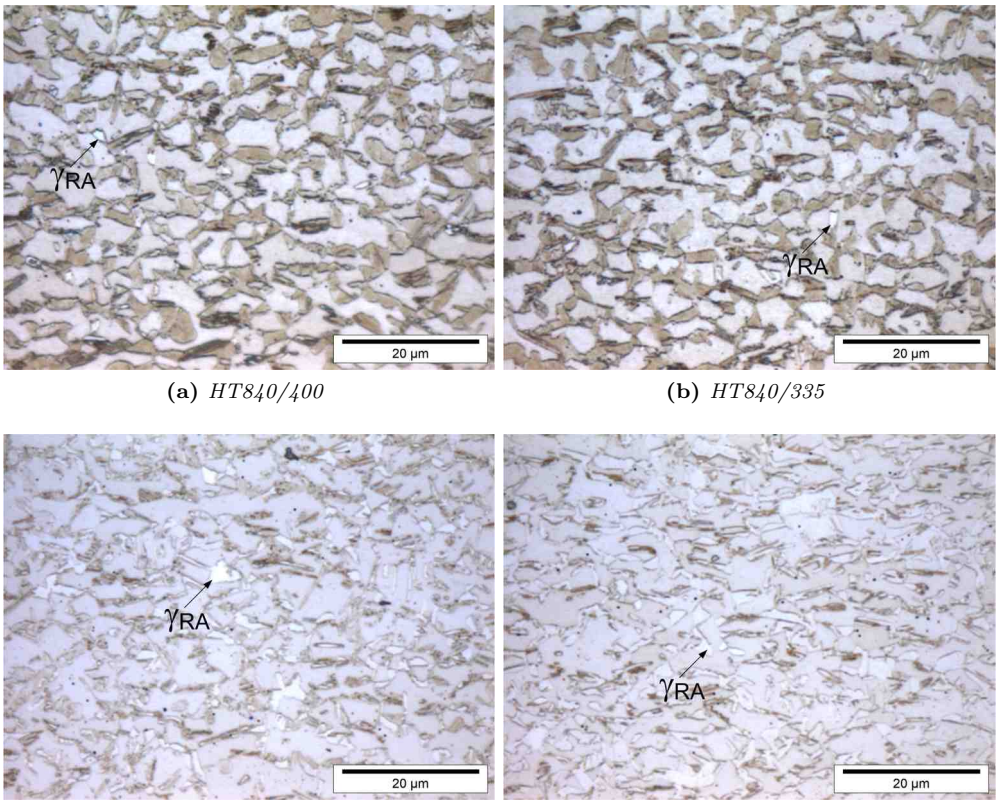

(a) *HT840/400* **(b)** *HT840/335*

(c) *HT800/400* **(d)** *HT800/335*

Figure 3.4: *Optical micrographs of High - Al base metals after the four heat treatments 'a' to 'd' respectively (see figure 3.3) showing the presence of retained austenite (γ_{RA}, bright) along with ferrite (matrix) and bainite (dark). The labels indicate the inter-critical annealing and isothermal bainitic holding temperatures.*

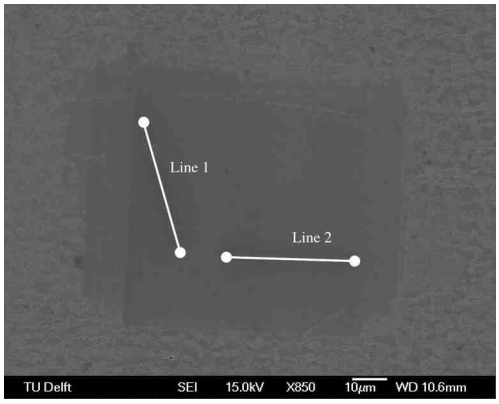

(a) *Secondary electron image*

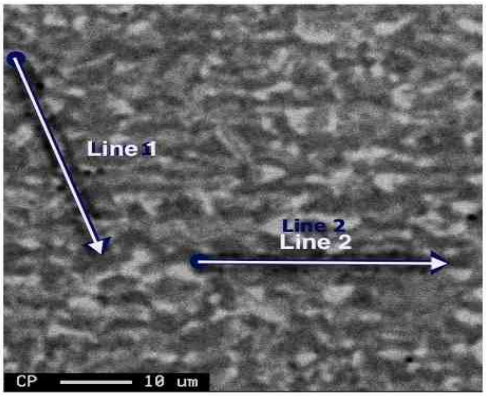

(b) *Back scattered electron image*

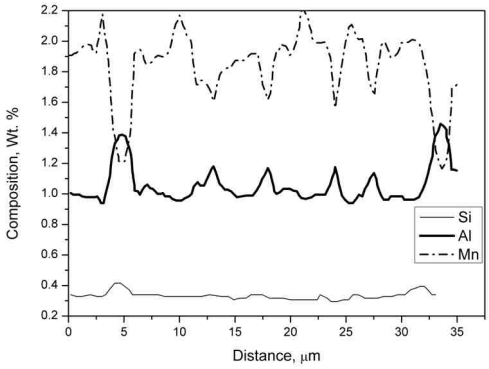

(c) *Line 1*

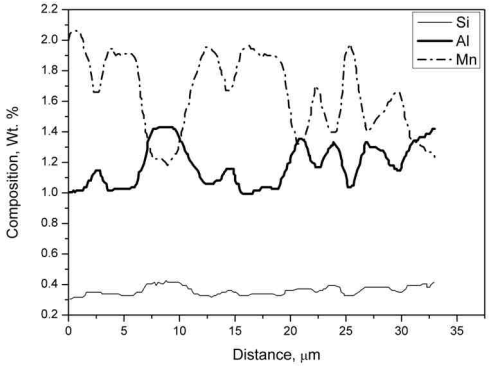

(d) *Line 2*

Figure 3.5: *EPMA analysis indicates that the ferrite grains in High-Al TRIP steel are richer in aluminium than carbide free bainite or retained austenite grains. This EPMA analysis was carried out on a HT800/400 heat treated sample.*

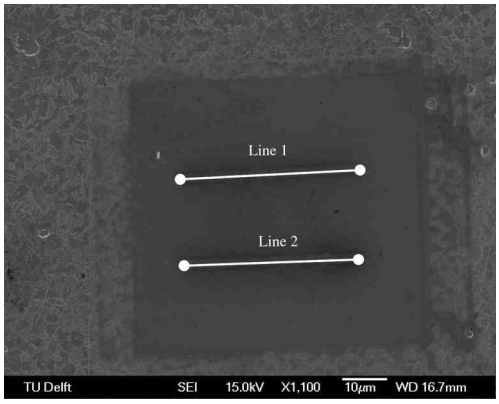

(a) *Secondary electron image*

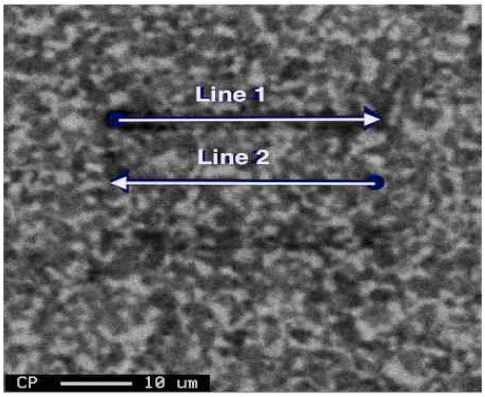

(b) *Back scattered electron image*

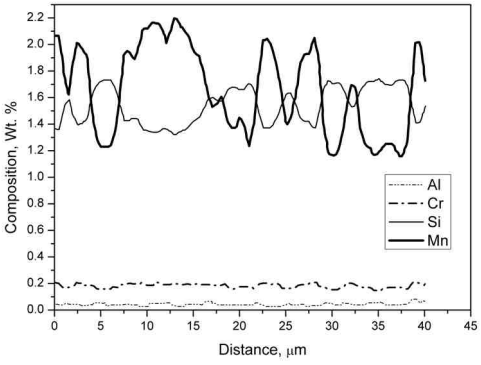

(c) *Line 1*

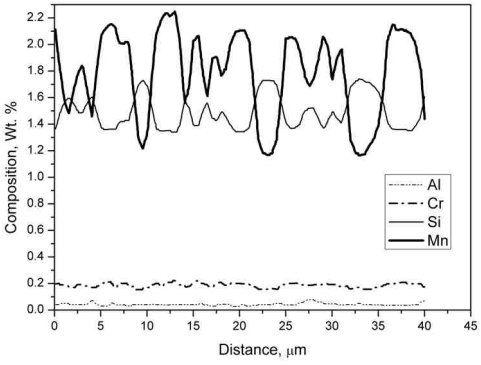

(d) *Line 2*

Figure 3.6: *EPMA analysis indicates that the ferrite grains in High-Si TRIP steel are richer in silicon than carbide free bainite or retained austenite grains. This EPMA analysis was carried out on a HT800/400 heat treated sample.*

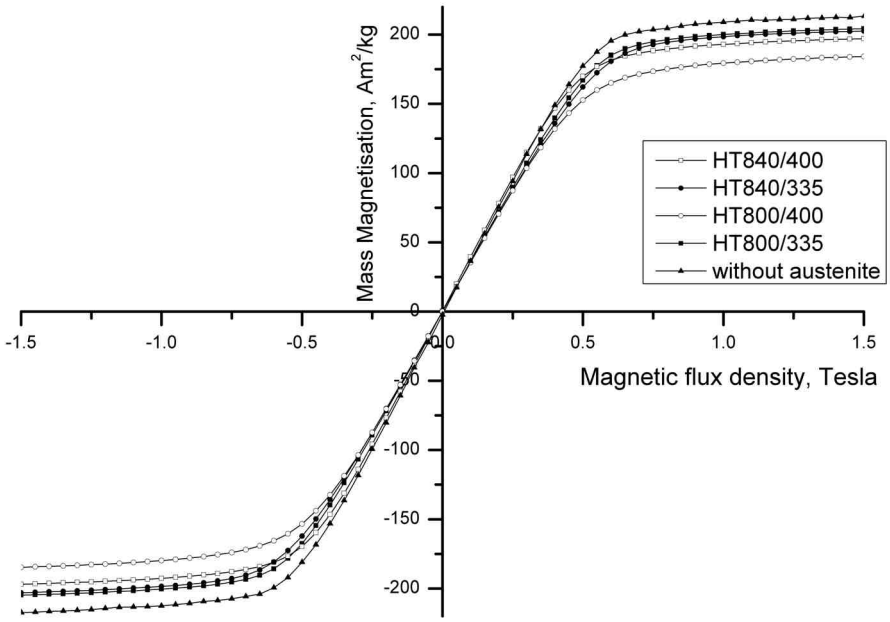

Figure 3.7: *Magnetisation of heat treated High - Al TRIP steel samples and a sample without austenite as a function of magnetic flux density.*

$$f_\gamma = 1 - \beta \left(\frac{M^s(c)}{M^s(f)} \right) \tag{3.3}$$

where $M^s(c)$ is the saturation magnetisation of austenite containing samples (in A m^2 kg^{-1}) and the coefficient β is 0.99 [14], which takes into account the effect of cementite on the saturation magnetisation. It can be seen form the magnetisation curves of the heat treated samples and the sample without austenite that the approach to the saturation magnetisation clearly differs in all cases. The saturation magnetisation of the sample without austenite ($M^s(f)$) was found to be 216.47 A m^2 kg^{-1}. Table 3.2 shows the saturation magnetisation values of heat treated samples and their corresponding austenite contents calculated using equation 3.3. The heat treatment condition HT800/400 yielded a base metal microstructure with a higher amount of austenite (15.0 %) compared with other heat treatment conditions. It should also be noted that conditions with higher isothermal bainitic transformation temperatures (in this case, HT840/400 and HT800/400) generated more austenite in the microstructures.

Figure 3.8 shows the X-ray diffraction patterns of High-Si (figure 3.8a) and High-

Table 3.2: *Saturation magnetisation and austenite content in heat treated High-Al TRIP steel plates*

Heat treatment condition	Saturation magnetisation, A m^2 kg^{-1}	Austenite, %
(a) HT840/400	197.12	8.9
(b) HT840/335	208.75	3.6
(c) HT800/400	186.24	15
(d) HT800/335	207.25	4.3

Al (figure 3.8b) TRIP steel samples after the radial integrations of $\{hkl\}$ reflections over 180^o. The mean lattice parameters of austenite and ferrite in the HT800/400 samples was determined from the experimental mean scattering angle ($2\theta_i$) of the (hkl) reflections using the following relationship [18];

$$a = \frac{1}{N}\sum_{i=1}^{N}\left(\frac{\lambda}{2}\right)\frac{\sqrt{h_i^2 + k_i^2 + l_i^2}}{sin(\theta_i)} \tag{3.4}$$

where a is the lattice parameter, N is the number of $\{hkl\}$ reflections of austenite and ferrite considered and λ is the wavelength of the beam (0.1732 Å). Table 3.3 shows the lattice parameters of retained austenite and ferrite in the High-Si and High-Al HT800/400 samples.

The carbon concentration of retained austenite was then estimated from the calculated lattice parameter (a_γ) using the relationship [18];

$$a_\gamma = 3.556 + 0.0453x_c + 0.00095x_{Mn} + 0.0056x_{Al} \tag{3.5}$$

where x_c, x_{Mn} and x_{Al} are the carbon, manganese and aluminium in austenite (wt. %). The influence of Si on the lattice parameter of austenite was found to be negligible within the experimental accuracy and thus it is not considered here [20]. Assuming the austenite manganese and silicon content are as the bulk manganese and aluminium contents, the retained austenite carbon concentration (x_c) in the High-Si and High-Al HT800/400 samples was found to be 1.2 and 1.04 wt. % respectively. The measured x_c in both steels are plotted with the calculated T_0 allotropic phase boundaries in figure 3.9.

The volume fraction of retained austenite present in the High-Al steel sample was found to be higher (15.4 %) than that of High-Si steel sample, which contained only 10.9 % after the heat treatment (HT800/400).

3.4 Discussions

3.4.1 Effect of heat treatment parameters

Optical microscopy (figure 3.4) shows that heat treatment with a higher inter-critical annealing temperature (840 ^{o}C) results in a coarse and polygonal bainitic structure

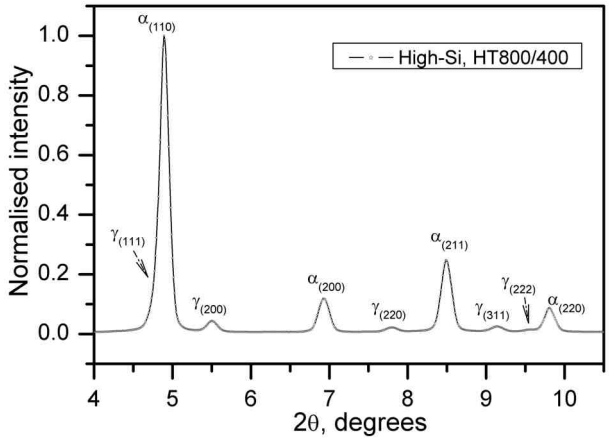

(a) *High-Si*

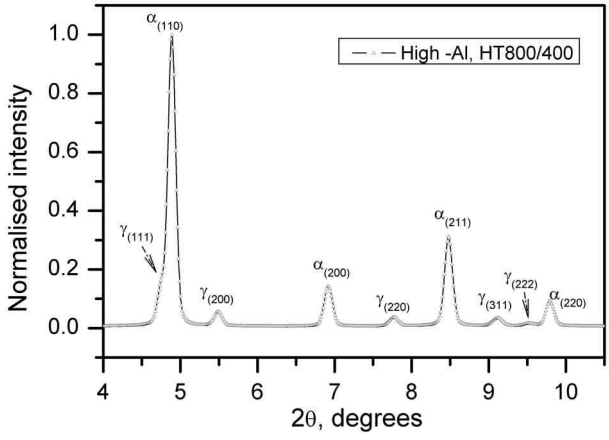

(b) *High-Al*

Figure 3.8: *The integrated diffraction rings of TRIP steel samples showing the normalised intensity as a function of 2θ for different austenite and ferrite (hkl) reflections in (a) High - Si and (b) - High - Al TRIP steels.*

Table 3.3: *Lattice parameters of retained austenite (a_γ) and ferrite a_α in Å, retained austenite content (γ_{RA}) and carbon in retained austenite (x_c) in HT800/400 heat treated TRIP steels.*

Steel	a_γ, Å	a_α, Å	γ_{RA}, %	x_c, wt. %
High-Si	3.60709	2.86450	10.9	1.2
High-Al	3.61791	2.87002	15.4	1.04

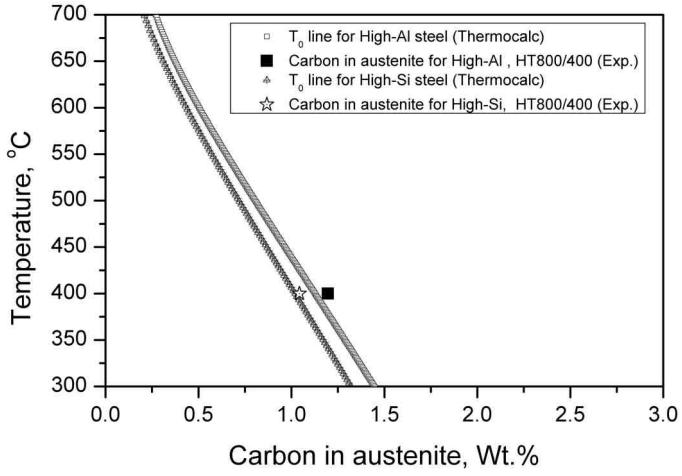

Figure 3.9: *Experimentally measured retained austenite carbon concentration of High-Si and High-Al TRIP steel samples showing higher values than the calculated T_0 allotropic phase boundaries.*

compared with a lower inter-critical annealing tempeature (800 ^{o}C). This result indicates that austenite grains which form during inter-critical annealing can grow faster at higher inter-critical annealing temperature and bainitic grains formed from this austenite grains maintain their prior austenite grain sizes during cooling from the inter-critical annealing temperature.

The magnetic saturation measurements indicates that the four different TRIP heat treatment cycles (figure 3.3) applied to the High - Al TRIP steel, generated base microstructures with austenite contents varying from 3.6 to 15.0 %. For the conditions HT840/400 and HT800/400, where the isothermal bainitic holding temperature was 400 ^{o}C, a higher amount of retained austenite was obtained (8.9 % and 15.0 % respectively), whilst samples held at 335 ^{o}C for isothermal bainitic transformation (condition HT840/335 and HT800/335), the austenite content was found be 3.6 and 4.3 % respectively. Similar behaviour was also observed by Saleh *et al.* [21], where lower bainitic holding temperatures resulted in lesser austenite fractions in the microstructures. During isothermal bainitic holding, the austenite formed after the inter-critical annealing transforms to carbide free bainite and the transformation ceases incompletely once the untransformed austenite is sufficiently enriched in carbon. The incomplete bainitic transformation time increases with decreasing isothermal bainitic holding temperature [10]. Minote *et al.* [22] showed that for a 0.2 wt. % carbon TRIP steel, the incomplete bainitic transformation time varied from 80 s to 1000 s when the isothermal bainitic holding temperature was reduced from 450 ^{o}C to 300 ^{o}C. During the base metal heat treatments, isothermal bainitic transformation (IBT) was carried out by holding at 400 ^{o}C and 335 ^{o}C for 60 s. This holding time was not sufficient to enrich the austenite and, especially in the cases of HT840/335 and HT800/335, there was not enough time for the enrichment of carbon in austenite, in contrast to the samples held at 400 ^{o}C. Due to this, the untransformed austenite after isothermal bainitic holding decomposes during subsequent cooling to room temperature and results in reduced austenite contents in the HT840/335 and HT800/335 samples. Optical microscopy analysis also shows the presence of bulky austenite grains (about 5 μm in diameter) in the higher austenite containing base metals (condition HT840/400 and HT800/400), which indicates that more of the austenite grains, formed during inter-critical annealing, remain untransformed during isothermal bainitic holding. Nevertheless, these heat treatments generated microstructures with varying content of retained austenite which were subsequently used to compare the effects of weld thermal cycles on the theses different microstructures in a given TRIP steel composition.

3.4.2 Effect of steel compostion

EPMA analyses indicated that in both steels, the HT800/400 TRIP heat treatment resulted in heterogeneity in the amount of alloying elements in the co-existing ferritic and austenitic phases. The ferritic grains were richer in aluminium in High-Al steel and silicon in High-Si steels, whereas retained austenite and bainitic grains were found to be richer in manganese. This partitioning behaviour did not however result in

complete equilibrium of subsititional alloying element contents within the co-existing phases. In general, it is assumed that the phase transformations occur during a TRIP heat treatment under para-equilibrium conditions, where the parent and product have the same amount of substitutional alloying elements. Under ideal para-equilibrium conditions, the TRIP heat treatment should always result in equal amounts of substitutional solid solutions between ferrite and austenite. Conversely, if a TRIP heat treatment is applied to a commercially produced (cold rolled, continuously annealed) steel, which contains a microstructure with heterogeneous distribution of alloying elements, the resultant TRIP microstructure would also show heterogeneity in substitutional alloying elements. This is because shorter annealing times (1800 s) will not be sufficient to homogenise the substitutional alloying elemental distributions which are very sluggish at the inter-critical annealing temperatures (840 and 800 ^{o}C).

The volume fraction of retained austenite present in the High-Al HT800/400 sample was found to be higher (15 %) than in the High-Si steel HT800/400 sample, which contained only 10.9 %, although both steels underwent the same TRIP heat treatment (inter-critical annealing at 800 ^{o}C and isothermal bainitic holding at 400 ^{o}C). It can be seen from figure 3.1b, where the pseudo binary phase diagram of High-Al steel is given, that the addition of aluminium in steels increases the equilibrium carbon content of austenite in the inter critical ($\alpha + \gamma$) region and extends the region to higher temperature. The equilibrium carbon content of austenite at 800 ^{o}C in High-Al steel is 0.77 wt. % which is higher than that of the High-Si steel (0.43 wt. %). Due to this, the austenite is enriched in carbon during inter-critical holding at 800 ^{o}C in High-Al steels, resulting in higher austenite stabilisation during isothermal holding at 400 ^{o}C and subsequent cooling to room temperature.

3.4.3 Retained austenite measurement

The retained austenite measurements using magnetic saturation and synchrotron X-ray diffraction show that both techniques measure the same retained austenite content in a HT800/400 High-Al TRIP steel sample (15 and 15.4 % respectively, table 3.2 and table 3.3). It is also found that both techniques measure the retained austenite with same accuracy with their own merits and drawbacks. The magnetic saturation technique measures the bulk magnetic properties of the specimen and, in comparison to other experimental techniques, is easy to use without complex sample preparation. However, with magnetic saturation techniques, it is not possible to extract the carbon concentration and lattice parameter information of retained austenite. Moreover, due to a relatively large sample size in the magnetic measurements (0.025 m^3), correlation of large temporal and spatial gradient thermal cycles (such as occur during welding) with the volume fraction and carbon concentration of austenite retained in the welded samples requires synchrotron X-ray diffraction.

3.5 Concluding remarks

It is found that, for a given TRIP steel composition, by altering the heat treatment parameters, it is possible to generate microstructures with retained austenite contents varying from 3.6 to 15 %. TRIP heat treatments with a higher inter-critical annealing temperature (840 ^{o}C) results in a coarse and polygonal bainitic structure. Conversely, with lower inter-critical annealing tempeature (800 ^{o}C), smaller and less well defined bainitic grains were obtained. The heat treatment results also indicates that a combination of lower inter-critical temperature (800 ^{o}C) and higher iosthermal bainitic temperature resulted in a high amount of retained austenite (15 %). After an identical heat treatment, the retained austenite content in a High-Al TRIP steel was found to be higher (15.4 %) than in a High-Si TRIP steel, which contained about 10.9 %). The elemental analysis indicates that the co-existing ferrite and bainite and retained austenite show partitioning of substitutional alloying elements in the TRIP heat treated microstructure. The consistency in the measurements of retained austenite contents using magnetic saturation and synchrotron X-ray diffraction show that both techniques can be used to quantify retained austenite in TRIP steels.

References

[1] O.Matsumura, Y.Sakuma and H.Takechi, 'TRIP and its kinetics aspects in austempered 0.4C-1.5Si-0.8Mn steels', *Scripta Metallurgica*, 21, 1301–1306, 1987.

[2] O.Matsumura, Y.Sakuma and H.Takechi, 'Mechanical properties and retained austenite in intercritically heat-treated bainite-transformed steel and their variation with Si and Mn additions', *Metallurgical Transactions A*, 22A, 489–498, 1991.

[3] B.C.De Cooman, 'Structure-properties relationship in TRIP steels containing carbide-free bainite', *Current Opinion in Solid State and Material Science*, 8, 285–303, 2004.

[4] S.J.Kim, C.G.Lee, I.Choi and S.Lee, 'Effects of heat treatment and alloying elements on the microstructures and mechanical properties of 0.15 wt. % C transformation induced plasticity aided cold rolled steel sheets', *Metallurgical and Material Transactions A*, 32A, 505–514, 2001.

[5] J.Mahieu, S.Claessens and B.C.De Cooman, 'Galvanisability of high-strength steels for automotive applications', *Metallurgical and Materials Transactions A*, 32A, 2905–2907, 2001.

[6] C.Garcia-Mateo, F.G.Caballero and H.K.D.H.Bhadesia, 'Acceleration of low-temperature bainite', *ISIJ International*, 43, 1821–1825, 2003.

[7] H.C.Chen, H.Era and M.Shimizu, 'Effect of phosphorous on the formation of retained austenite and mechanical properties in si-containing low carbon steel sheet', *Metallurgical Transactions A*, 20A, 437–445, 1989.

[8] J.Wang and S.van der Zwaag, 'Theoritical study of P-containing transformation induced plasticity steel - part 2', *Zeitschrift fr Metallkunde*, 92, 1306–1311, 2001.

[9] G.Ghosh and G.B.Olson, 'Simulations of paraequilibrium growth in multicomponent systems', *Metallurgical and Materials Transactions A*, 32A, 455–467, 2001.

[10] E.Girault, P.Jacques, P.Ratchev, J.van Humbeeck and B.Verlinden, 'Study of the temperature dependence of the bainitic transformation rate in a multiphase TRIP-assisted steel', *Material Science and Engineering A*, A273-275, 471–474, 1999.

[11] H.K.D.H.Bhadesia, Bainite in steels; Transformations, Microstructure and Properties, 2nd edn., IOM Commuication Ltd, 1 Carlton House terrace, SW1Y 3DB, London, 2001.

[12] F.S.LePera, 'Improved etching technique for the determination of percent martensite in high-strength dual-phase steels', *Metallography*, 12, 263–268, 1979.

[13] A.K.De and J.G.Speer, 'Color tint-etching for multiphase steels', *Advanced Materials & Processes*, February, 27–30, 2003.

[14] L.Zhao, N.H.van Dijk, E.Bruck, J.Sietsma and S.van der Zwaag, 'Magnetic and X-ray diffraction measurements for the determination of retained austenite in TRIP stees', *Material Science and Engineering A*, A313, 145–152, 2001.

[15] B.D.Cullity, Introduction to Magnetic Materials, Addition-Wesley, Reading, MA, USA, 1972.

[16] N.Luzginova, L.Zhao and J.Sietsma, 'Evolution and thermal stability of retained austenite in SAE 52100 bainitic steel', *Material Science and Engineering A*, A448, 104–110, 2007.

[17] L.Zhao, M.K.Wibowo, M.J.M.Hermans and S.M.C.van Bohemen, 'Retention of austenite in the welded microstructure of 0.16C-1.6Mn-1.5Si(wt.%) TRIP steels', *Journal of Materials Processing Technology*, 209, 5286 – 5292, 2009.

[18] N.H.van Dijk, A.M.Butt, L.Zhao, J.Sietsma, S.E.Offerman, J.P.Wright and S.van der Zwaag, 'Thermal stability of retained austenite in TRIP steels studied by synchrotron X-ray diffraction during cooling', *Acta Materialia*, 53, 5439–5447, 2005.

[19] B.K.Jha and N.S.Mishra, 'Microstructural evolution during tempering of a multiphase steel containing retained austenite', *Material Science and Engineering A*, A263, 42–55, 1999.

[20] D.J.Dyson and B.Holmes, 'Effect of alloying additions on the lattice parameter of austenites', *Journal of the iron and steel institute*, May, 469 – 474, 1970.

[21] M.H.Saleh and R.Priestner, 'Retained austenite in dual-phase silicon steels and its effect on mechanical properties', *Journal of materials processing technology*, 113, 587–593, 2001.

[22] T.Minote, S.Torizuka and M.Niikura, A., 'Modeling of transformation behaviour and compositional partitioning in trip steel', *ISIJ International*, 36, 201–207, 1996.

Chapter 4

Elemental behaviour during welding of TRIP steels[1]

The thermal cycle of a welding process destroys the original microstructure of a TRIP steel, resulting in inferior mechanical properties of the weld compared to the base metal. The presence of alloying elements such as silicon and aluminium limit the weldability of TRIP steel and thereby its commercial applications. In order to improve the weldability, it is desirable to understand the behaviour of TRIP steel with emphasis on the thermal cycles of specific welding processes and the effects of alloying additions on the evolution of the weld and heat affected zone (HAZ) microstructures. This chapter describes microstructural evolution during welding of commercially processed silicon and aluminium based TRIP steels. These steels were welded by means of Gas Tungsten Arc (GTA) welding, Laser Beam (LB) welding and Resistance Spot (RS) welding. The influence of the weld thermal cycles and composition on the nature of microstructrual constituents formed in the heat affected zone (HAZ) and fusion zone (FZ) after welding were studied. The role of alloying additions such as silicon and aluminium on the phase transformation behaviour of TRIP steels during welding was thoroughly analysed. Partitioning behaviour in various microstructrual constituents which were formed in a given weld thermal cycle were studied in order to understand their role in retained austenite stabilisation, inclusion formation at the fusion zone and the stabilisation of δ-ferrite in the fusion boundaries of the welded TRIP steels.

[1] "Microstructural Development during Welding of Silicon and Aluminum Based Transformation Induced Plasticity Steels - Inclusion and Elemental Partitioning Analysis", M.Amirthalingam, M.J.M.Hermans and I.M.Richardson, Met. Mat. Transactions A, 40A, 2009, 901-909.

4.1 Base materials

Commerical grade and industrially processed high silicon bearing (High-Si) and high aluminum (High-Al) bearing TRIP steels were used in this study (Table 3.1). Sample plates for Gas Tungsten Arc (GTA) and Laser Beam (LB) welding experiments with a length of 250 mm and a width of 100 mm were cut from the steel plates and subjected to a TRIP heat treatment cycle HT800/400 using salt baths (figure 3.3). Sample plates of 45 mm width and 100 mm length were cut from the heat treated plates and used for the Resistance Spot (RS) welding experiments. The details of the base metal microstructures and the variation of retained austenite in both steels can be found in section 3.3.6.

4.2 Welding

Heat treated TRIP steel plates were welded in a bead on plate configuration using an automated Gas Tungsten Arc (GTA) welding and continuous wave (CW) Nd:YAG laser beam welding equipment. Resistance spot welding was carried out in overlap configuration.

GTA welding was carried out using a Migatronic Commander 400 AC/DC power source. An automatic voltage control algorithm was used to keep the voltage constant during welding. The conditions shown in table 4.1 resulted in full penetration welds of about 5 mm width. The welding parameters were adjusted to have a similar width fusion zone despite the differences in the thickness of the TRIP steel plates used (1.25 and 3 mm thick High-Al and High-Si plates respectively). During welding, the samples were clamped to a steel backing plate with a 20 mm wide central groove for purging the backing gas (argon). At 125 mm from the starting edge of the samples, the backing plate has a 20 mm wide grove perpendicular to the welding direction, to allow thermocouple measurements to be made on the bottom side of the samples. *In-situ* temperature measurements were performed during bead-on-plate welding using 0.25 mm diameter k-type thermocouples which were discharge welded to the bottom of the plates on a line perpendicular to the weld seam on either side of the weld centre line with inter distances of approximately 3 mm between measurement points.

Laser Beam (LB) welding was carried out using a continuous wave (CW) Nd:YAG laser beam oriented perpendicular to the plate surface. Using a power of 2000 W and a speed of 25 mm s^{-1}, fully penetrated welds with a width of 2.5 mm were obtained. During LB welding, a continuous flow of argon (35 L min^{-1}) was maintained behind the weld pool with a gas nozzle oriented 60^o to the plate surface. The working distance and focal length of the laser in LB welding was 150 mm. The spot size of the laser was 0.45 mm. Temperature measurements during welding were carried out using 0.15 mm diameter k-type thermocouples with the same measurement configuration as during GTA welding.

Resistance spot welding was carried out using a Schlatter-50 Hz AC welding machine. An ISO5821, B type 16/6 electrode with a holding force of 4.5 kN was employed.

Table 4.1: *Welding parameters used in Gas Tungsten Arc (GTA) welding.*

Parameters	High-Si	High-Al
Electrode	W + 2 % La_2O_3	W + 2 % La_2O_3
Electrode diameter	2.4 mm	2.4 mm
Electrode angle	60 deg	60 deg
Arc length	3 mm	3 mm
Voltage	10.7 V	10.7 V
Current	145 A	65 A
Welding speed	3 mm s^{-1}	7 mm s^{-1}
Shielding gas	Ar, 10 L min^{-1}	Ar, 10 L min^{-1}
Shielding cup diameter	8 mm	8 mm

By applying a current of 8.5 kA (RMS) during a welding time of 420 ms (including 20 ms cooling time), about 7 mm diameter weld nuggets were obtained.

After welding, the plates were cross sectioned in the transverse direction for metallography analysis. Optical, scanning electron microscopy and elemental analysis were carried out using the procedures described in section 3.3.2 and 3.3.3.

4.3 Thermal cycle of the welding processes

The thermal profile of a welding process dictates the microstructural evolution in the heat affected (HAZ) and fusion zone (FZ). Figure 4.1 shows the temperature variation across the width of the High-Si and High-Al steel plates during GTA welding. The maximum temperature measured at 3.5 mm from the High-Si steel weld centre line was 1058 ^{o}C. This measurement point had average heating and cooling rates of 520 ^{o}C s^{-1} and 200 ^{o}C s^{-1} respectively from the peak temperatures to room temperature. A maximum temperature of 440 ^{o}C was measured at 12 mm from the weld centre line with average heating and cooling rates of 80 ^{o}C s^{-1} and 40 ^{o}C s^{-1}. During GTA welding of High-Al steel plate, a maximum temperature of 980 ^{o}C was measured 2.6 mm from the weld centre line, where the maximum cooling and heating rates (200 to 550 ^{o}C s^{-1}) were also observed. The width of the fusion zones obtained after GTA welding of these TRIP steel plates was about 5 mm.

Compared to GTA welding, LB welding differs significantly in terms of welding time, heating and cooling rates. Figure 4.2 shows the temperature variation during GTA and LB welding at a point 2.6 mm from the weld centre line. During GTA welding, a maximum temperature of 980 ^{o}C was observed at this point. However, due to a smaller weld pool (2.5 mm) and steep temperature gradients in LB welding a much lower peak temperature (215 ^{o}C) was observed at the measured point. Thus, a narrow heat affected zone (HAZ) was obtained in the case of LB welding. A peak temperature of 300 ^{o}C was recorded 11 mm from the weld centre line during GTA

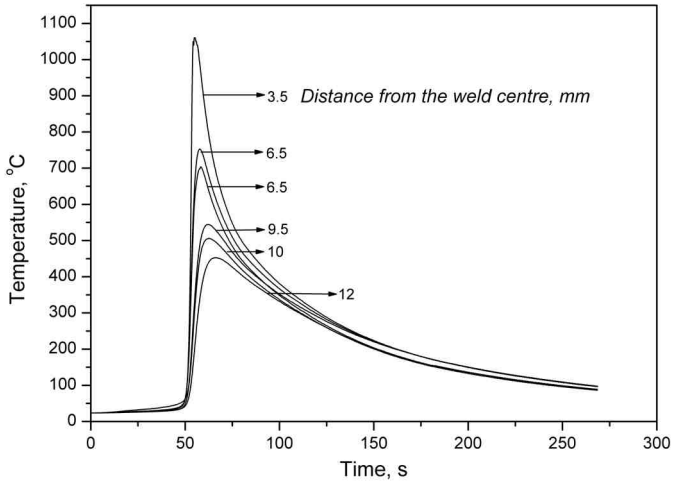

(a) *High-Si*

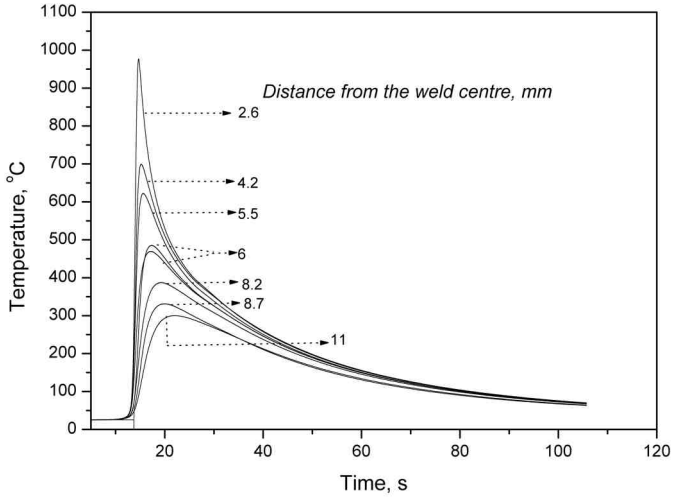

(b) *High-Al*

Figure 4.1: *Thermal cycle during GTA welding of TRIP steel plates at different distances from weld centre line.*

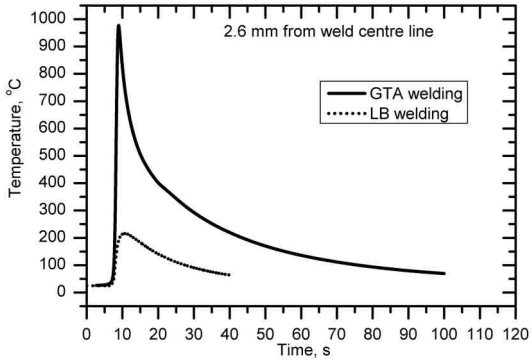

Figure 4.2: *Thermal cycle during GTA and LB welding measured at a point 2.6 mm from the weld centre line in a High - Al steel plate.*

welding indicating a wider HAZ (Figure 4.1b).

In the case of RS welding, the entire welding was completed within 420 ms, resulting in heating and cooling rates several times higher than that encountered in GTA and LB welding. Finite element simulation of RS welding thermal cycles for the welding parameters used here indicated maximum heating and cooling rates in the order of 2100 ^{o}C s^{-1} [1].

4.4 Microstructural characteristics of welded TRIP steel plates

The fusion and heat affected zones contain primarily a martensitic structure in LB and RS welded TRIP steels and, occasional grain boundary Widmanstätten, bainite and intragranular acicular ferrite in GTA welded steels. The average grain size in the coarse grained heat affected zone in both steels is about 120 μm (figure 4.3). The fusion zones of both steels show the presence of inclusions, mainly with a random distribution, in some places decorating the grain boundaries. The average size of the inclusions in the fusion zone of the High-Si steel are found to be smaller in size compared with those in the High-Al fusion zone. A distinctive zone of soft allotriomorphic ferritic grains was found across the fusion line of High-Al steel welds which is not present in welded High-Si steel samples. In addition, the presence of grain boundary ferrite is also observed in the fusion zones of welded High-Al steel samples. In TRIP steels, the formation of hard inter-metallic inclusions in the fusion zone and the presence of soft ferritic grains at the fusion line are invariably detrimental to the mechanical properties.

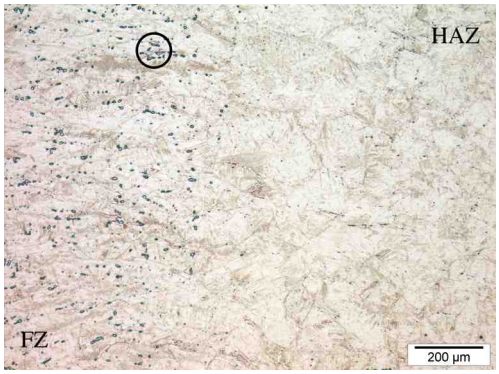

(a) *High-Si GTA welded; the black circle indicates inclusions in the fusion zone (FZ).*

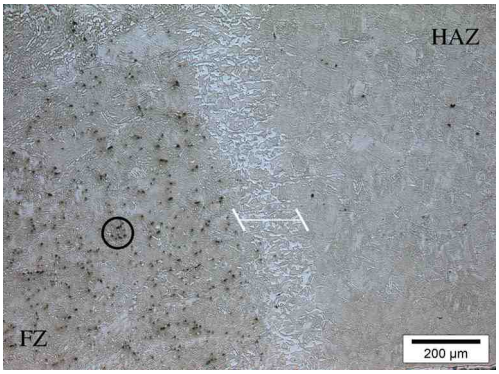

(b) *High-Al GTA welded; the black circle indicates the presence of inclusions in FZ and the white line shows the presence of polygonal ferrite at the fusion boundary.*

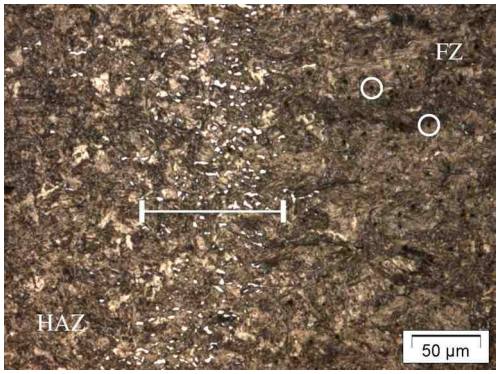

(c) *High-Al LB welded; white circles and the line indicate the presence of inclusions in the FZ and ferrite at the fusion boundary respectively.*

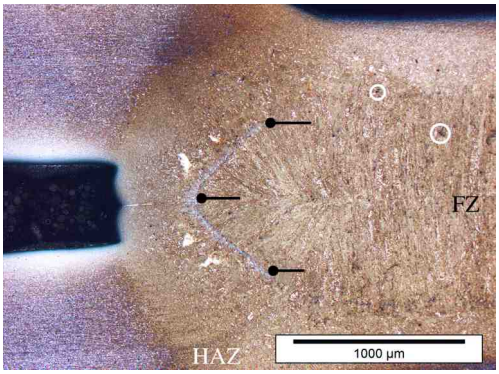

(d) *High-Al RS welded; pointers indicate the presence of polygonal ferrite at the fusion boundary and white circles show the presence of inclusions in the FZ.*

Figure 4.3: *Optical microscopy images of welded TRIP steel samples. (FZ - fusion zone, HAZ - heat affected zone, GTA - gas tungsten arc, LB - laser beam, RS - resistance spot).*

4.4.1 Inclusion formation in fusion zones

The fusion zones of both High-Si and High-Al steels contain complex inclusions. Optical microscopy analysis shows that these inclusions are generally found at the grain boundaries and occasionally they have also been seen in the grain interiors. Figure 4.4 gives an overview of inclusion distribution in the fusion zone of GTA welded High-Si steel and shows that the columnar grain boundaries are decorated with inclusions. At the centre of the fusion zone, the presence of inclusions is also found inside the equi-axed grains. Inclusions in the High-Al welds show a similar distribution to the High-Si steel welds, but the inclusions in the High-Al steel weld (figure 4.5b) are found to be larger in size (5 to 6 μm) than in the High-Si steel, where the average inclusion size is estimated to be 2 to 3 μm (figure 4.5a).

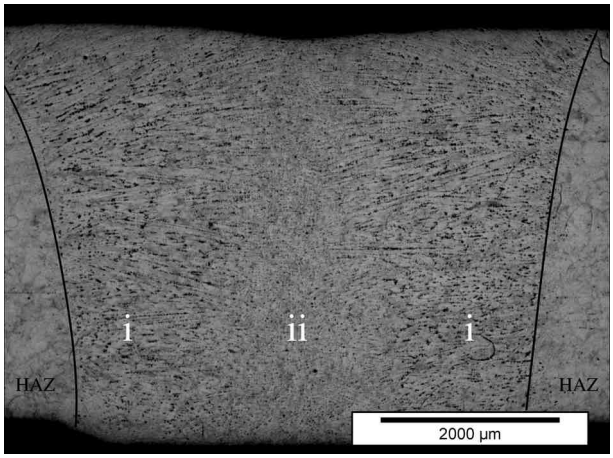

Figure 4.4: *Overview of a GTA welded High-Si steel weld showing (i) the presence of inclusions in the columnar grain boundaries and (ii) a random inclusion distribution in the equi-axed grain zone. The black lines indicate the fusion boundaries.*

Morphological analysis of the inclusions in the fusion zones of GTA welded TRIP steels using electron microscopy indicates that inclusions contain several substructural features. Figure 4.6 shows the secondary electron images of fusion zones delineating the inclusions with a spherical inner core, indicating the primary inclusion, surrounded by secondary inclusions. The inclusions in the laser welded TRIP steels show a similar inclusion morphology as seen in GTA welds. However, in resistance spot welded samples, the inclusions in the fusion zone do not show a complex structure and only a primary core is observed (figure 4.7).

It is known that the first reaction which influences the final weld microstructure is inclusion formation. The presence of high amounts of strong deoxidisers such as silicon and aluminium, as in the case of the TRIP steels under investigation, leads to the formation of oxide inclusions during welding [2, 3]. It is also known that the

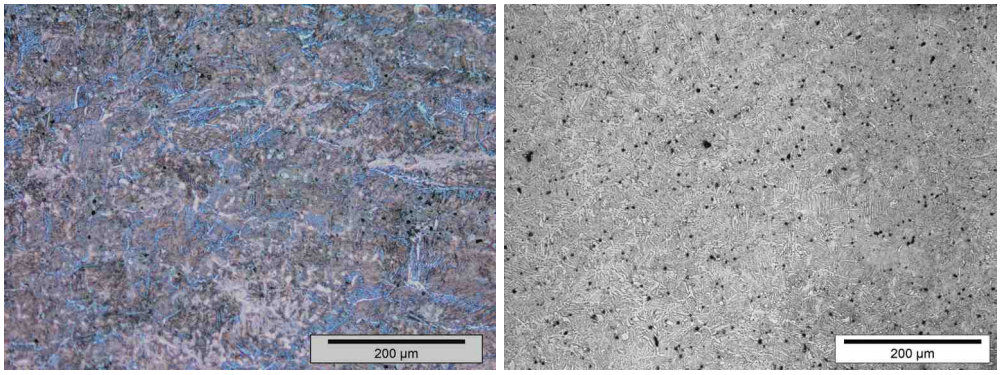

(a) *High-Si* **(b)** *High-Al*

Figure 4.5: *Inclusions in the centre of the fusion zone of GTA welded TRIP steels, showing a random distribution. The inclusion size of High-Si steel welds (a) show comparitively smaller in size than in High-Al steel welds (b).*

reaction between the dissolved alloying elements in the weld pool with the available oxygen, nitrogen and carbon forms non-metallic inclusions. In TRIP steels, strong oxidizing elements such as Al and Si are added to suppress the formation of cementite and thereby to stabilise the austenite by enriching it with carbon [4]. However, due to the strong affinity for oxygen, the added Al and Si readily form oxides during welding, leaving the weld pool depleted of these elements. This can be seen from figure 4.8, where the energy dispersive elemental analysis of the inclusions present in the fusion zone of the GTA welded High-Si steel show a higher silicon concentration at the centre core as well at the sides of the inclusion. Although, the bulk manganese content is higher than that of silicon, the amount of manganese found in the inclusion is less than that of silicon. A similar behaviour in elemental distribution was found in High-Al steel GTA weld inclusions, where the cores were found to be richer in aluminium with epitaxial enrichment of silicon and manganese (figure 4.9).

During welding, aluminium present in the liquid weld pool combines with available atmospheric oxygen and forms oxides, due to its higher affinity for oxygen compared to silicon. The formation of aluminium oxides leads to solute entrapment in the surroundings and to the subsequent formation of silicon oxides and epitaxially grown manganese sulfides when the liquid weld pool cools down below the solidification temperature. The Energy Dispersive X-ray Spectroscopic (EDS) analysis of inclusions in the High-Al steel fusion zone (figure 4.9) confirms this mechanism, where the aluminium content is found to be higher at the centre core of the inclusion. In the case of High-Si steel which contains only silicon as a strong deoxidizing element, the oxides of the silicon generally form at a lower temperature than those of aluminum, and the average size of the inclusions in the High-Si steel welds is therefore smaller. This can also be confirmed from the inclusion stability diagrams for the steels under

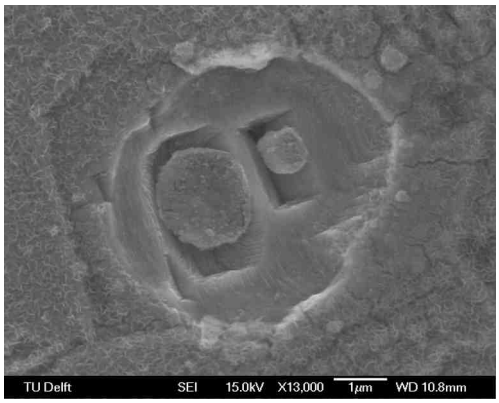

(a) *High-Si*

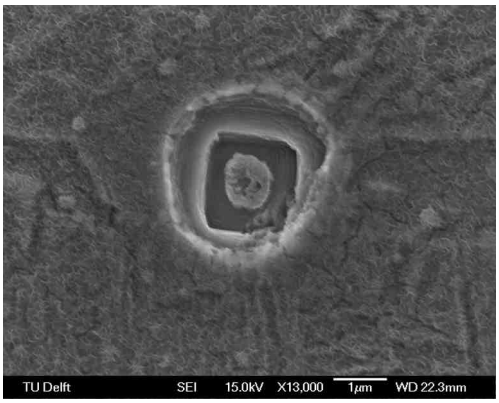

(b) *High-Si*

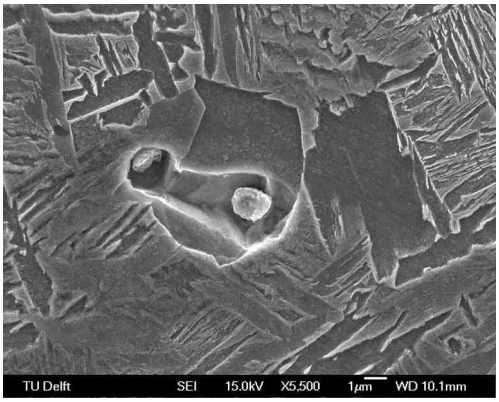

(c) *High-Al*

Figure 4.6: *Secondary electron images indicateing the presence of complex sub-structures with a primary inner core and surrounding secondary surfaces in inclusions of GTA welded TRIP steels.*

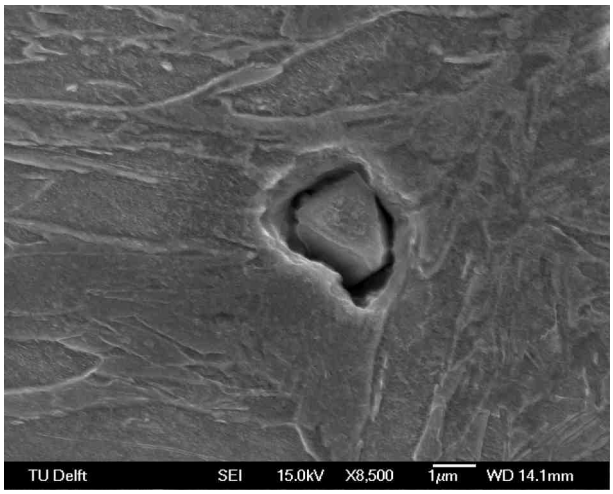

Figure 4.7: *An inclusion in the fusion zone of resistance spot welded High-Al TRIP steel showing only the primary core.*

investigation (figure 4.10), where equilibrium inclusion contents are given with respect to temperature for both steels with two different oxygen contents. Figure 4.10b indicates that for a High-Al steel liquid weld pool with an oxygen content of 0.002 wt. %, the nucleation temperature of Al_2O_3 is found to be 2008 ^oC whereas in High-Si steel, SiO_2 is found to nucleate at 1596 ^oC (figure 4.10a). If the oxygen content of the liquid weld pool increases from 0.002 to 0.004 wt. %, the nucleation temperature of oxides increases by about 75 ^oC in both steels. In all cases, MnS appears to form at about 1425 ^oC (below the solidification start temperature, 1536 ^oC) and the oxygen content in steel is not found to affect the formation of MnS.

By contrast to GTA and laser welding, the inclusions in the fusion zones of RS welded TRIP steels are mainly comprised of primary silicon or aluminium rich core (figure 4.11. During RS welding where the total welding process was completed in less than half a second (a total time of 420 ms including 20 ms cooling time), the epitaxial enrichment of substitutional manganese on the already formed oxides of aluminium or silicon was retarded due to sluggish diffusion, resulting primarily in aluminium or silicon oxide inclusions in the fusion zones.

The observation of inclusions in the fusion zones of low alloyed steel welds is not new; in fact, extensive research had been performed in the past to study the formation mechanism of inclusions, their effects on subsequent phase transformations and final mechanical properties of the welds [2, 3, 5–7]. In TRIP steels, which exhibit superior mechanical properties compared with many other low alloyed automotive grade steels, the presence of inclusions is detrimental to the mechanical properties of the weld. The non-metallic inclusions formed in the weldpool are also known to favour the formation of intragranular acicular ferrite by acting as potential nucleation

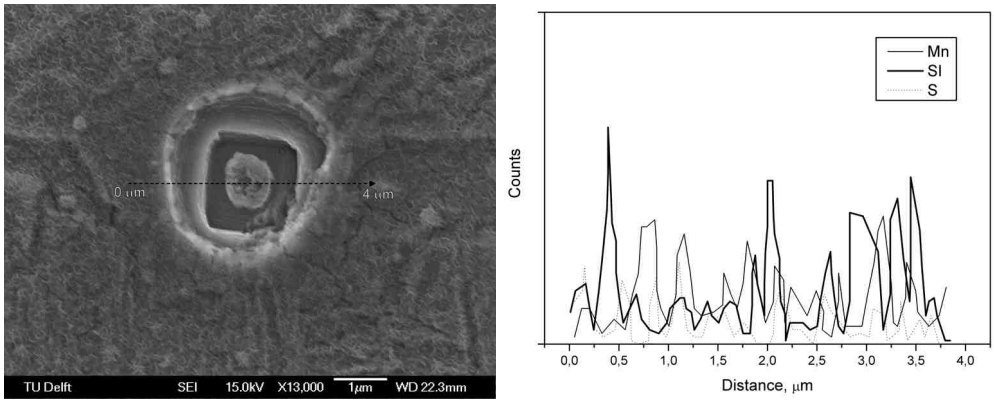

(a) **(b)**

Figure 4.8: *An inclusion in a GTA welded High-Si steel fusion zone showing a silicon rich primary inner core and epitaxial enrichment of manganese and sulphur, forming the secondary inclusion surfaces.*

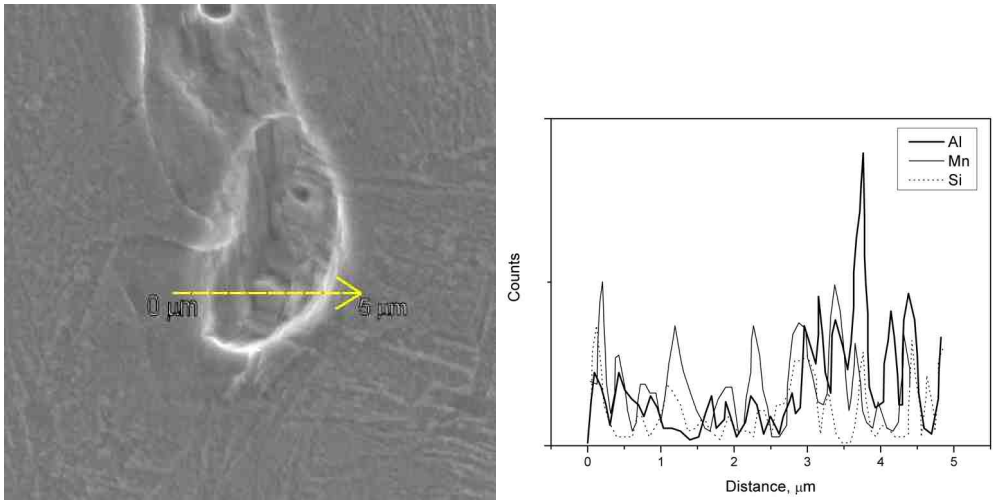

(a) **(b)**

Figure 4.9: *EDS measurement showing an aluminium rich primary inner core in an inclusion in the fusion zone of GTA welded High-Al steel. Epitaxial enrichment of silicon and manganese can also be seen on the aluminium rich core. (Note: The inclusion is not parallel to the plane of observation).*

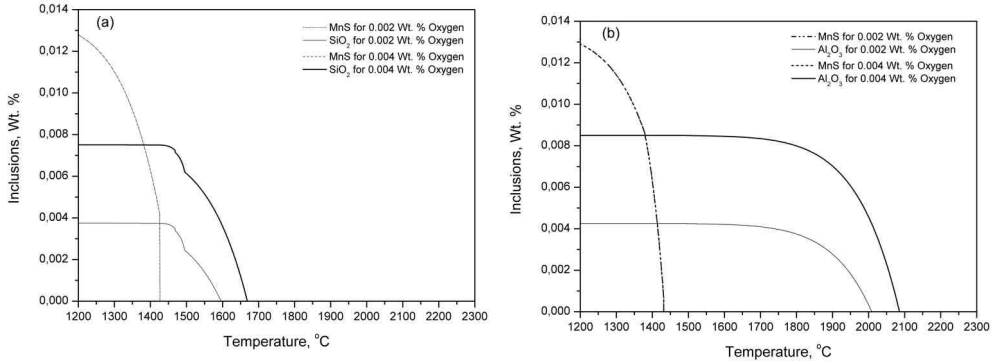

(a) *High-Si* **(b)** *High-Al*

Figure 4.10: *Calculated inclusion stability diagrams for TRIP steels showing the equilibrium inclusion percentage with respect to temperature for two different oxygen contents. It can also be seen that the oxygen content does not influence the MnS formation.*

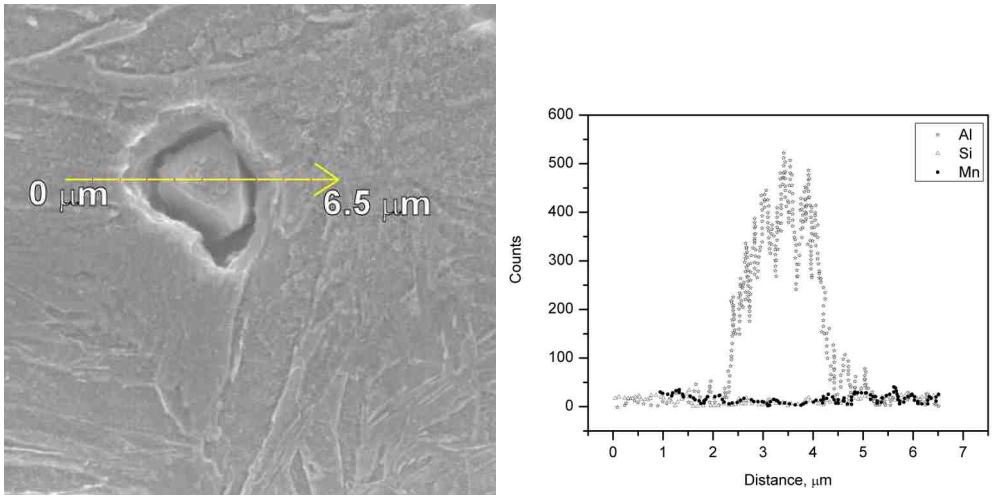

(a) **(b)**

Figure 4.11: *An inclusion in the fusion zone of an RS welded High-Al TRIP steel showing mainly a primary aluminium oxide inclusion and no epitaxial enrichment of manganese.*

sites. Increased volume fraction of acicular ferrite leads to an optimum combination of strength and toughness. The formation of acicular ferrite is also strongly influence by the thermal cycle of the welding process, inclusion size distribution, number density, volume fraction and composition of the inclusions [3, 8]. Microstructural analysis indicates that acicular ferrite is found only in GTA welded TRIP steel samples. In the case of LB and RS welded samples, the fusion zones contain a martensitic structure (figures 4.3 and 4.5). However, the inclusion volume fraction in the fusion zones was estimated to be 2.5 to 3 % (see chapter 5 for the quantification method used) and was similar for of all three welded samples. Thus, fusion zones with non-metallic inclusions in a martensitic matrix may lead to inferior strength - ductility combinations in LB and RS welded TRIP steel samples.

The size (> 2 μm) and volume fraction (2.5 to 3 %) of inclusions present in the fusion zones of welded TRIP steels is higher than reported inclusion contents in the automotive grade DP600 steel [9]. To confirm this finding, a dual phase steel plate (DP600, with a composition of C 0.09, Mn 1.7, Si 0.29 and Cr 0.55 wt.%) was welded in a bead-on-plate geometry using the welding procedure given in table 4.1. A microstructural analysis of the fusion zones was carried out to study and compare the inclusion formation in this steel with TRIP steel welds. Optical microscopy analysis did not reveal any coarse or large amounts of inclusions in the fusion zone of the GTA welded DP600 weld (figure 4.12). The volume fraction of inclusions found in DP steels was also lower (<0.2 %) than inclusions in TRIP steel welds. The DP600 steel studied here does not contain a large amount of oxide forming elements such as silicon or aluminium. The presence of strong oxidising elements such as silicon and aluminium in the steel plays a major role in the formation of coarse and large amount of inclusions in the fusion zones. Although, the presence of silicon and aluminium is necessary to generate a retained austenite containing TRIP steel microstructure, due to their strong affinity to oxygen, they will however lead to the formation of oxide containing inclusions in the weld pool.

There are four possibilities for the formation of oxide inclusions in the fusion zone of welded steels during welding [10].

1. Oxide inclusion arising from oxidation at the weld pool surface when there is oxygen in the shielding gas or when oxygen is available in the welding atmosphere.

2. Oxide inclusions arising from the oxidised plate surface prior to welding. The oxide scales present at the plate surface will tend to float, transported with the motion of the weld pool and be retained during subsequent solidification.

3. Inclusions forming from the de-oxidiser in the filler metal while welding is carried out using filler metal additions and

4. The interaction of oxygen dissolved in the parent material combines with alloying elements to form oxide inclusions.

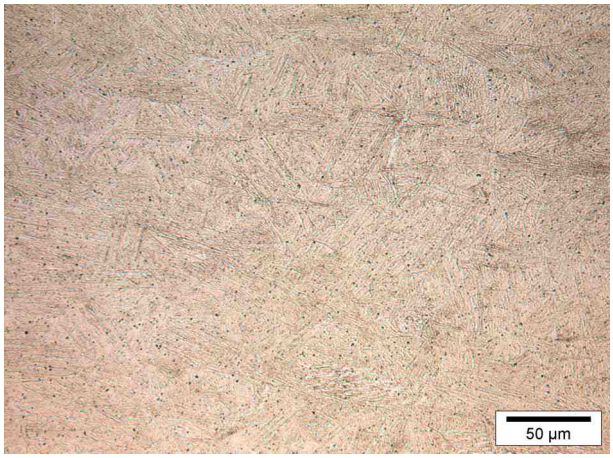

Figure 4.12: *The fusion zone of a GTA welded DP600 steel does not show the presence of coarse or large amounts of inclusions, unlike the GTA welded TRIP steels. In contrast, only a few small (<1µm) inclusions were observed (little black dots in the microstructure).*

In this work and also during commercial welding of automotive grade steels, welding of TRIP steels is generally carried out without the addition of filler metals which eliminates the third possibility for the formation of non-metallic inclusions. The presence of oxide scales on the base metal plate surface may play a role in the formation of oxide inclusions in the solidified fusion zone microstructures. In order to study the role of oxide scales on the base metal plate surface, RS welding was carried out using the procedure given in section 4.2 on the heat treated High-Al TRIP steel base metal plates with and without the surface oxide scales. The oxide scales on the surface of the plate were removed using an acid pickling bath and subsequent ultrasonic vibration bath cleaning in acetone. After welding, both with and without oxide, the microstructural analysis indicated similar sizes, shapes and distributions of oxide inclusions in the fusion zones (figure 4.13). This result shows that in TRIP steels, the presence of surface oxides does not play a major role in the formation of non-metallic inclusions in the fusion zones of welded TRIP steels. Moreover, the elemental analysis of inclusions showed that the primary core is comprised mainly of oxides of aluminium and silicon and there is no evidence of the presence of iron based oxides which would have been present if surface oxide scales promoted inclusion formation. This result leads to the conclusion that the interaction of silicon and aluminium with available oxygen during welding forms oxide inclusions in the weld pool of the TRIP steels. After welding, the total oxygen content of the fusion zones of welded steels also increased to 0.007 from 0.002 wt. %, which is present in the base metal, confirming oxygen pick-up during welding. In GTA and LB welding, commercial purity shielding gas was used which generally contain residual oxygen, and in RS welding, the entrapped air between the

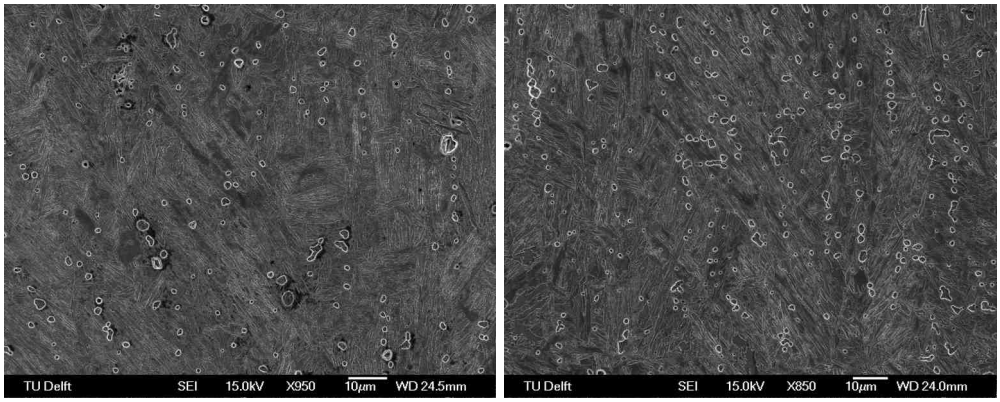

(a) *without surface oxide cleaning* **(b)** *with cleaning and no surface oxides*

Figure 4.13: *Resistance spot welding of High - Al TRIP steel plates with and without surface oxides showing similar inclusions in the fusion zones (a) - without surface oxide cleaning and (b) with cleaning and no surface oxides.*

overlapped plates provides the necessary oxygen for the formation of oxide inclusions. Figure 4.14 shows the effect of entrapped air on the variation of inclusion distribution density on a RS welded High-Al TRIP steel plate. It can be seen from this figure that the density of inclusions is higher close to the prior weld plate interface due to the entrapment of air during the overlapping of the plates and the interaction of oxygen with the aluminium in the weld pool, leading to the formation of non-metallic oxide inclusions in the final solidified fusion zone microstructure.

4.4.2 Partitioning behaviour of Aluminium and Silicon

The microstructural analysis of the welded TRIP steels indicates that the fusion boundaries of High-Al steel welds contain a zone of polygonal ferrite grains. This ferrite formation was not observed in the High-Si steel welds. The thickness of ferrite zone was different in each welding condition, varying from about 200 μm in GTA welded to 60 μm in LB welded and 20 μm in RS welded High-Al TRIP steel (figure 4.15).

The elemental analysis shows that the ferritic grains in the fusion boundaries of welded High-Al steel welds are richer in aluminium, indicating a partitioning of aluminium to the fusion boundaries from adjoining fusion and heat affected zones (figure 4.16). During solidification of the weld pool, the alloying elements present in the steel redistribute and partition to the solidified δ-ferrite based on their solubility. Figure 4.17 shows equilibrium concentrations of alloying elements and inclusion content of the liquid during solidification. Once the temperature reaches the solidification start temperature (1536 ^{o}C), due to the lower solubility of C, Mn, Si and S in the solidified

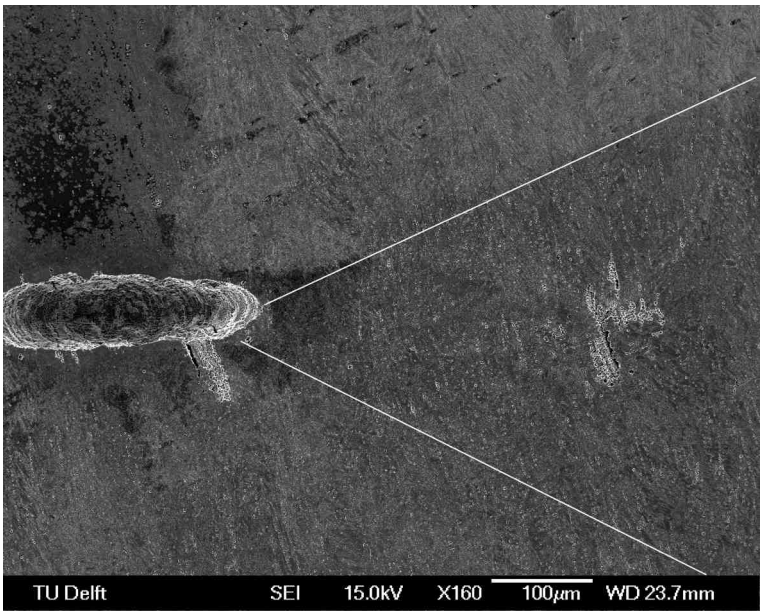

(a)

(b)

Figure 4.14: *Secondary electron image showing the inclusion density at the prior weld plate interface. The cavity indicates the plate interface at the overlap position and the white lines show the inclusion distribution (a) and (b) with higher magnification.*

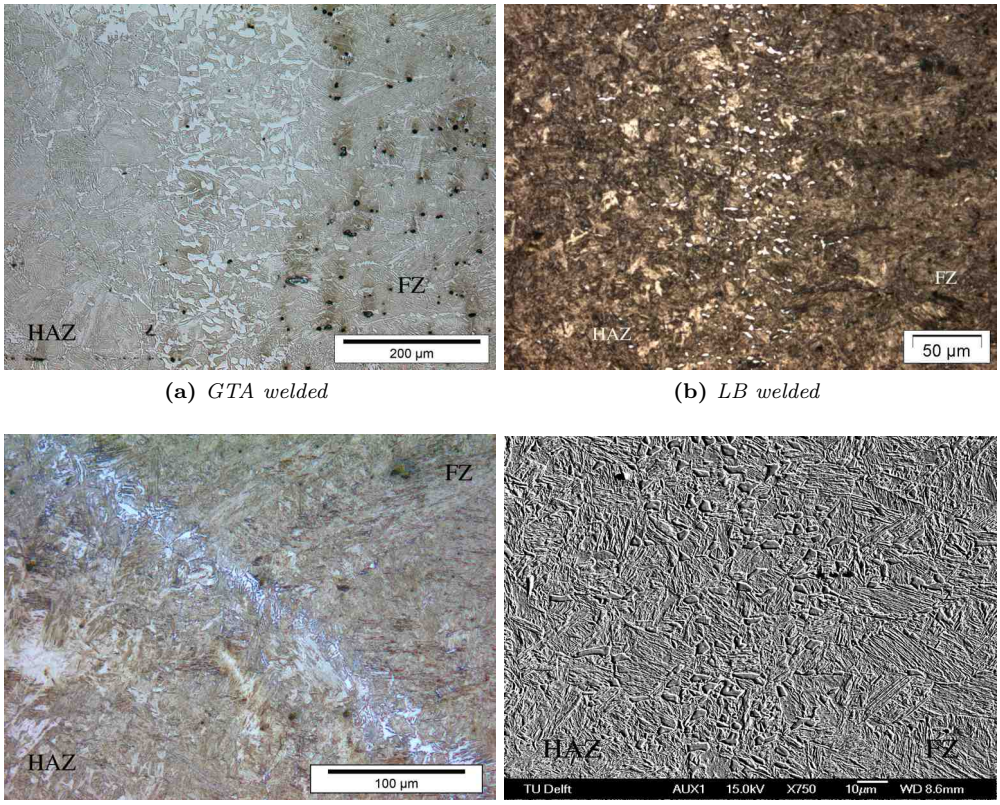

(a) *GTA welded* **(b)** *LB welded*

(c) *RS welded* **(d)** *LB welded*

Figure 4.15: *Fusion boundaries of welded High - Al TRIP steels showing the presence of polygonal ferritic grains for different welding processes (a,b and c). (d) back scattered electron image showing the compositional contrast of the fusion line ferritic zone.*

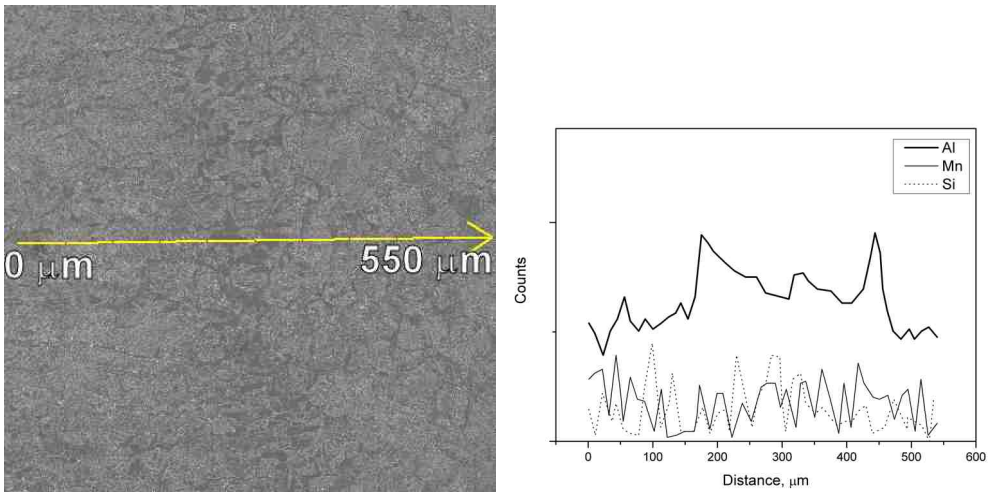

(a) *High - Al, GTA welded* **(b)** *Elemental distribution*

Figure 4.16: *The fusion boundary (a) showing increased aluminium content at the ferrite zone in a GTA welded High-Al steel and (b) the elemental distribution across this boundary.*

δ-ferrite, these elements tend to segregate to the liquid pool. However, due to higher solubility of aluminium in ferrite, aluminium partitions to the solidified δ-ferrite and enriches it. It can be seen from figure 4.17 that only the aluminium content in the liquid pool starts decreasing when solidification starts, while other alloying element contents increase due to their lower solubility in ferrite.

The aluminium based TRIP steels generally contain about 1 to 1.3 wt. % of aluminium. During welding and subsequent solidification of the molten weld pool, the equilibrium aluminium content in ferrite was calculated to rise as high as 1.35 wt. % at 1400 ^{o}C for the steel under consideration (figure 4.18a). According to the corresponding binary Fe-Al phase diagram (figure 4.18b), if the aluminium content exceeds 1.15 wt. %, the ferrite is stabilised. When the liquid weld pool starts to solidify to δ-ferrite at the fusion lines and at the columnar grain boundaries, the aluminium starts to partition to the newly solidified δ-ferrite from the liquid weld pool. Once the aluminum in the δ-ferrite reaches the critical stabilization limit, (1.15 wt. %), the δ-ferrite stabilizes at the fusion lines and at the grain boundaries and does not undergo any further transformation into inter-critical austenite and subsequent martensite. Thus soft ferritic zones are formed close to the fusion lines and columnar grain boundaries. The thickness of the ferrite zone in the fusion boundaries of GTA welded TRIP steel was found to be higher (about 200 μm) than LB welded steel (60 μm). In the case of GTA welding, the width of the weld pool was larger due to which more aluminium can diffuse to the solidified δ-ferrite. In addition, a larger area in the HAZ adjacent to the fusion boundary in GTA welding reaches a temperature where

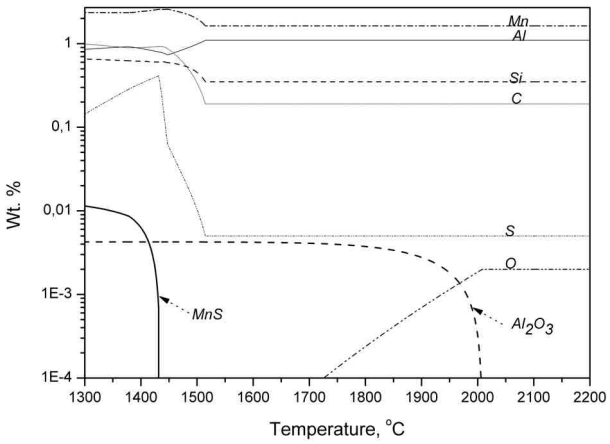

Figure 4.17: *Equilibrium element and inclusion content in liquid High-Al TRIP steel, indicating that once the solidification starts at 1536 °C, Al starts to partitioning from the weld pool to solidified δ-ferrite.*

δ-ferrite is stable; this, combined with a slower cooling rate (40 °C s^{-1}) for the GTA welding process, results in a wider ferrite zone. Conversely, RS welded TRIP steels show that only very small areas in the fusion boundaries contain δ-ferrite grains due to faster welding and thus a limited time for aluminium to partitioning to the solidified δ-ferrite compared with the other two processes.

Although the solidification of the liquid pool cannot occur under equilibrium conditions due to the rapid heating and cooling rates encountered during welding, without a thorough mixing or convection close to the solidification front, the solute elements partitioning into or out of the liquid pool can only be transported away from the solid-liquid interface by the diffusional process [11]. This results in a build-up of solute elements ahead of the growing crystals, with a corresponding rapid increase in alloying content of the solid that forms. It is also obvious that the thickness of this build-up area is strongly based on the thermal cycle of the solidification process. In addition, due to the higher solubility of aluminium in solidifying δ-ferrite, there is an increased possibility of aluminium build-up at the solidification front which in-turn results in the stabilisation of ferrite. This stabilisation of soft polygonal ferritic grains at the fusion boundaries leads to heterogeneity in the microstructure, which otherwise predominantly contains martensite in the adjoining fusion and coarse grained heat affect zones; this results in inferior mechanical properties of the weld. The hardness variation over the weld zone of GTA welded High-Al steel shows a large decrease in hardness at the fusion boundary (point-b in figure 4.19) due to the presence of soft ferrite grains. This result shows that the amount of aluminium added in the TRIP

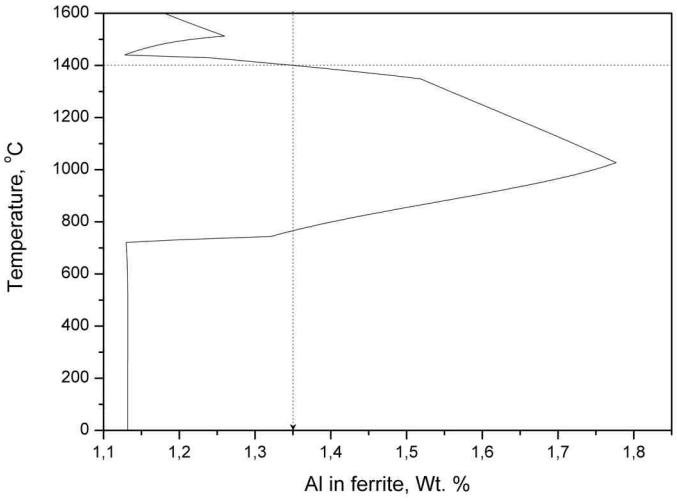

(a) *Equilibrium Al content in ferrite*

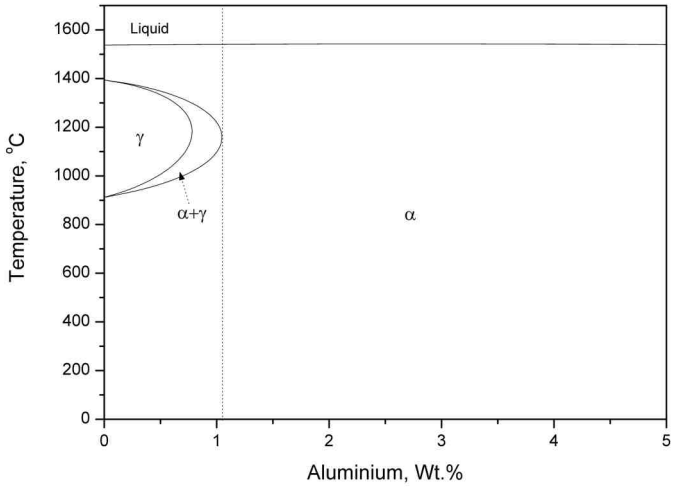

(b) *Fe-Al phase diagram*

Figure 4.18: *(a) - the aluminium content in ferrite in the steel can rise to 1.35 wt. % at 1400 °C (a), and once the aluminium content exceeds 1.15 wt. % ferrite is stabilised (b).*

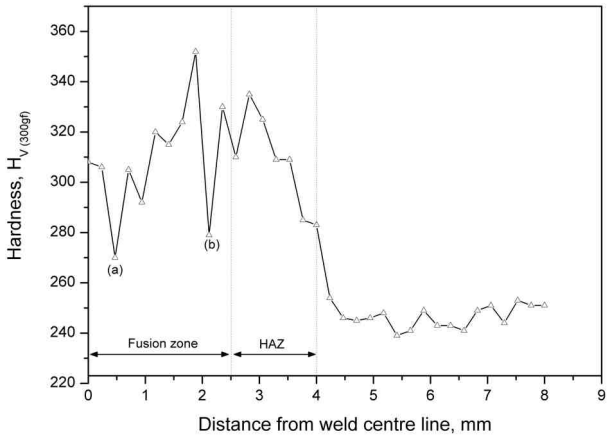

Figure 4.19: *The hardness variation over the weld zone of GTA welded High - Al steel showing a decrease in hardness near the fusion boundary (b). The hardness value at this point is close to the centre of the fusion zone where coarse-grained equi-axed grains show generally reduced hardness. The point (a) indicates a softer zone adjacent to an equi-axed grained weld centre line.*

steel should be carefully controlled to minimise the effect of aluminium partitioning on the fusion boundaries during the solidification under a given weld thermal cycle.

4.5 Conclusions

The microstructural analysis during welding of silicon and aluminium based Transformation Induced Plasticity (TRIP) steels shows the formation of complex inclusions in the fusion zones of High-Si and High-Al TRIP steels. Depending on the welding process these inclusions can contain several sub-structural features with different compositions. The formation of allotriomorphic ferrite is found at the fusion line and the grain boundaries of High-Al steel welds due to partitioning of aluminium to the solidified δ-ferrite, which leads to stabilisation of ferrite.

References

[1] N.J.den Uijl, 'Post weld heat treatments of advanced high strength steel for automotive joining', *Mathematical modelling of weld phenomena*, 8, 217–223, 2007.

[2] S.S.Babu and S.A.David, 'Inclusion formation and microstructure evolution in low alloy steel welds', *ISIJ international*, 42(12), 1344–1353, 2002.

[3] T.Koseki and G.Thewlis, 'Inclusion assisted microstructure control in cmn and low alloy steel welds', *MaterialsScienceandTechnology*, 21, 867–879, 2005.

[4] B.C.De Cooman, 'Structure-properties relationship in TRIP steels containing carbide-free bainite', *Current Opinion in Solid State and Material Science*, 8, 285–303, 2004.

[5] T.Hong, T.Debroy, S.S.Babu and A.David, S., 'Modeling of inclusion growth and dissolution in the weld pool', *Metallurgical and Materials Transactions B*, 31B, 161 – 169, 2000.

[6] H.Yin, 'Inclusion characterization and thermodynamics for high-al advanced high-strength steels', *Iron and Steel Technology*, 6, 64 – 73, 2006.

[7] M.A.Quintana, J.McLane, S.S.Babu and S.A.David, 'Inclusion formation in selft-shielded flux cored arc weld', *Welding Research Supplement*, 4, 98s – 105s, 2001.

[8] S.S.Babu, S.A.David, J.M.Vitek, K.Mundra and T.DebRoy, 'Development of macro- and microstructure of carbon-manganese low alloy steel welds:inclusion formation', *Material Science and Technology*, 11(2), 186–199, 1995.

[9] C.Ma, D.L.Chen, S.D.Bhole, G.Boudreau, A.Lee and E.Biro, 'Microstructure and fracture characteristics of spot-welded DP600 steels', *Material Science and Engineering A*, 485, 334 – 346, 2008.

[10] G.Thewlis and D.R.Milner, 'Inclusion formation in arc welding', *Welding research supplement*, 281s–288s, 1977.

[11] K.Easterling, Introduction to the physical metallurgy of welding, Butterworths and co. ltd, 1983.

Chapter 5

Quantitative phase analysis in welded TRIP steels[2]

The addition of alloying elements ensures the presence of required microstructural constituents; a mixture of ferrite, carbide free bainite and retained austenite in a TRIP steel microstructure after the heat treatment. The required combination of strength, ductility and crash worthiness is achieved by deformation induced transformation of retained austenite to martensite. These properties strongly depend on the volume fraction, size, shape and distribution of retained austenite grains in the microstructure. A weld thermal cycle destroys microstructure containing the retained austenite. This leads to strong heterogeneity between weld and base metal, which may in turn result in inferior mechanical properties of the welded TRIP steel. Therefore, it is important to quantify the microstructural constituents, with an emphasis on retained austenite across the weld region. The effect of a GTA weld thermal cycle on the retained austenite volume fraction in the heat affected and fusion zone with various initial base metal microstructural conditions are presented in this chapter. The thermal stability of retained austenite in the base metal and fusion zone is analysed in a study of decomposition kinetics of austenite during welding. A quantitative analysis of retained austenite across the weld zone of the GTA weld was carried out using magnetic saturation methods and synchrotron X-ray diffraction and, the results are presented and analysed in this chapter.

[2] "Quantitative analysis of microstructural constituents in welded Transformation Induced Plasticity Steels", M.Amirthalingam, M.J.M.Hermans L.Zhao and I.M.Richardson, Met. Mat. Transactions A, 41A, 2010, 431-439.

5.1 Magnetic saturation measurements

5.1.1 Introduction

The alloy composition and the heat treatment parameters used to generate a TRIP steel microstructure determine the fraction, size and distribution of retained austenite. For a given steel composition, by varying the heat treatment parameters, it is possible to generate microstructures with different amounts of retained austenite as, described in chapter 3. In order to understand the effect of the starting base metal microstructure on the variation of retained austenite in welded samples, the High-Al TRIP steel base metals, which were generated using the heat treatment procedures in section 3.3.1, were welded using the GTA welding parameters given in table 4.1. Quantitative microstructural analysis was carried out on the welded TRIP steels using a magnetic saturation method to study the variation of retained austenite across the heat affected and fusion zone. The amount of non-metallic inclusions present in the fusion zone of GTA welded High - Al TRIP steel was also measured using this technique.

5.1.2 Effect of base metal conditions

The heat treated base metal High-Al steel plates, HT840/400, HT840/335, HT800/400 and HT800/335 (figure 3.3) were GTA welded using the procedure explained in section 4.2. The volume fractions of retained austenite in the welded TRIP steel plates were measured by a magnetic saturation technique using a vibrating sample magnetometer (section 3.3.4). Cylindrical samples of 1.25 mm diameter were cut by means of electro discharge machining from the welded plates at 5 different places in and around the weld zone for the magnetic saturation measurements. Figure 5.1 schematically shows the positions from which samples were taken. Three samples along the length of the weld were taken at different transverse locations to ensure repeatability, and measurements were averaged over the three samples to improve the statistical relevance. Note that the left and right sides of the weld centre line are treated separately for this purpose.

The magnetisation measurements were performed in a LakeShore 7307 Vibration Sample Magnetometer (VSM) and were carried out by applying magnetic fields starting from 2 Tesla to zero and then to -2 Tesla with a step size of 0.05 Tesla. Section 3.3.4 describes the measurement procedures used to determine the mass magnetisation of the samples for the applied magnetic flux density. The saturation magnetisation (M^s) of each sample from the welded plates was then calculated from these magnetisation curves by fitting equation 3.2. Quantitative measurement of austenite contents in the heat affected zones (the samples 5 mm and 2.7 mm from the weld centre line (WCL)) were carried out using equation 3.3. However, the samples from the fusion zones also contain paramagnetic non-metallic inclusions and measurements of retained austenite contents in the fusion zones were corrected for the amount of non-metallic inclusions. The magnetisation behaviour of samples from the heat affected and fusion

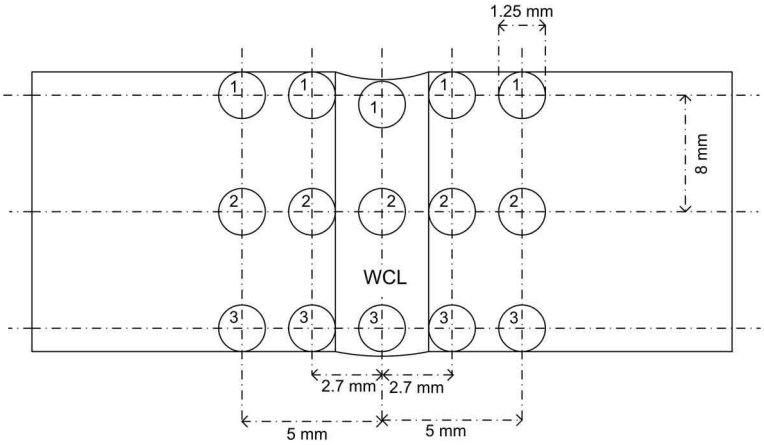

Figure 5.1: *Schematic representation of various places from which samples were cut from the welded plate. Here, WCL is the weld centre line. Samples representing the heat affected zone were taken at 2.7 and 5 mm from the weld centre line. (Note: Measurements from samples 1 to 3 at each transverse location were averaged.)*

zones showed differences in the saturation magnetisation, which indicated variations in the amount of paramagnetic phases, in this case austenite and non-metallic inclusions. This is reflected in figure 5.2 where the magnetisation behaviour of the samples taken from the heat affected (5 mm from WCL) and fusion zones of welded plates is shown.

In order to calculate the non-metallic inclusion contents, the saturation magnetisation of fusion zone samples without austenite ($M^s(i)$) was measured after transforming the austenite present in the sample to ferromagnetic ferrite and cementite by tempering while continuously heating to 600 ^{o}C. The non-metallic inclusions present in the fusion zone is stable during this tempering process [1]. The mass fraction of inclusions (f_i) was calculated by comparing the saturation magnetisation of a fusion zone sample without austenite ($M^s(i)$) to the base metal sample without austenite ($M^s(f)$) using the relationship similar to equation 3.3,

$$f_\gamma = 1 - \beta \left(\frac{M^s(i)}{M^s(f)} \right) \tag{5.1}$$

The average saturation magnetisation of the fusion zone samples without austenite but with inclusions ($M^s(i)$) was found to be 210.90 A m^2 kg^{-1} as compared to 216.47 A m^2 kg^{-1} for the base metal sample without austenite or inclusions. Thus, the average inclusion content in the fusion zones of welded TRIP steels was 2.6 $\pm$0.2 % (see section 3.3.4).

The variation in the austenite contents in the welded High-Al TRIP steel plates are shown in figure 5.3, after correcting for the non-metallic inclusion content in the

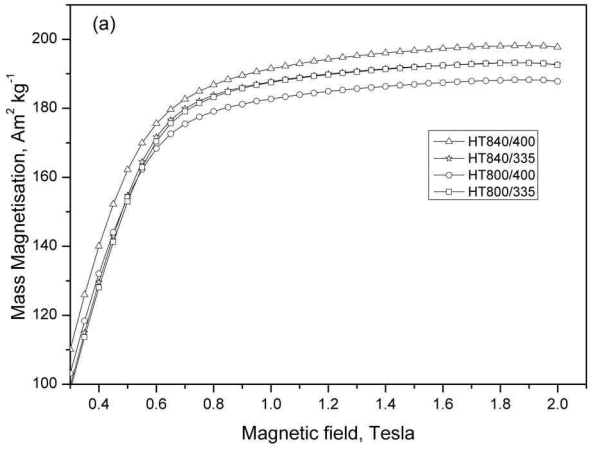

(a) *in HAZ, 5 mm from WCL*

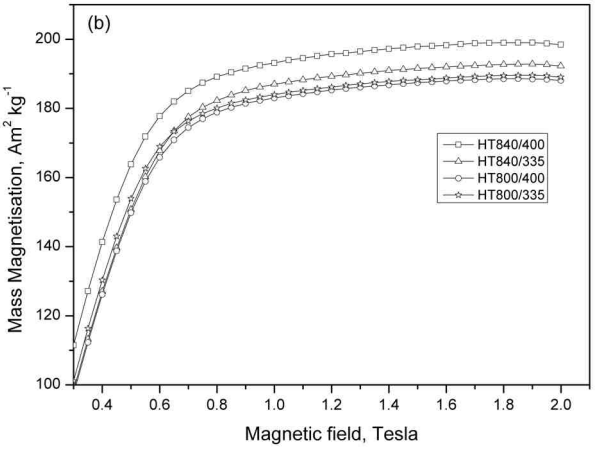

(b) *fusion zone*

Figure 5.2: *Magnetisation behaviour of samples from (a) heat affected and (b) fusion zones of High-Al TRIP steel welds.*

fusion zones. It should be noted that the magnetic measurements were carried out on 1.25 mm diameter samples and thus represent averages over the volume of the sample. In figure 5.3, the average austenite contents of the samples are plotted against the distance of the centre of the samples from the weld centre line. It is interesting to note that about 4.1 to 12.7 % of austenite is found in the heat affected zones and 5.7 to 9.6 % in the fusion zones despite the fact that both the fusion and heat affected zones undergo a weld thermal cycle with heating and cooling rates varying from 550 to 200 ^{o}C s^{-1}.

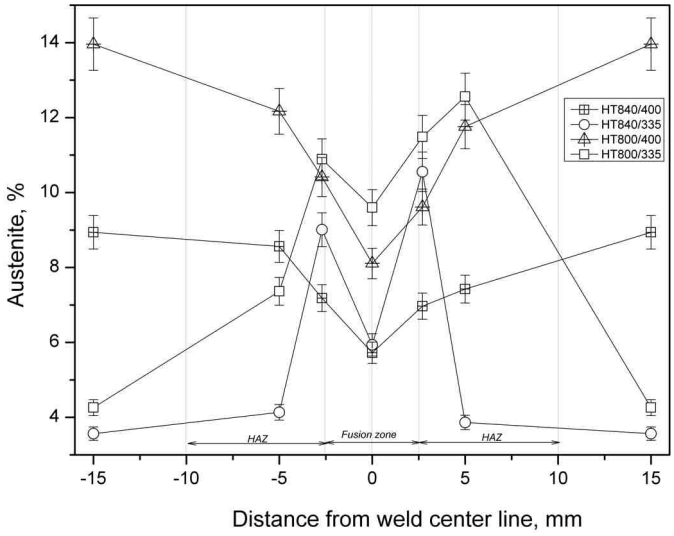

Figure 5.3: *Austenite variation across the width of welded High - Al TRIP steel plates (with ±0.2 % accuracy).*

Magnetic saturation measurements show that significant amounts of austenite have been retained in the heat affected and fusion zones of High -Al TRIP steel welds. The austenite contents in the centre of the fusion zones were found to vary from 5.7 to 9.6 %. This indicates that despite the use of the same welding parameters, the degree of partitioning of alloying elements during solidification can vary. Local variations in compositions due to the formation of non-metallic inclusions can also affect the stabilisation of austenite (section 4.4.1), which finally leads to variation in the austenite content in the fusion zone.

In the case of base metal conditions HT840/400 and HT800/400, where the starting austenite contents were higher (8.9 and 14.0 % respectively), the heat affected zones were found to contain less austenite than the base metals. Conversely, after starting from a microstructure containing less austenite, as in the conditions

HT840/335 and HT800/335 (3.6 and 4.3 %), the austenite contents increased in the heat affected zones during welding. In the weld microstructures, the coarse and fine grained heat affected zones were found at 2.6 to 4.5 mm from the weld centre lines respectively. A major portion of these zones, subjected to temperatures ranging from 980 ^{o}C to 650 ^{o}C, with heating rates close to 500 ^{o}C s^{-1}, does not attain the equilibrium austenite fraction corresponding to their respective peak temperatures. In the case of base metal conditions HT840/400 and HT800/400, the austenite grain sizes were found to be larger compared with the base metal conditions HT840/335 and HT800/335 (see section 3.3.6). The higher isothermal holding temperature (400 ^{o}C) also resulted in lesser enrichment in carbon, as a result, the chemical stability and the stability due to the increased size of austenite in condition HT840/400 and HT800/400 is lowered and austenite in these samples decomposes more easily during weld heating cycles compared with the austenite formed in HT840/335 and HT800/335 [2]. Hence, it appears that during welding, less stable austenite in the base metals decomposes, more stable austenite grains grow with the expense of co-existing phases and new austenite grains nucleate after the A_{c_1} temperature is passed. These grains are retained at room temperature upon cooling after sufficient enrichment of carbon.

5.1.3 Thermal stability of retained austenite

During welding, in the region directly alongside the fusion lines (in the present case, about 2.5 mm from the weld centre line), the peak temperature could reach above (A_{c3}) and depending on the location, steel becomes fully austenitic. The peak temperature reached during welding decreases with the distance from the weld centre line. In the regions where the peak temperature during welding remains lower than the austenite nucleation temperature during heating (A_{c_1}), no austenite is formed, instead the originally retained austenite in the base metal may decompose. Therefore to study the effect of such thermal cycles on the stability of retained austenite, a heat treated base metal (condition HT840/400) sample was heated to 600 ^{o}C and cooled to room temperature at a rate of 0.03 ^{o}C s^{-1}. The saturation magnetisation during heating ($M_{1H}(T)$) was measured as a function of temperature (T) by applying a constant field of 1 Tesla. During this treatment, it can be expected that the retained austenite present in the samples decomposes into ferrite and cementite. After cooling, this sample was again heated to 600 ^{o}C at the same heating rate (0.03 ^{o}C s^{-1}) and the saturation magnetisation without austenite ($M_{2H}(T)$) was measured as a function of temperature. The difference between $M_{1H}(T)$ and $M_{2H}(T)$ yielded the decomposition behaviour of austenite during heating (figure 5.4). The temperature dependent saturation magnetisation of the samples with and without austenite were fitted within the temperature region of 20 to 290 ^{o}C with the well-known thermo-magnetic equation [3–5];

$$M(T) = M_o \left[1 - k(T + 273)^{\frac{3}{2}}\right] \tag{5.2}$$

where k is a constant which after fitting was found to be 1.1x10^{-5} K$^{-3/2}$ for $M_{1H}(T)$ and 1.5x10^{-5} K$^{-3/2}$, for $M_{2H}(T)$. M_o is the saturation magnetisation at -273 ^{o}C,

measured by extrapolating the thermo-magnetic curves after fitting and was found to be 165.8 A m^2 kg^{-1} for the base metal sample with austenite (before first heating) and 192.1 A m^2 kg^{-1} for the base metal sample without austenite (after first heating).

Figure 5.4a shows the variation of saturation magnetisation ($M_{1H}(T)$) and ($M_{2H}(T)$) of the base metal sample (condition HT840/400) as a function of the temperature during heating. $M_{1H}(T)$ initially starts reducing with increasing temperature due to the increase in spin-wave fluctuations. Once the temperature reaches 295 ^{o}C, $M_{1H}(T)$ gradually starts increasing due to the formation of ferrite and ferromagnetic hexagonal ϵ-carbide ($Fe_{2.4}C$) from the paramagnetic austenite. Upon further heating, there is an obvious decrease in saturation magnetisation in the temperature range from 390 ^{o}C to 400 ^{o}C, which may be due to the formation of a paramagnetic transient phase. The saturation magnetisation increases again after this obvious decrease and further increase in the temperature results in the formation of stable cementite, which is paramagnetic above 210 ^{o}C, after which the saturation magnetisation decreases continuously until the final measurement temperature (600 ^{o}C). However, in the case of the second heating, the saturation magnetisation ($M_{2H}(T)$) decreases continuously with increasing temperature following equation 5.2, which indicates that there are no further transformations.

Thermo-magnetic measurements were also carried out on a sample from the fusion zone of a welded TRIP steel in order to compare the decomposition behaviour of austenite in the fusion zone to that of the base metal (figure 5.4b). After fitting temperature dependent saturation magnetisation of the fusion zone sample with equation 5.2, the constant k is found to be 1.2x10^{-5} $K^{-3/2}$ for both $M_{1H}(T)$ and $M_{2H}(T)$. The saturation magnetisation at -273 ^{o}C (M_o) was measured to be 187.5 A m^2 kg^{-1} for the fusion zone sample with austenite (before the first heating) and 209.8 A m^2 kg^{-1} for the fusion zone sample without austenite (after the first heating). Table 5.1 summarises the thermo-magnetic parameters determined for the base metal and fusion zone samples. The calculated saturation magnetisations at -273 ^{o}C (M_o) were found be to higher than those for the base metal samples, whilst the magnetisation behaviour of the fusion zone sample appears to be similar to that of the base metal sample. However, the gradual increase in the magnetisation, which indicates the formation of ferrite and ϵ-carbide ($Fe_{2.4}C$) is found at 240 ^{o}C, which is lower than for the base metal (290 ^{o}C). Moreover, the sudden decrease in the magnetisation, which was found in the base metal sample, appears to occur over a slightly wider range of temperatures (370 ^{o}C to 410 ^{o}C) and the decrease in saturation magnetisation occurs to a lesser degree in this temperature range.

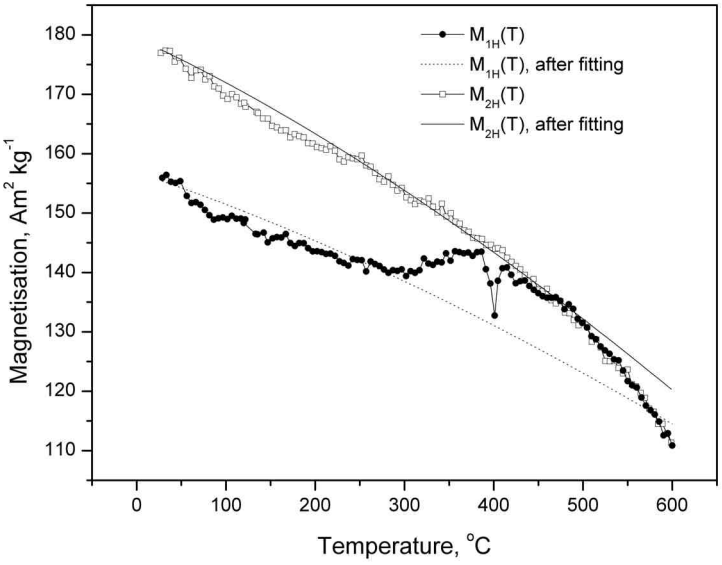

(a) *base metal sample*

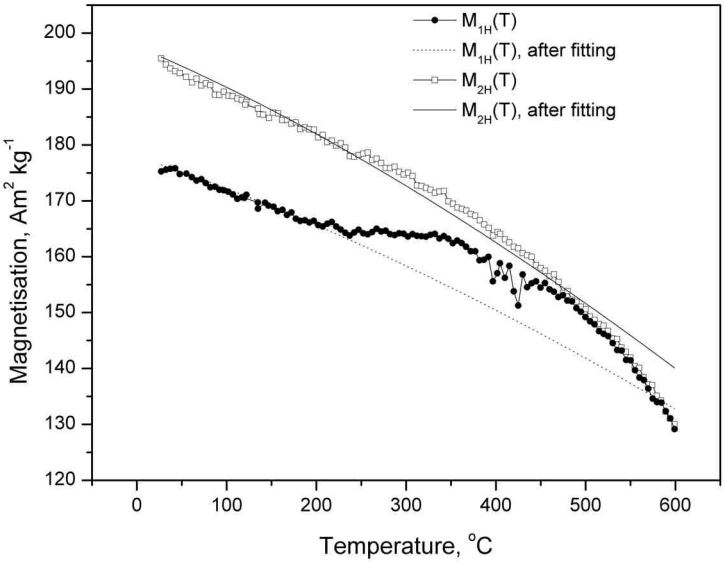

(b) *fusion zone sample*

Figure 5.4: *Saturation magnetisation as a function of temperature of the (a) base metal sample (b) fusion zone sample ($M_{1H}(T)$- saturation magnetisation of sample with austenite, $M_{2H}(T)$ - saturation magnetisation of sample without austenite). These lines are fitted with equation 5.2*

.

Table 5.1: *The measured thermo-magnetic parameters for High-Al steel base metal and GTA welded fusion zone samples.*

Base metal			
First heating, 1H(T)		Second heating, 2H(T)	
k, $K^{-3/2}$	M_o, A m^2 kg^{-1}	k, $K^{-3/2}$	M_o, A m^2 kg^{-1}
$1.1x10^{-5}$	165.8	$1.5x10^{-5}$	192.1
Fusion zone			
First heating, 1H(T)		Second heating, 2H(T)	
k, $K^{-3/2}$	M_o, A m^2 kg^{-1}	k, $K^{-3/2}$	M_o, A m^2 kg^{-1}
$1.2x10^{-5}$	187.5	$1.2x10^{-5}$	209.8

The thermo-magnetic measurements indicate that the austenite in the base metal started decomposing to ferromagnetic ϵ-carbides above 290 ^{o}C while heating at a rate of 0.03 ^{o}C s^{-1}. In the range of 390 to 400 ^{o}C, there is a sudden decrease in saturation magnetisation, which can possibly attributed to the formation of $\eta(\epsilon')$ transient carbides. It is reported that at 400 ^{o}C, orthorhombic $\eta(\epsilon')$ transient carbide (Fe_2C) forms upon ordering from ϵ-carbide by lowering the overall symmetry of the carbide phase on transiting from the hexagonal ϵ-carbide to orthorhombic cementite (Fe_3C). In most of the cases described in the literature, it is observed in high carbon steels [6–8], with the exception of the observations by Jha *et al.* [9], where the formation of $\eta(\epsilon')$ carbides was observed while tempering retained austenite at around 400 ^{o}C in low carbon steels . However, the magnetic properties of this $\eta(\epsilon')$ transient carbide are not reported anywhere, due to the low stability. It appears from the present observation that this transient $\eta(\epsilon')$ carbide is paramagnetic as observed in the temperature range (390 to 400 ^{o}C). Upon heating further, the saturation magnetisation increases again (400 to 415 ^{o}C), indicating that the paramagnetic transient carbides might transform back to ferro magnetic components. However, the transformation sequences of transient carbides cannot be verified from this study due to lack of proper magnetic properties data.

The thermo-magnetic measurements on the fusion zone sample showed that the decomposition of austenite to ferrite and ϵ-carbide ($Fe_{2.4}C$) started at 240 ^{o}C with a gradual increase in saturation magnetisation. This is a lower temperature than that of the base metal which showed an increase in magnetisation only above 290 ^{o}C. The difference may be attributed to the continuous cooling of the liquid weld metal to room temperature. Any austenite left in the fusion zone would be more enriched in carbon compared with the base metal sample, which was held at 400 ^{o}C for the isothermal bainitic holding. This results in an earlier precipitation of ϵ-carbide from the enriched austenite in the fusion zone sample compared to the base metal sample.

The increase in the saturation magnetisation in the fusion zone sample also occurs over a wider temperature range, from 240 to 460 ^{o}C, compared with the base metal samples. The base metal samples showed a narrow increased magnetisation zone from 290 to 440 ^{o}C, despite the fusion zone sample containing less austenite (5.7 %) compared with the base metal (8.9 %). This indicates that the decomposition kinetics of austenite in the fusion zone sample is slower due to its size and carbon enrichment. The appearance of several sudden decreases in the magnetisation indicates that the formation and decomposition of $\eta(\epsilon')$ transient carbides may occur in several stages due to the compositional heterogeneity of retained austenite in the fusion zone (section 4.4.2).

In summary, the magnetic saturation measurements showed that about 4.1 to 12.6 % austenite is found in the heat affected zones and 5.7 to 9.6 % is found in fusion zones after welding, depending on the thermal history of the samples. The mass fraction of austenite present in the heat-affected and fusion zones reduces after welding the base metals containing higher fractions of austenite. Conversely, after starting from microstructures containing less austenite, the austenite contents increased in the heat-affected and fusion zones after welding. This is due to the presence of coarse and less stable austenite grains in the base metals with higher austenite contents. Thermo-magnetic measurement showed that the retained austenite present in the microstructure decomposes during heating and the kinetics of retained austenite decomposition in the fusion zone is slower than in the base metal. This measurement also suggests the formation of a paramagnetic orthorhombic $\eta(\epsilon')$ transient carbide (Fe_2C) during the decomposition of austenite.

5.2 Quantitative analysis using synchrotron X-ray diffraction

Quantitative analysis of retained austenite in the heat affected zones (HAZ) and fusion zones (FZ) of the welded TRIP steel with various starting microstructural conditions using a magnetic saturation method revealed that a significant amount of austenite was retained after welding. However, due to a relatively large sample size in the magnetic measurements (1.53 mm^3), large thermal gradients are expected and therefore correlation of weld thermal cycles with the volume fraction and carbon concentration of austenite, retained in the welded samples, was found to be difficult. An experimental study was made to quantify retained austenite in Gas Tungsten Arc (GTA) welded silicon and aluminium based TRIP steels using 2-D synchrotron X-ray diffraction analysis. The quantitative diffraction analysis was carried out transverse to the weld centre line. Variations in RA content were measured across the width of the welded plates. The effect of the weld thermal cycles on the partitioning of alloying elements such as carbon, silicon and aluminium was studied. Based on the results a possible mechanism for the stabilisation of RA in weld zones was deduced for both silicon and aluminium based TRIP steels. The effect of stabilisation of δ-ferrite in the fusion boundary (see section 4.4.2) and the resultant enrichment of carbon to the

HAZ are discussed and an analysis of the retained austenite contents in the welded TRIP steels is presented.

5.2.1 Experimental procedure

Quantitative analyses were carried out in GTA welded High - Si and High - Al TRIP steel plates (See table 3.1 for the composition). These plates were heat treated in HT800/400 condition shown in figure 3.3. Bead-on-plate welding was performed on these heat treated plates (dimensions 200 x 100 x 1.25 mm^3 High - Al plate and 200 x 100 x 3 mm^3 High - Si plate) using the welding parameters shown in table 4.1 and the procedures explained in section 4.2. After welding, three-dimensional images of the welded plates were generated using a Konica Minolta VI-910 3D laser scanner in order to estimate the plate deformations with a measurement accuracy of ± 0.1 mm. The results of the deformation measurements were then used to adjust the detector to sample distance during the diffraction measurements.

Synchrotron X-ray diffraction measurements were carried out on the welded plates at beamline ID11 of the European Synchrotron Radiation Facility (ESRF) Grenoble, France, using a three-dimensional X-ray diffraction microscope (3DXRD). A monochromatic X-ray beam with an energy of 71.64 keV (wavelength 0.1732 Å), a horizontal beam size of 0.24 mm and a vertical size of 0.2 mm was used to illuminate the steel plates. Plates were mounted on an xyz-table in longitudinal direction and measurements were carried out transverse to the weld centre line. By moving from the top edge of the plate through the weld zone in a straight line with a step size of 0.2 mm, measurements were carried out to 75 mm from the top edge of the plates. With an exposure time of 6 s, the 2D diffraction rings from austenite and ferrite were recorded in transmission geometry using a FreLon 2D area detector. In both welded plates, the weld centre line was situated at $\simeq$ 50 mm; The measurement thus followed a line from the base material, through the fusion zone and the heat affected zone either side of the fusion zone. Figure 5.5 shows the measurement arrangements used to analyse the welded plates at ID-11 of ESRF, where the weld in sample plates was kept parallel to y direction and the measurements were carried out in z direction.

In order to characterise the base metal, cylindrical samples with a diameter of 1 mm and a length of 3 mm were electro-discharge-machined (EDM) from the TRIP heat treated plates with the cylindrical axis oriented in the rolling direction of the plate. These samples were then mounted on an xyz-table and illuminated with a synchrotron X-ray beam of the same energy as used for the welded plates, but a different horizontal and vertical beam size (1.2 mm and 0.6 mm, respectively). During the illumination of the base metal samples, they were continuously rotated around the sample axis, between -90^o to +90^o. Measurements were integrated over successive angles of 10^o using an exposure time of 6 s in each step.

The 2D diffraction patterns obtained from the welded plates and base metal samples were then corrected for detector background and distortion statistics. The volume fraction of austenite was calculated from the integrated intensities of two austenite ($\gamma_{(200)}, \gamma_{(220)}$) and two ferrite ($\alpha_{(200)}, \alpha_{(210)}$) rings using the procedure given

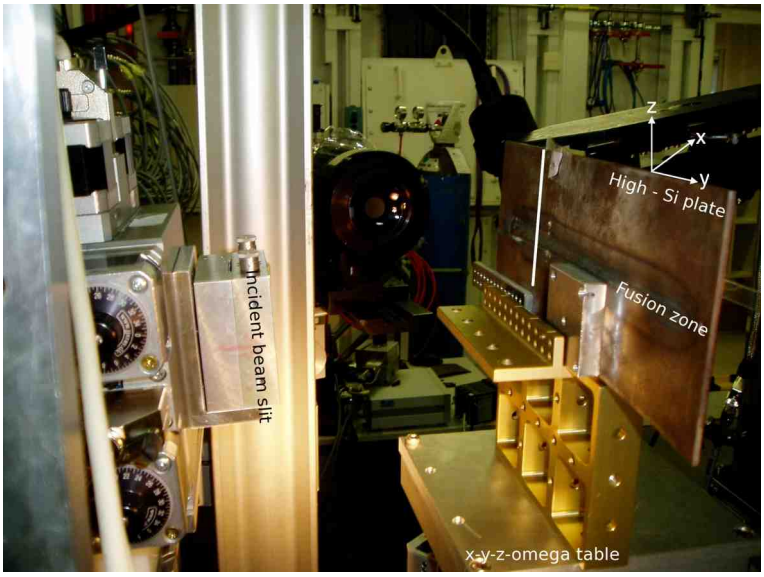

Figure 5.5: *Synchrotron X-ray diffraction set-up used for welded TRIP steel plates. The white line indicates the measurement line.*

in section 3.3.5 and [10]. The lattice parameters of the base metal austenite and ferrite were estimated from the experimental mean scattering angle (2θ). Section 3.3.5 describes the measurement procedures used to quantify retained austenite volume fraction and lattice parameters.

5.2.2 Influence of weld thermal cycle on plate distortion

The thermal cycles of the welding process used here (table 4.1) generate thermal stresses which in combination with phase transformation stresses result in out-of-plane deformation of the plates after welding (figures 5.6 and 5.7). Despite the thickness difference (1.25 mm High-Al and 3 mm High - Si plate), the weld thermal cycle caused a similar degree of out-of-plane deformation along the transverse direction, with a maximum of 1.5 mm at the transverse plate edges. In the fusion zone, High-Si steel shows slightly more out-of-plane deformation (0.5 mm) than that of High-Al steel plate. The width of the fusion zone is about the same (5 mm) in both steel plates. The thicker High-Si steel plates contain a greater volume of liquid in the weld pool and thus sagging of the weld pool under the influence of the gravitational force results in more out-of-plane deformation of the fusion zone. At the longitudinal edges, the thinner High-Al steel plate shows a higher degree of out-of-plane deformation (6 mm) than in High-Si steel which showed about 3.2 mm distortion.

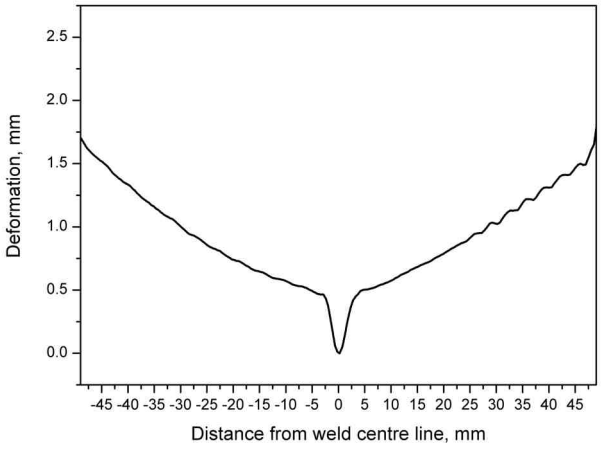

(a)

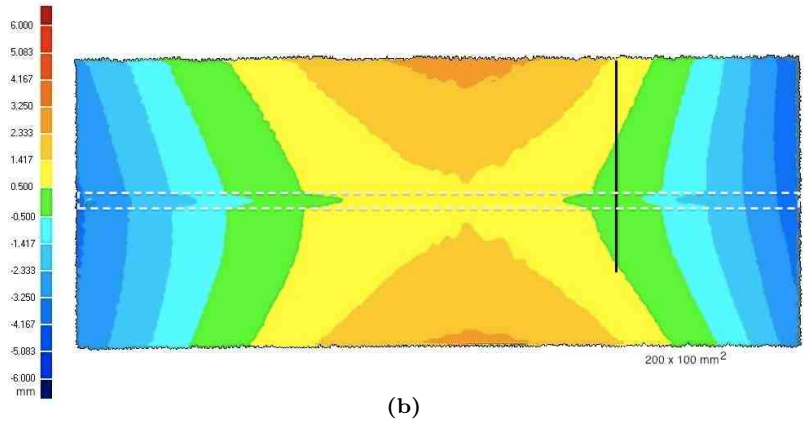

(b)

Figure 5.6: *(a) Deformation in the welded High-Si TRIP steel plate along the transverse direction at the synchrotron diffraction measurement locations. (b) the deformation of the entire plate. The black line schematically shows the position of the synchrotron X-ray diffraction measurement line and the white dotted lines indicates the fusion boundary. (The measurements are shown in mm).*

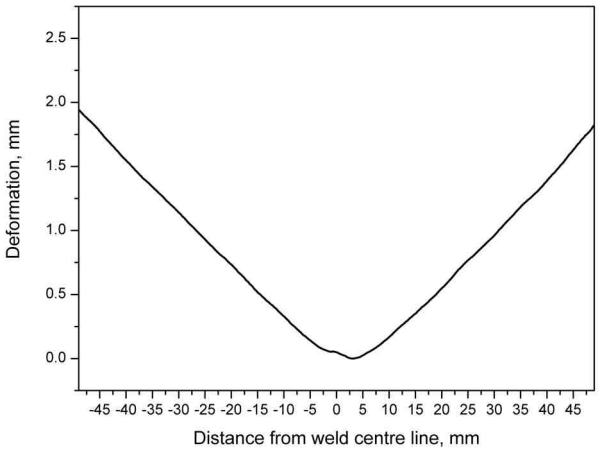

(a)

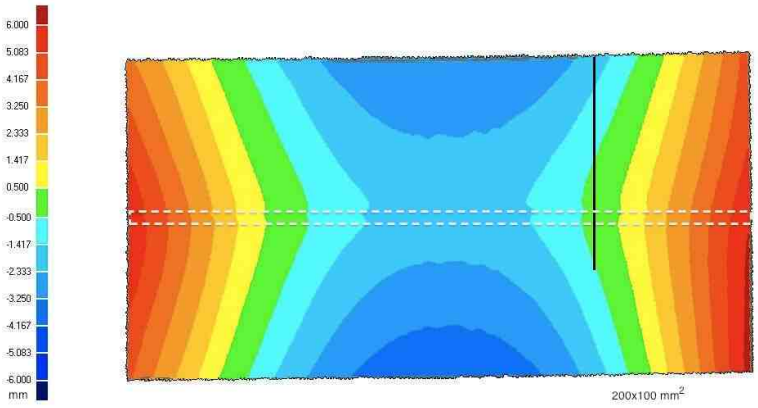

(b)

Figure 5.7: *(a) Deformation in the welded High-Al TRIP steel plate along the transverse direction at the synchrotron diffraction measurement. (b) the deformation of the entire plate. The black line shows the position of the synchrotron X-ray diffraction measurement line and the white dotted lines indicates the fusion boundary. (The measurements are shown in mm).*

5.2.3 Diffraction analysis of welded plates

The synchrotron diffraction measurements on the welded TRIP steel plates yielded 2D diffraction patterns in the transverse direction across the weld centre line. Figure 5.8a schematically shows the measurement profile used for the welded plates, where the transverse line running over the points A-B-C-D indicates the measurement line used. The distance from the plate edge (point A) to point D is 75 mm. In both steel welds, the width of the fusion zone is 5 mm and the point C shows the weld centre line. Figure 5.8 shows the 2D-diffraction rings obtained corresponding to the point A (base metal), point B (heat affected zone) and point C (weld centre line) of the High-Al steel weld. After detector background and distortion statistics correction, the 2D diffraction patterns obtained along the transverse line to the weld were radially integrated and 2θ - intensity plots were obtained (figure 5.9).

The retained austenite content transverse to the weld centre line of welded TRIP steel samples was calculated from the integrated intensities of of $\gamma_{(200)}, \gamma_{(220)}$ and $\alpha_{(200)}, \alpha_{(211)}$ using the procedure explained in section 3.3.5.

Figure 5.10 shows the variation of retained austenite content and the linear interpolation of measured peak temperature reached during GTA welding of TRIP steel plates. The austenite fraction increases from the fusion boundaries in welded High-Al TRIP steel up to 4 mm from the weld centre line whereas in High Si steel, the austenite fraction decreases. It is confirmed from the previous section (section 4.4.2) that, during welding of High-Al steel, the partitioning of aluminium to the solidified ferrite leads to the stabilisation of polygonal ferrite grains in the fusion boundaries. This ferrite stabilisation leads to the diffusion of carbon into the adjoining austenite grains in the heat affected zone (HAZ), enriching them. As a result, the austenite content is found to increase in High-Al steel at these locations. This partitioning behaviour is not found in welded High-Si steels. Thus, there is no increase in austenite content found in this region (figure 5.10).

The austenite fraction is further found to increase from 4 mm from the weld centre line and both steels showed a maximum amount of austenite in the HAZ (12 % in High-Al and 10 % in High-Si) in the location where the peak temperature during welding was about 800 ^{o}C. This increase in austenite fraction is mainly because the peak temperature is in the inter-critical ($\alpha + \gamma$) region. In this region, the austenite is enriched in carbon due to partitioning of carbon from co-existing ferrite; a higher amount of austenite is therefore stabilised compared with other locations in the heat affected zone.

Apart from this, in the case of welded High-Si steel, at about 8 mm from the weld centre line, there is a distinctive zone with very small austenite content (about 1 %). The peak temperature reached during welding at this location is found to be 600 ^{o}C, which is lower than the A_{c_1} temperature (temperature above which austenite starts forming during heating). In a previous section (5.1.3), it is shown, while studying the thermal stability of austenite during continuous heating to 600 ^{o}C, that the retained austenite decomposes into a ferrite and cementite mixture. Thus during welding, in the zones where the peak temperature is below A_{c_1}, the retained austenite present in

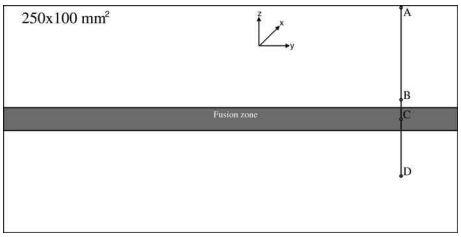

(a) *Schematic illustration*

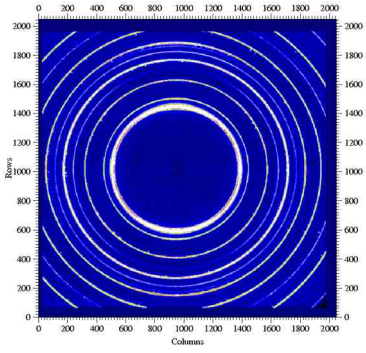

(b) *Point A, base metal*

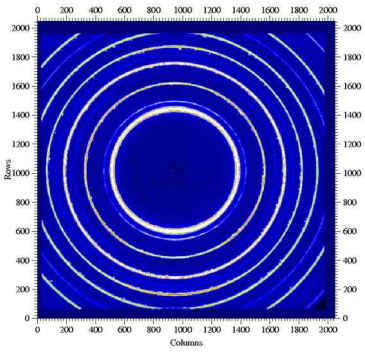

(c) *Point B, in HAZ*

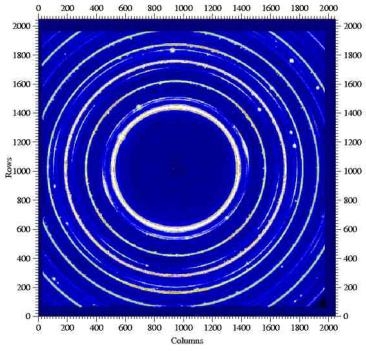

(d) *Point C, at the weld centre line*

Figure 5.8: *(a) The schematic illustration of the measurement profile used for synchrotron diffraction analysis of welded TRIP steel plates. Figure (b), (c) and (d) show the 2D diffraction patterns obtained in the base metal (point A), in HAZ (point B, 4 mm from weld centre line) and at the weld centre line (point C). From inside towards outside, the patterns shows the diffraction rings of* $\gamma_{(111)}$, $\alpha_{(110)}$ *(merged with* $\gamma_{(111)}$*),* $\gamma_{(200)}$, $\alpha_{(200)}$, $\gamma_{(220)}$, $\alpha_{(211)}$, $\gamma_{(311)}$, $\gamma_{(222)}$ *and* $\alpha_{(220)}$ *respectively.*

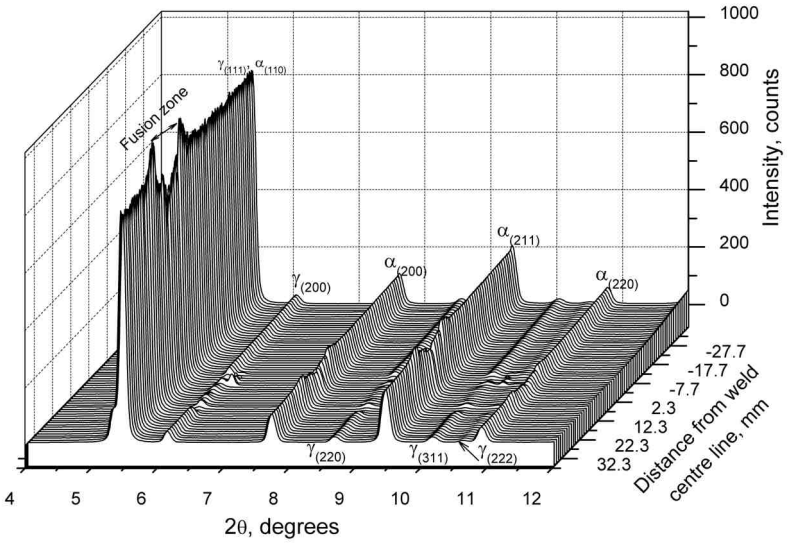

(a) *High - Si*

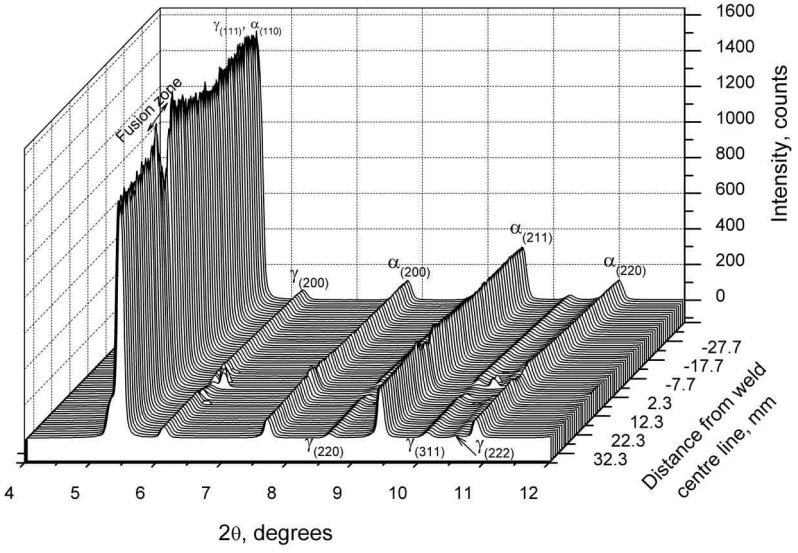

(b) *High - Al*

Figure 5.9: *The intensity - 2θ patterns along the transverse direction of welded High-Si (a) and High-Al (b) steel plates.*

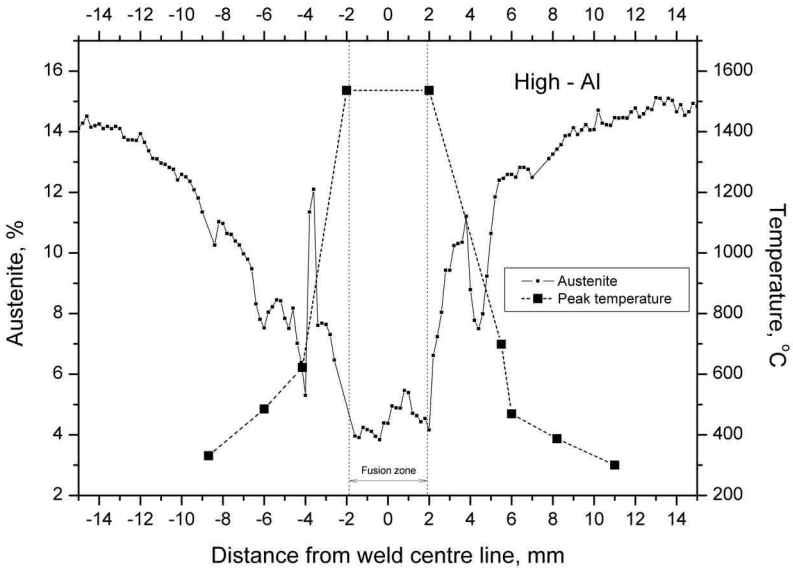

(a) *High - Al*

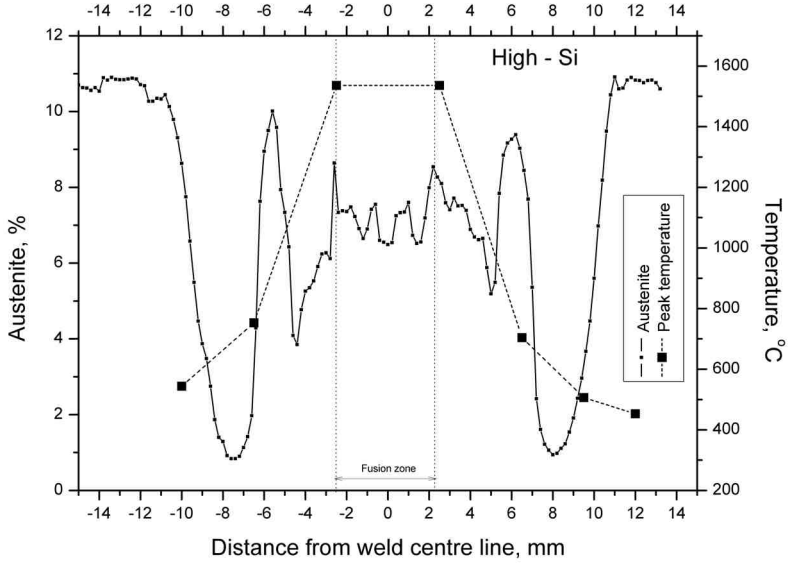

(b) *High - Si*

Figure 5.10: *Variation of retained austenite content in the welded High-Al (a) and High-Si (b) steel plates.*

the microstructure is decomposed into ferrite + cementite. However, this effect is not seen to any significant extent in the High-Al steel, due to the increased stability of aluminium containing austenite and the use of thinner plates (1.25 mm) as compared with the High-Si steel (3 mm).

5.3 Conclusions

Quantitative phase analyses in welded TRIP steels were carried out using magnetic saturation and synchrotron X-ray diffraction methods. The amount of retained austenite present in the weld metal reduces after welding, the base metals containing higher amounts of austenite. Conversely, welding TRIP steels base metals with lesser retained austenite results in an increased amount of austenite in weld metal compared with the base metal. Thermo-magnetic measurements showed that heating the TRIP steel to 600 ^{o}C resulted in the decomposition of austenite into a ferrite and cementite mixture. This is also confirmed from the synchrotron diffraction analysis where the regions in the heat-affected zone which attained peak temperatures of about 600 ^{o}C contained less retained austenite (1 %). Regions in the heat-affected zone where the peak temperatures during welding reached the inter-critical ($\alpha + \gamma$) temperature region contained higher amounts of retained austenite after welding compared to other regions in the heat affected zones. The partitioning of aluminium and subsequent stabilisation of δ-ferrite in the fusion boundaries influenced the stabilisation behaviour of the retained austenite in the High-Al TRIP steel.

References

[1] H.Yin, 'Inclusion characterization and thermodynamics for high-al advanced high-strength steels', *Iron and Steel Technology*, 6, 64 – 73, 2006.

[2] J.Wang and S.van der Zwaag, 'Stablisation mechanisms of retained austenite in transformation-induced plasticity steels', *Metallurgical and Materials Transactions A*, 31A(6), 1527–1539, 2001.

[3] L.Zhao, F.J.Vermolen, J.Sietsma and S.van der Zwaag, 'Physical simulation of thermally induced martensite formation from retained austenite in TRIP steels', *Journal of Material Science and Technology*, 19, 105–108, 2003.

[4] A.S.Arrott and B.Heinrich, 'Application of magnetization measurements in iron to high temperature thermometry', *Journal of Applied Physics*, 52(3), 2113–2115, 1981.

[5] C.Kittle, Introduction to solid state physics, John Wiley and Sons Inc., New York, 1986.

[6] Y.Hirotsu and S.Nagakura, 'Crystal structure and morphology of the carbide precipitated from martensitic high carbon steel during the first stage of tempering', *Acta metallurgica*, 20, 645–655, 1972.

[7] Y.Hirotsu, Y.Itakura, K.Su and S.Nagakura, 'Electron microscopy and diffraction study of the carbide precipitation form martensitic low and high nickel steels at the first stage of tempering', *Transactions JIM*, 17, 503 – 513, 1976.

[8] E.J.Mittemeijer and I.A.Wierszyllowsky, 'The isothermal and non-isothermal kinetics of tempering iron-carbon and iron-nitrogen martensites and austenites', *Zeitschrift für Metallkunde*, 82, 419 – 429, 1991.

[9] B.K.Jha and N.S.Mishra, 'Microstructural evolution during tempering of a multiphase steel containing retained austenite', *Material Science and Engineering A*, A263, 42–55, 1999.

[10] N.H.van Dijk, A.M.Butt, L.Zhao, J.Sietsma, S.E.Offerman, J.P.Wright and S.van der Zwaag, 'Thermal stability of retained austenite in TRIP steels studied by synchrotron X-ray diffraction during cooling', *Acta Materialia*, 53, 5439–5447, 2005.

Chapter 6

In-situ phase transformation studies of TRIP steels

During a typical thermal cycle in the heat affected zone (HAZ), in the heating stage the steel reaches peak temperatures close to the liquidus temperature near the fusion boundary and progressively lower temperatures with increasing distance from the boundary. The welded steel is cooled continuously from the peak temperature at various cooling rates. Due to the imposed thermal cycle, the austenite grain size, volume fraction and composition (especially carbon) vary in the HAZ. Moreover, the variation in the thermal expansion behaviour of co-existing phases induce stresses and thus affect the stability of retained austenite in welded TRIP steels. Chapter 5 showed the variation of retained austenite in welded TRIP steels as a function of distance from the fusion line, indicating that peak temperatures reached during a weld thermal cycle influence the amount of austenite retained in the heat affected zones (HAZ). In this chapter the decomposition, formation and transformation behaviour of austenite in TRIP steels are described based on the measurements made, while subjecting the steels to thermal cycles applied *in-situ* in a synchrotron beam line using a unique high temperature furnace designed especially for this purpose. Time-temperature dependent diffraction patterns were collected to study the decomposition kinetics of retained austenite during initial heating, the kinetics of formation of austenite upon further heating and the transformation kinetics during subsequent cooling. The lattice parameters of austenite and co-existing phases during the applied thermal cycles were also calculated to study the thermal expansion behaviour of individual phases. This study also explores the possible mechanisms behind the time dependent transformation of retained austenite in welded TRIP steels. The results of the *in-situ* phase transformation behaviour obtained by synchrotron X-ray diffraction are also compared with dilatometry and magnetic saturation techniques.

6.1 *In-situ* synchrotron diffraction studies

In-situ synchrotron diffraction studies were carried out on High-Si and High-Al TRIP steel samples (table 3.1) using a specially designed furnace in ID-11 of the European Synchrotron Radiation Facility (ESRF) [1]. Cylindrical samples for *in-situ* synchrotron diffraction were electro discharge machined (EDM) from the TRIP heat treated plates (Condition HT800/400 in figure 3.3) with the axis of the samples oriented in the rolling direction. The sample design and dimensions are shown in figure 6.1. An S-type (Pt−Pt+10 wt. % Rh) thermocouple was spot welded on the top of the sample and was used to control the temperature using an Eurotherm^{TM} temperature controller. A 3D-XRD furnace was used to apply the thermal cycle to the samples. A detailed description of this furnace design, its characteristics and performance is given elsewhere [1]. Figure 6.2 shows the experimental set-up used for the *in-situ* synchrotron diffraction studies at the ID-11 of ESRF. A monochromatic X-ray beam with an energy of 78.395 keV (wavelength 0.15815 Å), a horizontal beam size of 1.2 mm and a vertical size of 0.55 mm was used to illuminate the steel sample. The furnace was mounted on an x-y-z-ω table. With an exposure time of 0.1 s, snap shots of 2D diffraction rings of austenite and ferrite were recorded in transmission geometry using a FreLon 2D area detector. Including data recording time, a time resolution of 0.6 s was achieved and powder diffraction rings were therefore recorded at 0.6 s intervals. During the in-situ experiments, samples were heated from room temperature to either 1000 or 1100 ^{o}C over 60 s and held there for 70 s in helium atmosphere at a pressure of 0.4 bar. Although a real weld thermal cycle does not contain an extended holding at peak temperature, due to experimental difficulties in turning on the cooling cycles, the holding period was extended. Holding ensured a complete austenisation during heating in the case of High-Si steel samples. After holding, the sample was cooled to room temperature over a period of 60 to 80 s by simultaneously purging helium to the sample chamber and switching of the power supply. This procedure generated a thermal cycle, which resembles the heating and cooling conditions experienced 4.2 mm from the weld centre line (non-linear heating and cooling rates), and closely matches the HAZ of a gas tungsten arc welded TRIP steel plate. (see section 5.2.3).

The 2D diffraction patterns obtained during the thermal cycles were then corrected for detector background and distortion statistics. The sample to detector distance and the position of the beam centre were determined using a standard LaB_6 powder diffraction pattern. The volume fraction of austenite was calculated from the integrated intensities of two austenite $\gamma_{(200)}$, $\gamma_{(220)}$ and two ferrite $\alpha_{(200)}$, $\alpha_{(211)}$ peaks using the procedure explained in section 3.3.5. The lattice parameters of austenite and ferrite are calculated as a function of temperature from the mean scattering angles (2θ) of the austenite ($\gamma_{(200)}$, $\gamma_{(220)}$ and $\gamma_{(311)}$) and ferrite rings ($\alpha_{(200)}$, $\alpha_{(211)}$ and α_{220}) using equation 3.4. The results of the *in-situ* diffraction analysis will be presented in two parts in the forthcoming section where, section 6.2 deals with the thermal cycle with a peak temperature of 1000 ^{o}C applied on both High-Al and High-Si steels and section 6.3 describes the results of the thermal cycle with a peak temperature of 1100 ^{o}C applied on High-Si steel. Thus, section 6.2 is concerned with the effect of

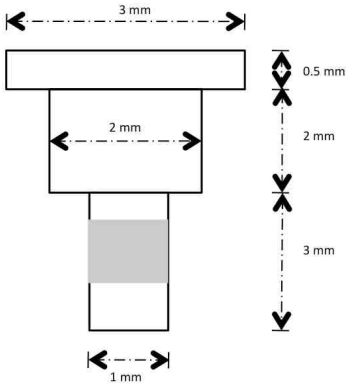

Figure 6.1: *Schematic illustration of sample geometry used for the in-situ synchrotron X-ray diffraction experiments. The grey area indicates the position of the beam.*

composition and section 6.3 with effect of austenisation temperatures on the kinetics of austenite transformation.

6.2 Effect of composition

In this section, results are reported from *in-situ* synchrotron diffraction studies carried out while imposing a thermal cycle with a peak temperature of 1000 ^{o}C on both High-Al and High-Si steels.

6.2.1 Thermal cycle applied

As described in the previous chapters, the thermal cycle of a welding process changes the base metal microstructure and alters the size, amount and distribution of retained austenite in the fusion and heat affected zones. Figure 6.3 shows the thermal cycle applied to TRIP steel samples during *in-situ* synchrotron diffraction studies where the samples were heated to 1000 ^{o}C . The thermal cycle is divided into three parts to facilitate the data analysis of the in-situ 2D diffraction patterns. The first comprises heating to 1000 ^{o}C from room temperature in 60 s and holding at that temperature for 70 s. During this part, the retained austenite present in the microstructure is expected to decompose. Nucleation and subsequent growth of new austenite from the ferritic + bainitic microstructure occurs once the temperature goes beyond the A_{c1} temperature (the nucleation temperature of austenite during heating). The second part of the thermal cycle involves cooling from 1000 ^{o}C to room temperature ($\simeq$24 ^{o}C). The austenite is expected to transforms into a mixture of ferrite, bainite and martensite. During the third part of the thermal cycle, the sample is held at room temperature for 2000 s. The diffraction patterns, which were recorded during this room temperature

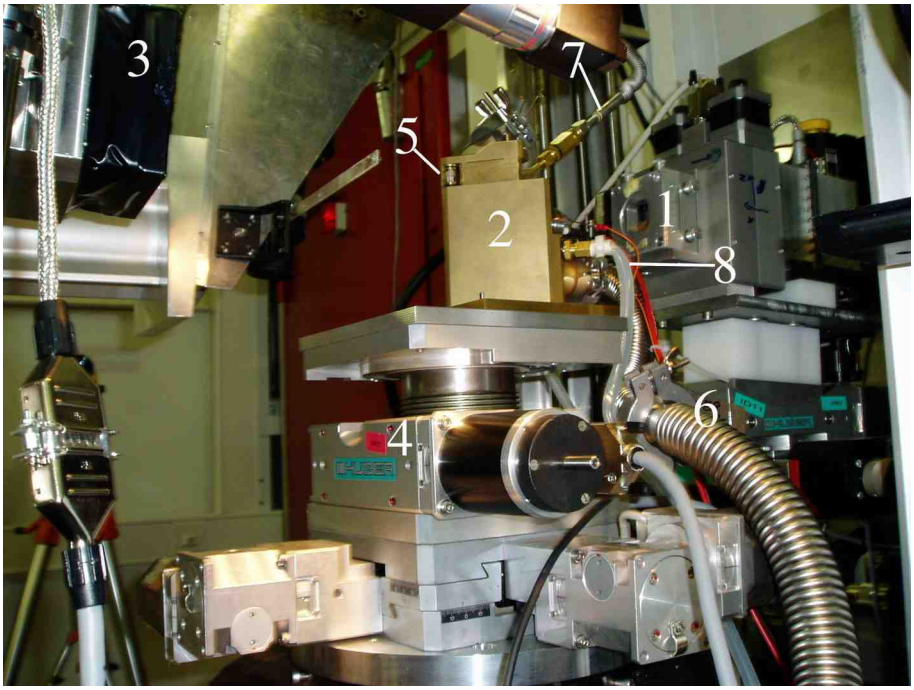

Figure 6.2: *Experimental set-up used for in-situ synchrotron diffraction studies at the ID-11 of ESRF. 1. beam entry slit, 2. 3D-XRD furnace, 3. 2D FreLon^{TM} area detector, 4. x-y-z-ω table, 5. sample chamber, 6. vacuum circuit 7. helium inlet via mass flow controller, 8. water cooling circuit.*

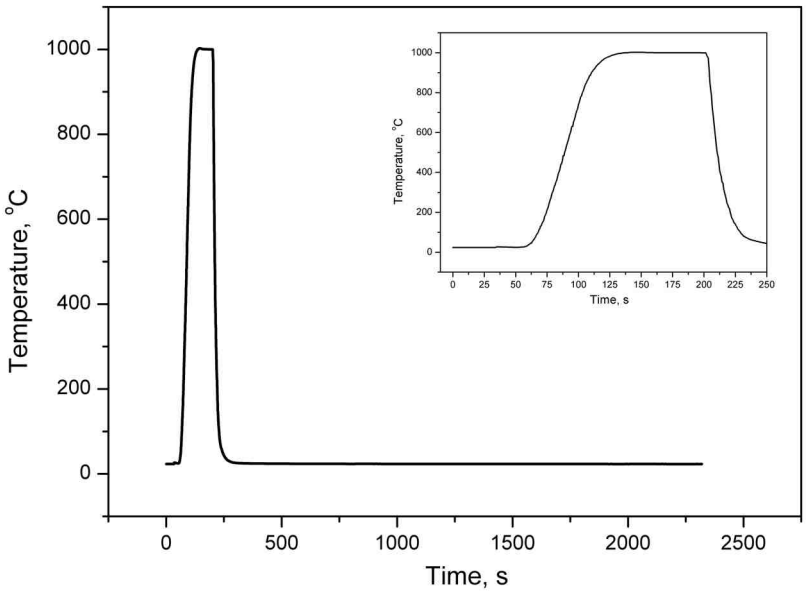

Figure 6.3: *The thermal cycle with a peak temperature of 1000 °C used for in-situ synchrotron diffraction. Insert shows the same thermal cycle without room temperature holding part.*

holding, were then analysed to study the stability of retained austenite upon holding. Figure 6.4 shows the recorded 2D diffraction patterns at 6 different temperatures while applying the thermal cycle using the furnace on a High-Al TRIP steel sample. In figure 5.8b, a diffraction pattern of the base metal sample without the background noise from the furnace was shown. The recorded 2D diffraction patterns were corrected for furnace background, detector noise and distortion corrections, before the quantitative phase and lattice parameters analyses were carried out.

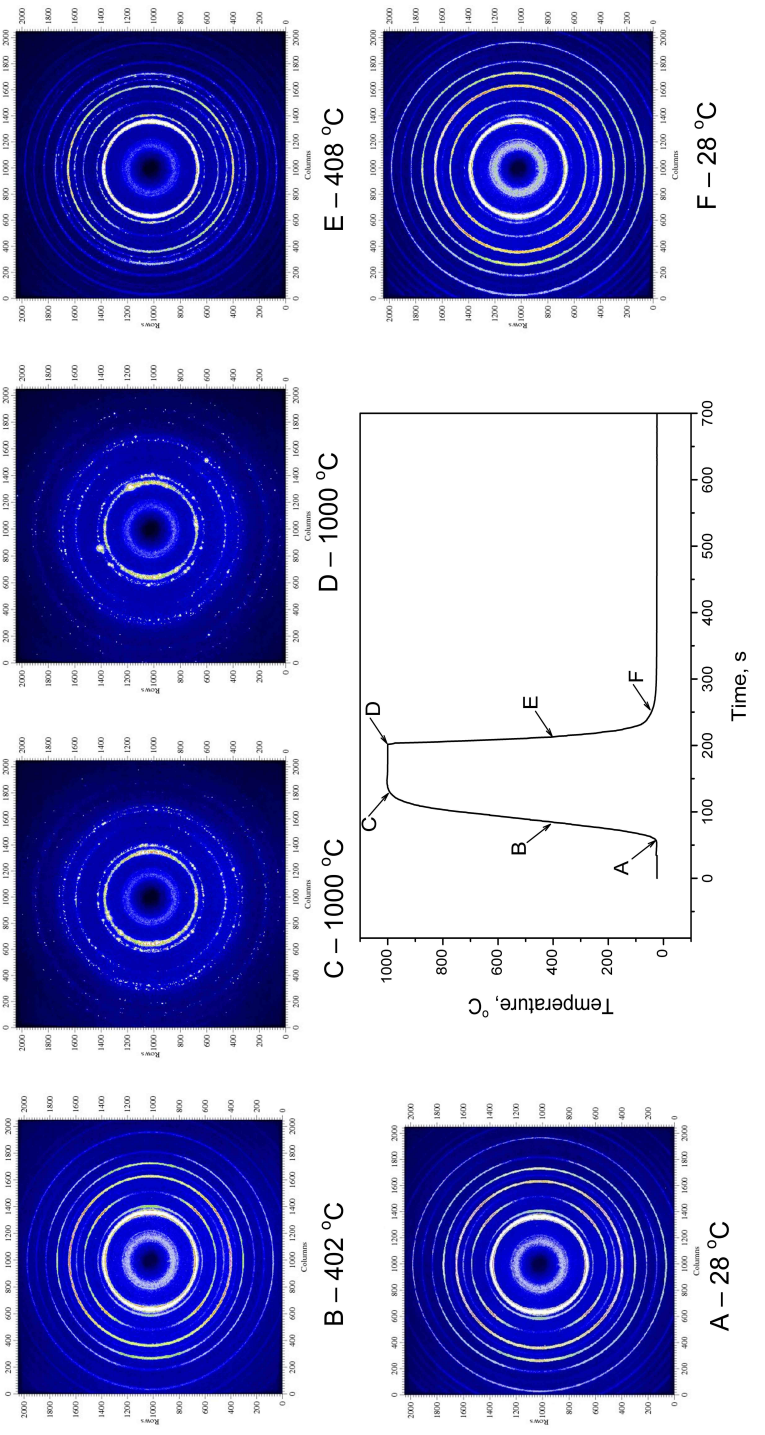

Figure 6.4: *Examples of the 2D diffraction patterns recorded while applying the thermal cycle on a High-Al steel sample. The inner most diffuse ring in "A, B and F" patterns are due to diffuse scattering from the quartz capsule of the furnace. In "A, B and F" from inside towards outside, the patterns show the diffraction rings of* $\gamma_{(111)}$, $\alpha_{(110)}$ *(merged with* $\gamma_{(111)}$*),* $\gamma_{(200)}$, $\alpha_{(200)}$, $\gamma_{(220)}$, $\alpha_{(211)}$, $\gamma_{(311)}$, $\gamma_{(222)}$ *and* $\alpha_{(220)}$ *respectively. Patterns "C and D" show diffraction rings of austenite only.*

6.2.2 Transformation kinetics during heating to 1000 ^{o}C

Figure 6.5 shows the austenite content during heating of High-Si and High-Al base metal samples. The retained austenite present in the High-Si and High-Al base metal samples (10.3 and 15.4 % respectively) is stable up to 290 ^{o}C. Upon increasing the temperature, the retained austenite fraction starts to decrease slowly above 290 ^{o}C and after reaching 400 ^{o}C, the kinetics of decomposition increase. Figure 6.6 shows the kinetics of austenite formation $\left(\frac{d(x_\gamma)}{d(t)}\right)$ as a function of heating temperature. When the temperature reaches 290 ^{o}C, the derivative $\frac{d(x_\gamma)}{d(t)}$ starts to deviate to negative values indicating that the decomposition of austenite was started. It reaches a maximum negative value at around 450 ^{o}C confirming a faster decompostion at this temperature. At 500 ^{o}C, the amount of retained austenite present in the High-Al and High-Si samples was 8.4 and 4.4 %, which is almost half of that present in the base metals. The samples were heated from 290 ^{o}C to 500 ^{o}C in about 13 s (figure 6.3).

Upon further heating, the austenite content decreases in the High-Al sample continuously up to 529 ^{o}C and reached to minimum level of 7.1 % during heating. In the case of the High-Si steel, the decrease in retained austenite content was evident up to 550 ^{o}C and was reduced to 3.6 %. A further increase in temperature resulted in an increase in austenite content, indicating that the samples reached the A_{c_1} temperatures (529 and 551 ^{o}C for High-Al and High-Si steels respectively) for the current average heating rate ($\simeq$16 ^{o}C s^{-1}). Figure 6.6 also confirms this as the kinetics of austenite formation move to positive values, indicating the nucleation of new austenite grains beyond this temperature. A complete austenisation of the High-Si steel sample is evident when the temperature reaches 802 ^{o}C. In the case of High-Al steel sample, the austenite fraction reaches 99 % once the temperature reaches 1000 ^{o}C.

6.2.3 Lattice parameters variation during heating to 1000 ^{o}C

The lattice parameter of the austenite in the High-Al steel sample is found to vary linearly with temperature between room temperature and 290 ^{o}C, during which time the retained austenite is stable (figure 6.7a). There is an additional increase in lattice parameter found once the retained austenite starts to decompose upon further heating and a deviation from linearity can be seen. The lattice parameter of austenite drops once the temperature reaches about 430 ^{o}C and starts to increase linearly again until the A_{c_1} temperature is achieved (529 ^{o}C). A further increase in temperature to 715 ^{o}C does not show any changes in the lattice parameter of austenite. At higher temperatures it again starts to increase with temperature and decreases again only as the sample approaches a fully austenitic structure (961 ^{o}C).

In contrast to the austenite lattice parameter, the lattice parameter of ferrite does not show any variation in slope during heating (figure 6.7b). It is found to increase linearly with temperature up to a temperature of 830 ^{o}C, where about 6.4 % of ferrite is left in the sample. A further increase in temperature results in scatter.

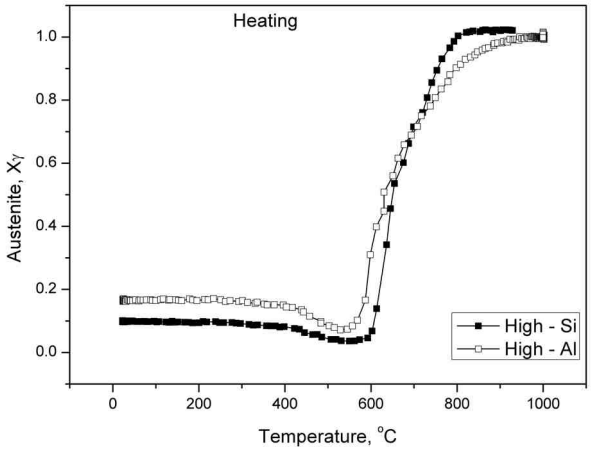

Figure 6.5: *Variation of austenite percentage with temperature during heating to 1000 °C.*

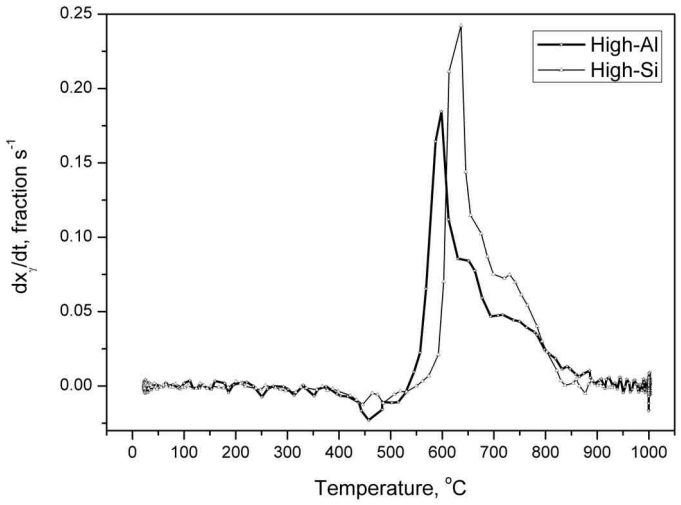

Figure 6.6: *The formation kinetics of austenite during heating to 1000 °C.*

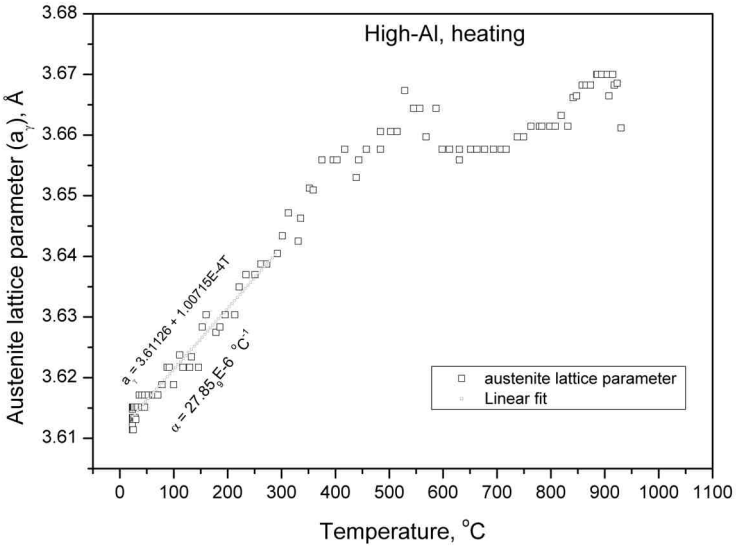

(a) *High-Al, austenite lattice parameter*

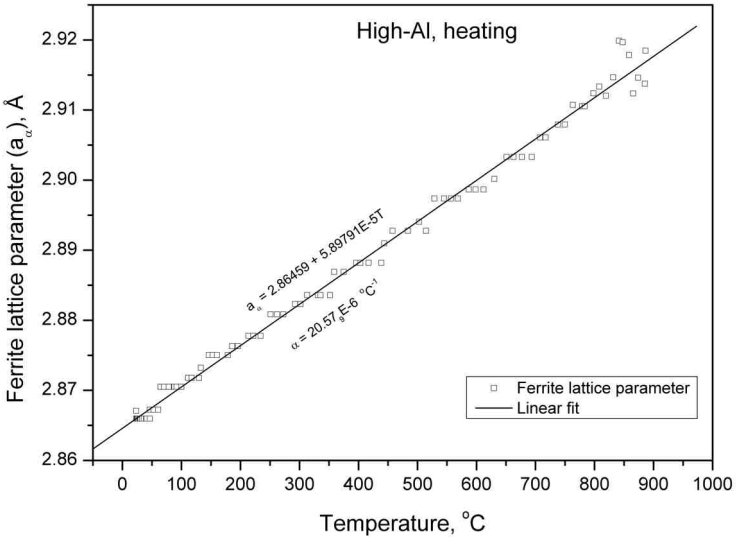

(b) *High-Al, ferrite lattice parameter*

Figure 6.7: *Variation of lattice parameter in High-Al steel during heating to 1000 °C.*

Table 6.1: *Thermal expansion coefficients of austenite and ferrite during heating.*

Steel	Austenite	Ferrite
High-Al	27.85_9x10^{-6} ^{o}C^{-1} (25 to 290 ^{o}C)	20.57_9x10^{-6} ^{o}C^{-1} (25 to 830 ^{o}C)
High-Si	28.81_9x10^{-6} ^{o}C^{-1} (25 to 290 ^{o}C)	19.41_2x10^{-6} ^{o}C^{-1} (25 to 740 ^{o}C)

The lattice parameter of austenite (below 290 ^{o}C) and the ferrite lattice parameter (up to 830 ^{o}C) in figure 6.7 can be described by the following expressions;

$$a_\gamma = 3.61126 + 1.00715X10^{-4}T \tag{6.1}$$

$$a_\alpha = 2.86459 + 5.8979X10^{-5}T \tag{6.2}$$

where 'a_γ' is the lattice parameter of austenite and 'a_α' is the lattice parameter of ferrite in $\mathring{A}$ and T is the temperature in ^{o}C. The lattice parameter of austenite and ferrite are related to the linear thermal expansion co-efficient 'α' using the equation;

$$a(T) = a_{25}(1 + \alpha[T - 25]) \tag{6.3}$$

where 'a_{25}' is the lattice parameter of austenite or ferrite at 25 ^{o}C [2]. For High-Al steel, the linear thermal expansion co-efficient of austenite is calculated to be 27.85_9x10^{-6} ^{o}C^{-1} from 25 to 290 ^{o}C and that of ferrite 20.57_9x10^{-6} ^{o}C^{-1} from 25 to 830 ^{o}C. The subscripts denote the uncertainty in the last digit.

The austenite lattice parameter of High-Si steel sample showed a similar behaviour to the High-Al steel sample during heating to 1000 ^{o}C (figure 6.8a). A similar change in slope was observed once the retained austenite started to decompose after 290 ^{o}C and a decrease in lattice parameter accurs at 400 ^{o}C. In the case of High-Al steel, this levelling off in lattice parameter during heating was observed at 430 ^{o}C. The lattice parameter of ferrite in the High-Si steel sample showed only a linear expansion behaviour as was also seen in the High-Al steel sample (figure 6.8b).

The lattice parameter of austenite from room temperature to 290 ^{o}C and the ferrite lattice parameters (up to 740 ^{o}C) of High-Si steel in figure 6.8 can be expressed similar to equation as,

$$a_\gamma = 3.59718 + 1.03765X10^{-4}T \tag{6.4}$$

$$a_\alpha = 2.86212 + 5.55826X10^{-5}T \tag{6.5}$$

Using the equation 6.3, the linear thermal expansion coefficients of austenite and ferrite in High-Si were 28.81_9x10^{-6} and 19.41_2x10^{-6} ^{o}C^{-1}, respectively.

Table 6.1 summaries the thermal expansion coefficients of austenite and ferrite in both steels with their calculated temperature ranges.

6.2.4 Transformation kinetics during cooling from 1000 ^{o}C

In the High-Al steel sample, the transformation of austenite to ferrite during cooling was observed when the sample temperature reached 974 ^{o}C, indicating the A_{c_3}

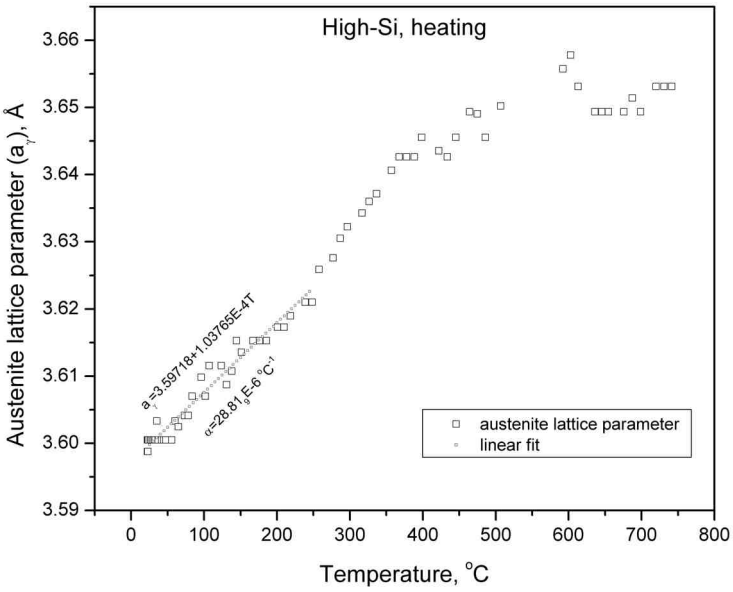

(a) *High-Si, austenite lattice parameter*

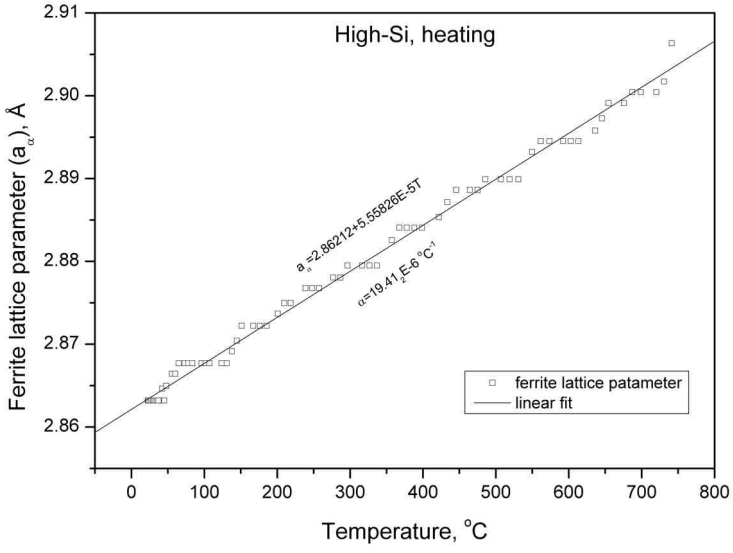

(b) *High-Si, ferrite lattice parameter*

Figure 6.8: *Variation of lattice parameter in High-Si steel during heating to 1000 °C.*

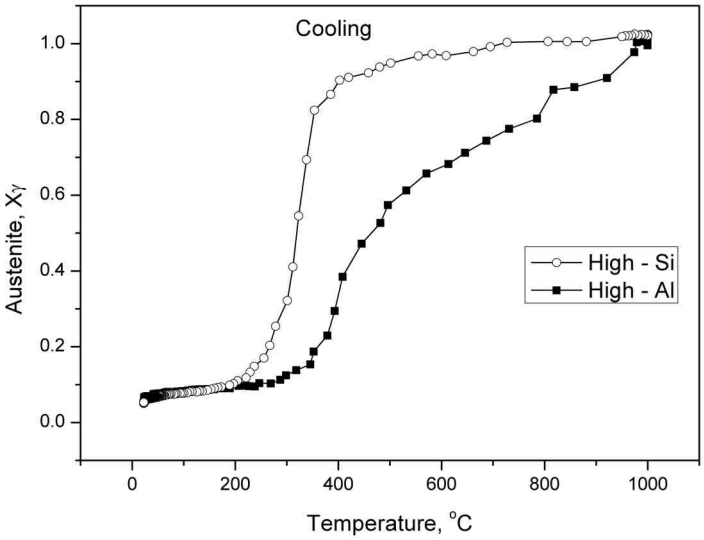

Figure 6.9: *Austenite fraction as a function of temperature during cooling from 1000 °C.*

temperature of this steel. The sample was cooled in 1.6 s from 1000 °C to 974 °C and ferrite rings were first observed at this temperature. In the case of High-Si steel sample, the appearance of the first ferritic rings was observed at 727 °C. Figure 6.9 shows the austenite fraction during cooling from 1000 °C in High-Al and High-Si steel samples. It can be seen from this figure that the transformation of austenite is initially sluggish in High-Si steel and even after reaching about 400 °C, 90.1 % of the austenite is left untransformed in this steel. Whereas in High-Al steel, at 400 °C, the amount of austenite left untransformed is about 35 %. This is also supported by the transformation rate of austenite with respect to the cooling temperature shown in 6.10. In the case of High-Si steel, the transformation rate of austenite is at about 1.4 % s^{-1} till 420 °C. The transformation rate increases steeply from the next recorded temperature (400 °C). A further decrease in temperature results in a rapid decomposition of austenite in High-Si steel in which at 300 °C, the total austenite content decreased to 32 %, with a maximium recorded rate of 22 % s^{-1} at 320 °C. When the temperature reached 200 °C, both steels contained a similar amount of untransformed austenite (about 10 %). Upon further cooling, the austenite content decreases gradually in both steels, reaching about 7 % in the High-Al steel sample and 6.5 % in the High-Si steel sample at 40 °C.

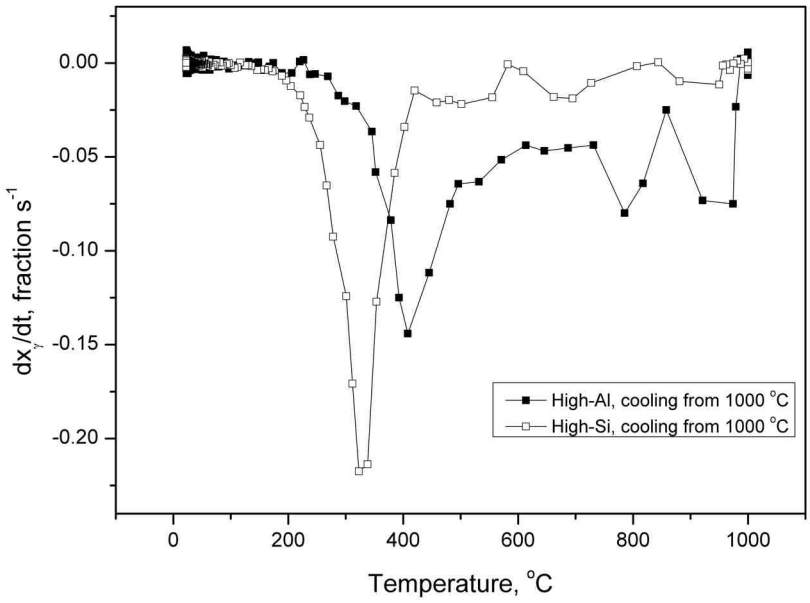

Figure 6.10: *Transformation rate of austentie during cooling from 1000 ^{o}C*

6.2.5 Lattice parameter variation during cooling from 1000 ^{o}C

Unlike in heating, the lattice parameters of austenite and ferrite show several deviations from linearity while cooling from 1000 ^{o}C. In High-Al steel samples, the lattice parameters decrease linearly down to about 550 ^{o}C (figure 6.11). A further decrease in temperature results in an increase of the austenite lattice parameter (a_γ) while it remains constant from 495 to 405 ^{o}C. Upon further decreasing the temperature, the a_γ continues to decrease to 270 ^{o}C after which again an increase is observed. The changes in a_γ appear random once the temperature decreases below 200 ^{o}C until the sample reached 100 ^{o}C. The ferrite lattice parameter a_α showed a similar decrease until about 600 ^{o}C and a further decrease in temperature showed an increase in lattice parameter up to 530 ^{o}C. After this temperature, the a_α decreases linearly to 445 ^{o}C. The measured a_α remains constant till the next temperature step where the sample temperature reached to 405 ^{o}C. Upon further cooling, the a_α decreases linearly albeit in several steps, indicating a possible thermal non-equilibrium during cooling.

The austenite and ferrite lattice parameters of High-Si steel showed a slightly different behaviour compared to the High-Al steel sample (6.12). Though the general variation pattern remains the same, compared to the High-Al steel, the temperatures at which changes in slopes are observed and the magnitude of the parameter shift dif-

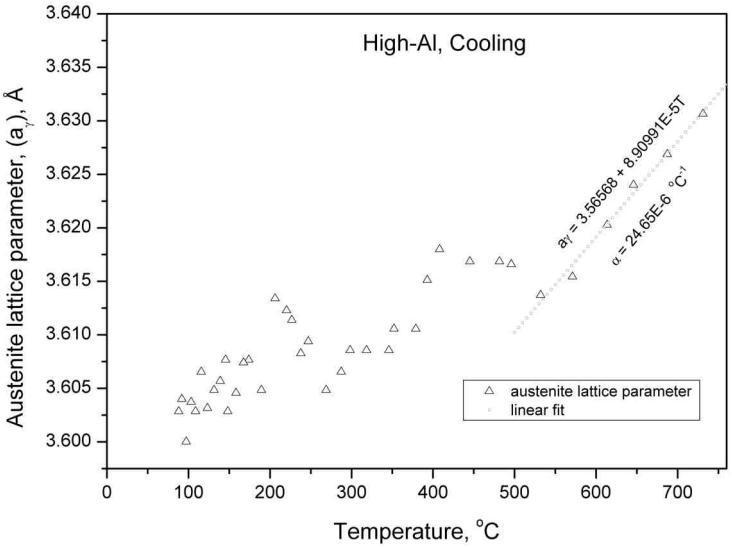

(a) *High-Al, austenite lattice parameter*

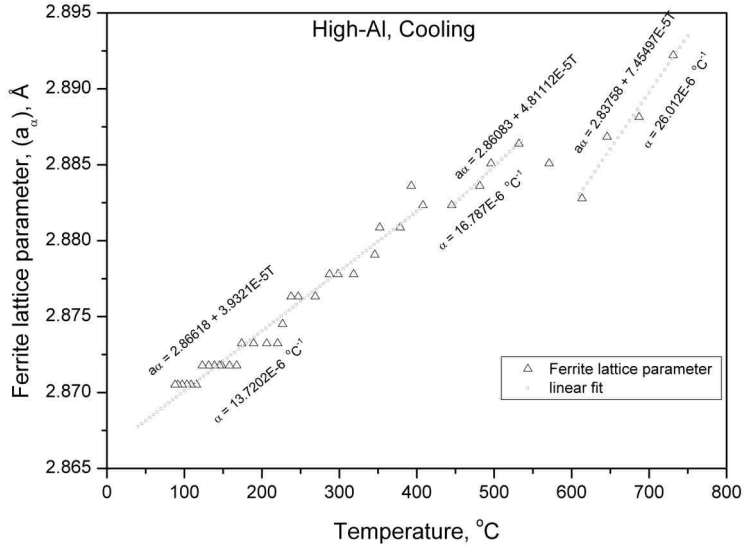

(b) *High-Al, ferrite lattice parameter*

Figure 6.11: *Variation of lattice parameter in High-Al steel during cooling from 1000 °C.*

Table 6.2: *Thermal expansion coefficients of austenite and ferrite during cooling.*

Steel	Austenite	Ferrite
High-Al	24.64_6x10^{-6} ^{o}C^{-1} (731 to 530 ^{o}C)	26.01_2x10^{-6} ^{o}C^{-1} (731 to 610 ^{o}C)
	-	16.78_7x10^{-6} ^{o}C^{-1} (532 to 445 ^{o}C)
	-	13.72_0x10^{-6} ^{o}C^{-1} (408 to 85 ^{o}C)
High-Si	27.41_1x10^{-6} ^{o}C^{-1} (727 to 500 ^{o}C)	23.97_4x10^{-6} ^{o}C^{-1} (311 to 204 ^{o}C)

fer for this steel. The austenite lattice parameter a_γ in High-Si steel decreases linearly until the temperature reaches about 500 ^{o}C. At the next measured temperature step, the sample cooled to 480 ^{o}C and an increase in lattice parameter is observed. The a_γ decreases further with cooling temperature and there are no distinctive shifting patterns observed henceforth. The ferrite lattice parameter a_α in this steel also initially decreases until the temperature reached 460 ^{o}C. Upon decreasing the temperature further to 400 ^{o}C, a steep increase in a_α is observed. a_α remains constant to 320 ^{o}C and at the next measured temperature step (310 ^{o}C) it starts to decrease. a_α decreases linearly from 310 ^{o}C to 205 ^{o}C. Upon further cooling, as in High-Al steel a_α decreases linearly albeit in several steps.

During cooling, the variation in the lattice parameters of ausenite and ferrite in both steels were fit with equation 6.3 between the temperature intervals where the variation appears linear and the thermal expansion coefficients were calculated. Table 6.2 summarises the calculated thermal expansion coefficients within the specified temperatures ranges.

6.2.6 Transformation of austenite at room temperature

In this section, the results of the third part of the thermal cycle are presented. The samples were kept at room temperature after cooling from 1000 ^{o}C and the diffraction patterns were recorded during the holding period. Surprisingly, the austenite content in the sample was found to decrease continuously during room temperature holding after cooling from 1000 ^{o}C. Figure 6.13 shows the variation of austenite content during cooling from 40 ^{o}C and subsequent holding at room temperature. The austenite fraction in the sample is not stable after cooling, but transforms continuously. The sample contained about 7 % of austenite at 40 ^{o}C. Cooling to 25 ^{o}C did not change the austenite content immediately; however, the austenite fraction decreased to 6.2 % after 100 s whilst the temperature remained stable at about 24 to 23 ^{o}C. After 2110 s holding at room temperature, the austenite content was 5.4 % (fig. 11b). A similar behaviour is also observed in the High-Si steel sample after cooling from 1000 ^{o}C to room temperature. At 40 ^{o}C, this steel contains about 6.5 % of untransformed austenite and upon further cooling to 25 ^{o}C, the austenite content is reduced to 6 %. The sample was held at room temperature ($\simeq$23 ^{o}C) for 2000 s and at the end of this holding period, the untransformed austenite content in this steel sample was reduced

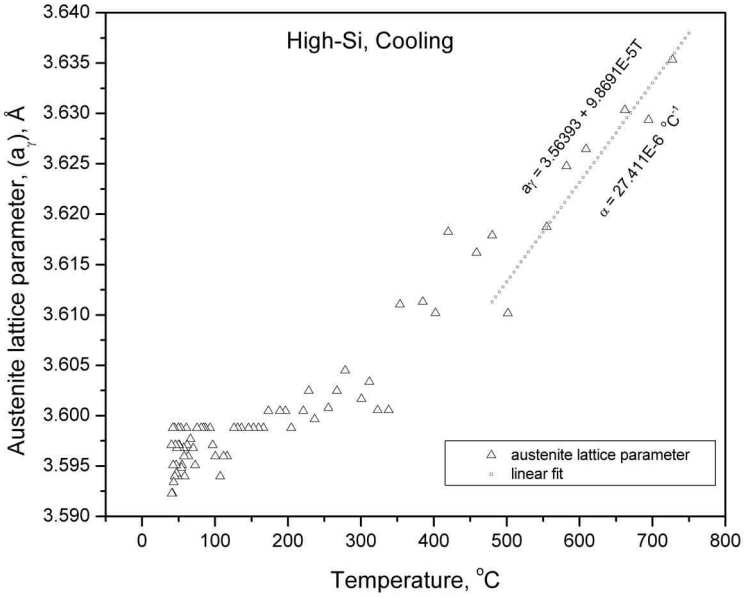

(a) *High-Si, austenite lattice parameter*

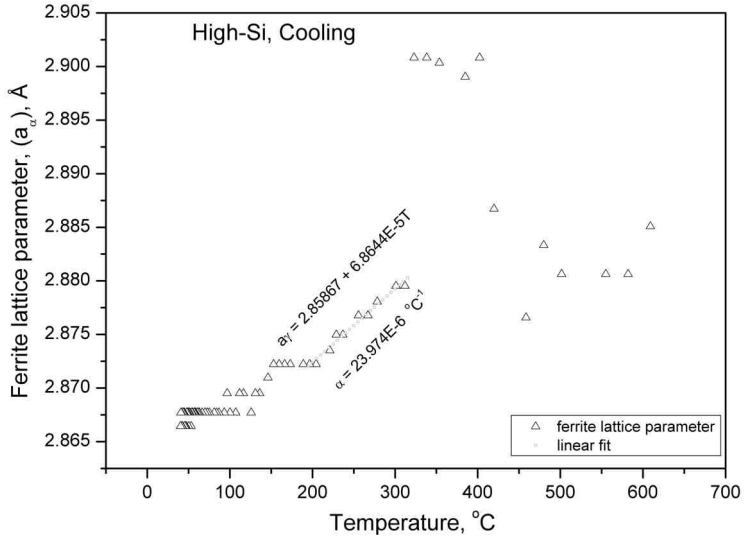

(b) *High-Si, ferrite lattice parameter*

Figure 6.12: *Variation of lattice parameter in High-Si steel during cooling from 1000 °C.*

to 5 %.

This result indicates that a significant amount of austenite (1.5 to 2 %) is transforming at room temperature holding after cooling from 1000 ^{o}C. This transformation becomes very critical because after commercial welding of the TRIP steel, the welded steel is immediately subjected to various mechanical operations. If the retained austenite fraction is not stable in the heat affected zone and the austenite continuously decomposes after welding, the properties of welded TRIP will also vary with time.

6.3 Effect of austenisation temperature

In this section, results are reported from *in-situ* synchrotron diffraction studies carried out on High-Si steel samples where samples were heated to 1100 ^{o}C.

6.3.1 Thermal cycle applied

During this thermal cycle, the High-Si steel samples were heated to 1100 ^{o}C with a similar heating and cooling rates used to those reported in section 6.2 (refer figure 6.3). Figure 6.14 shows the actual thermal cycles used for both experimental parts where the heating and cooling rates are almost identical. Samples were heated to 1100 ^{o}C in 80 s and held there for 68 s. After the holding, the sample was cooled to room temperature in 85 s by purging helium with a maximum achieved cooling rate of 90 ^{o}C s^{-1} in between 1100 to 1000 ^{o}C (in the experiments of section 6.2, this maximum was achieved between 1000 to 900 ^{o}C.) The average cooling rate between 900 to 400 ^{o}C was 60 ^{o}C s^{-1}. Here, the transformation kinetics of austenite during cooling a High-Si steel sample from 1100 ^{o}C are presented as compared to a sample cooled from 1000 ^{o}C. The decomposition and formation kinetics of austenite during heating to 1100 ^{o}C is not presented as the heating rates remain the same in both cases.

6.3.2 Transformation kinetics during cooling from 1100 ^{o}C

Apart from the composition, another rate controlling factor in the transformation of austenite is its grain size. In the case of High-Si steel, heating to 1000 and 1100 ^{o}C resulted in a complete austenisation in both cases. Thus, studying the austenite transformation during cooling from these temperatures gives an indication about the effect of austenisation temperature on the transformation behaviour of austenite in a TRIP steel. Figure 6.16 and figure 6.17 show the austenite fraction and the rate of transformation during cooling from 1000 and 1100 ^{o}C. When the sample was cooled from 1100 ^{o}C, the first ferrite diffraction spots were observed when the temperature reached 862 ^{o}C as compared to 727 ^{o}C for the sample cooled from 1000 ^{o}C. Cooling the sample below this temperature (862 ^{o}C) shows a slightly increased rate of transformation in the 1100 ^{o}C case. As mentioned earlier (section 6.2.4), the transformation of austenite after cooling from 1000 ^{o}C, is sluggish until 420 ^{o}C and an increase in rate of transformation is found once the sample is cooled below this temperature. In the

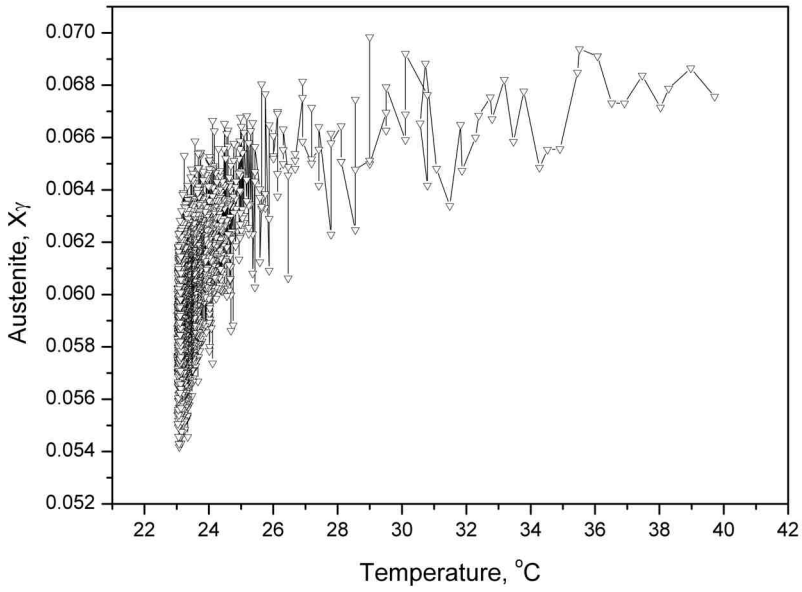

(a) *High-Al*

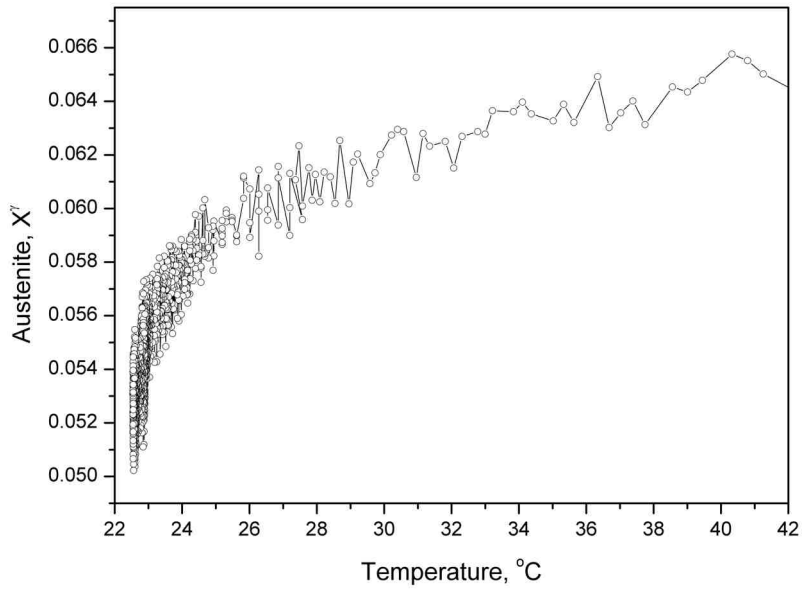

(b) *High-Si*

Figure 6.13: *Austenite fraction in High-Al and High-Si steels after cooling from 1000 °C shows that the untransformed austentie is not stable at room temperature and transforms continuously at the room temperature holding.*

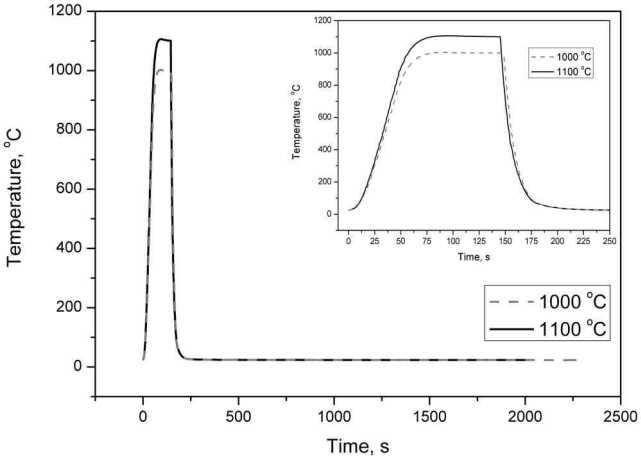

Figure 6.14: *Comparison of thermal cycles used for in-situ X-ray diffraction studies. Section 6.2 deals with the samples which were heated to 1000 °C, whereas in section 6.3 to 1100 °C. The insert focuses on the heating and cooling stage, showing the similarity in the rates.*

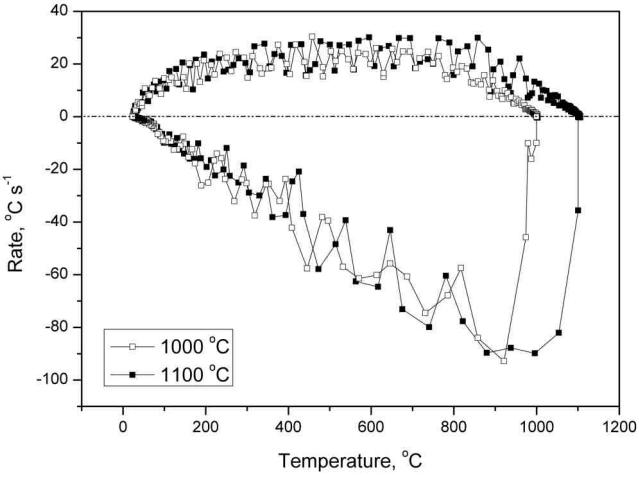

Figure 6.15: *Heating and cooling rates achieved during heating to 1000 and 1100 °C. Note that the heating is done using a PID controlling unit, whereas cooling is done by purging the helium gas after switching-off the power unit.*

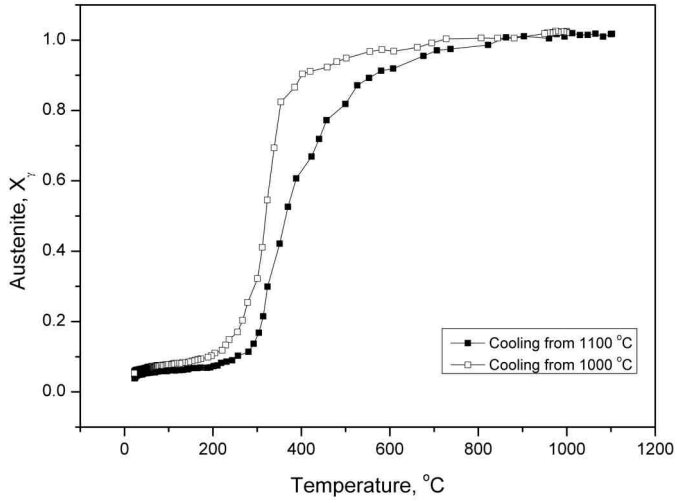

Figure 6.16: *Comparison of austenite fraction during cooling the High-Si steel samples from 1100 and 1000 °C.*

sample cooled from 1100 °C, the transformation rate increases rapidly after reaching 580 °C and at 500 °C, the transformation rate of austenite is about 8 % s^{-1}. The transformation rate remained constant in the next three measurement steps until the temperature of the sample reached 440 °C. Further cooling of the sample resulted in an increased rate of transformation of austenite with a maximum recorded rate of 18.5 % s^{-1} at 350 °C. A maximum transformation rate of austenite (22 % s^{-1}) was recorded at 320 °C for the sample cooled from 1000 °C. When the sample was cooled further, the austenite fraction decreases gradually and the transformation rate also decreases, indicating that the transformation becomes slower at lower temperatures. At 40 °C, the sample cooled from 1100 °C contained 5.3 % of untransformed austenite whereas cooling from 1000 °C resulted in 6.5 % of untransformed austenite at the same temperature.

6.3.3 Lattice parameters during cooling from 1100 °C

During cooling from 1100 °C, the lattice parameters of austenite a_γ and ferrite a_α also showed several deviations from linearity as during cooling from 1000 °C. Figure 6.18 shows the austenite and ferrite lattice parameters of High-Si steel while cooling from 1100 °C. The austenite lattice parameter decreases initially until the sample reached 960 °C. From the next recorded temperature step (903 °C), the austenite lattice parameter starts to increase down to 822 °C. At the next recorded temperature step

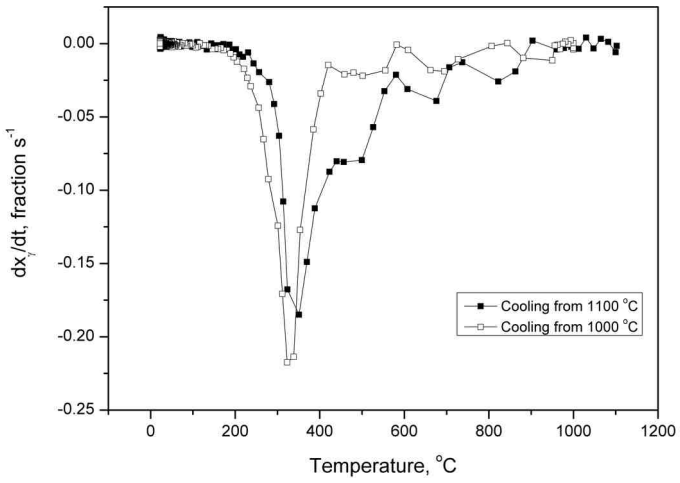

Figure 6.17: *Comparison of transformation rate of austenite during the High-Si steel samples from 1100 and 1000 ^{o}C.*

(737 ^{o}C), a decrease in lattice parameter is observed. A further cooling again increases the lattice parameter till 675 ^{o}C and a reduction from that temperature to 554^{o}C. In the next two recorded temperature steps (526 and 500 ^{o}C), the a_γ does not vary significantly and starts to increase when temperature goes down towards 440 ^{o}C. It remained the same in the next recorded temperature step (388 ^{o}C). From thereon, cooling the sample results initially in a more or less linear variation, albeit in several multiple steps. Finally, cooling below 250 ^{o}C leads to a scattering in a_γ.

Unlike in a_γ, the ferrite lattice parameter a_α shows a clear deviation pattern with cooling temperature. After a small initial change, a_α increases rapidly when the temperature decreased from 605 to 580 ^{o}C. a_α decreases gradually thereafter to a temperature of 440 ^{o}C. Cooling from this temperature results in a change in slope of the curve until the temperature 350 ^{o}C is reached. a_α further decreases with temperature linearly to 255 ^{o}C. Upon further cooling to room temperature from 255 ^{o}C, a_α decreases almost linearly but with several steps. This linear variation from 255 ^{o}C to room temperature is fit with with equation 6.3 and the thermal expansion co-efficient was calculated to be 17.78_3x10^{-6} ^{o}C^{-1}.

6.3.4 Transformation of austenite at room temperature after cooling from 1100 ^{o}C

The austenite content in the sample was also found to decrease continuously during room temperature holding after cooling from 1100 ^{o}C. Figure 6.19 shows the variation

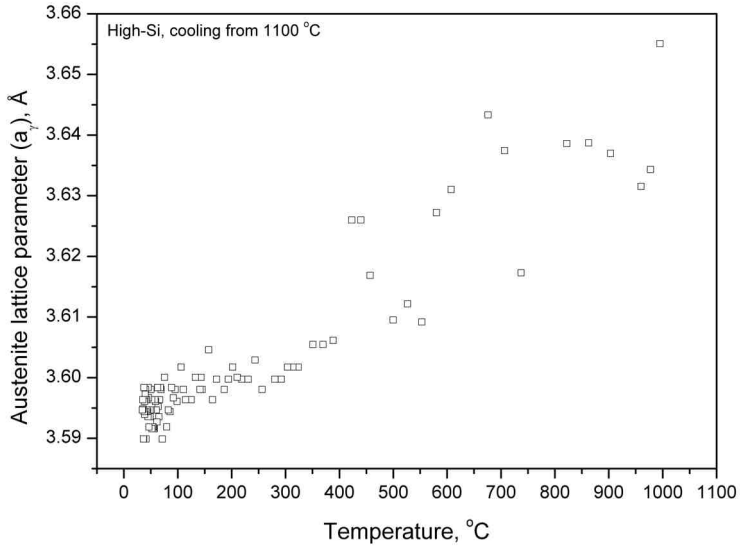

(a) *Austenite lattice parameter*

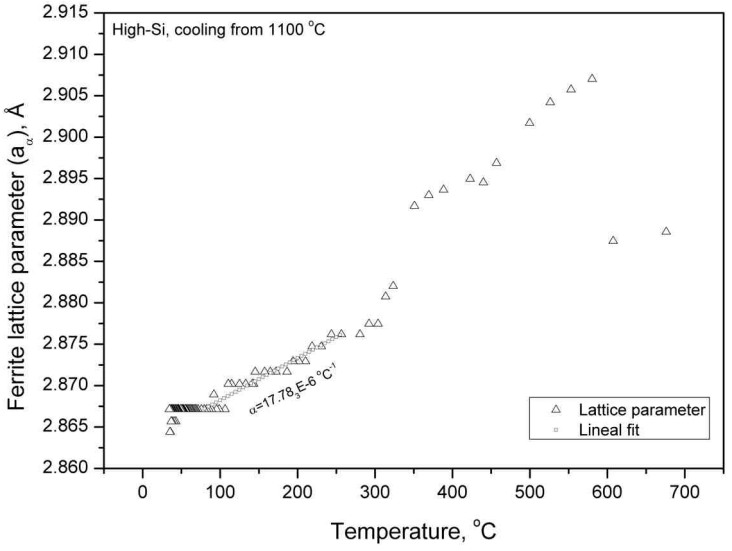

(b) *Ferrite lattice parameter*

Figure 6.18: *The austenite and ferrite lattice parameters of High-Si steels as a temperature while cooling from 1100 °C.*

in the austenite content during holding at the room temperature. After cooling from 1100 to 40 ^{o}C, the sample contained about 5.3 % of untransformed austenite. After cooling to room temperature (25 ^{o}C), the untransformed (retained) austenite content in the sample was 4.8 %. In this case also, the austenite is not found to be stable upon further holding at room temperature. After holding at room temperature for 1900 s, the untransformed austenite in this sample was reduced to 3.9 %. Thus, about 1.1 % of austenite was decomposed during the room temperature holding period.

6.4 *In-situ* dilatometry studies

The *in-situ* synchrotron diffraction results indicated that a significant amount of austenite ($\simeq$ 2 %) is transforming at room temperature after cooling from austenisation temperatures, as shown in figure 6.13 and 6.19. It is also reported that the properties of welded TRIP steel changes with time after welding [3]. In order to explore whether the possible room temperature transformation of austenite takes place after welding, dilatation measurements were carried out on the welded TRIP steel samples.

High-Al TRIP steel (table 3.1) plates with a heat treatment HT800/400 (table 3.3) were gas tungsten arc welded using the welding parameters given in table 4.1. Immediately after welding, samples with a size of 5 x 12 mm were cut from the welded plates, covering the fusion and heat affected zones. Figure 6.20 schematically shows the area from which the samples were taken for the dilatometry analysis. Samples were then transferred to a Bähr 805A dilatometer with a minimum possible time (50 minutes), 2 days and 5 hours and, 6 days after welding. With a minimum possible sample preparation time and equipment setting-up time, the dilatation measurements were able to be started within 50 minutes after welding. One sample, cut from the welded plate, was quenched in liquid nitrogen to facilitate the transformation of austenite retained at room temperature to martensite. Although, this cooling will not necessarily lead to complete transformation of retained austenite to martensite, it is known that a considerable decrease in retained austenite content occurs after cooling to liquid nitrogen temperature [4]. In order to avoid the effect of ambient temperature variation on the dilatation of the samples, samples were heated to 100 ^{o}C at 1 ^{o}C s^{-1} and held there for 50000 s. The thermal expansion of the samples while heating to 100 ^{o}C and the dilatation behaviour during holding at 100 ^{o}C were then recorded, together with heating temperature and time.

Figure 6.21 shows the thermal expansion behaviour of the samples while heating to 100 ^{o}C. It can be clearly seen that the expansion behaviour of the steel samples taken 50 minutes after the welding differ significantly from the samples quenched in liquid nitrogen, 2 days and 5 hours and, 6 days after welding. Moreover, the expansion behaviour of the sample quenched in liquid nitrogen is similar to that of sample kept at room temperature for 6 days after welding. This difference in the thermal expansion behaviour clearly indicates that changes are happening with time after welding. Ideally, if there is no change in microstructure with time, samples are expected to expand with temperature following the same expansion slope under the

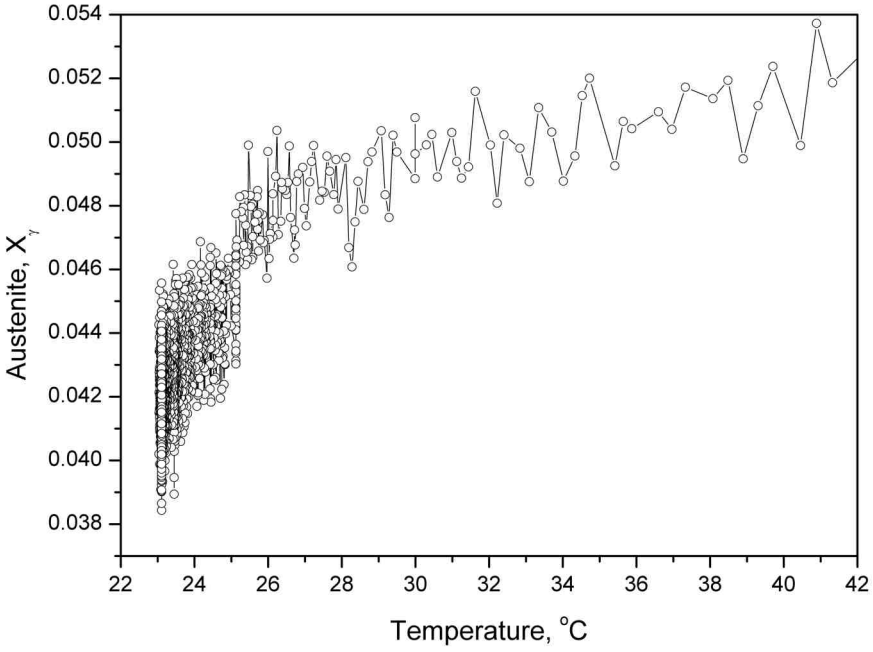

(a) *Austenite fraction with cooling temperature*

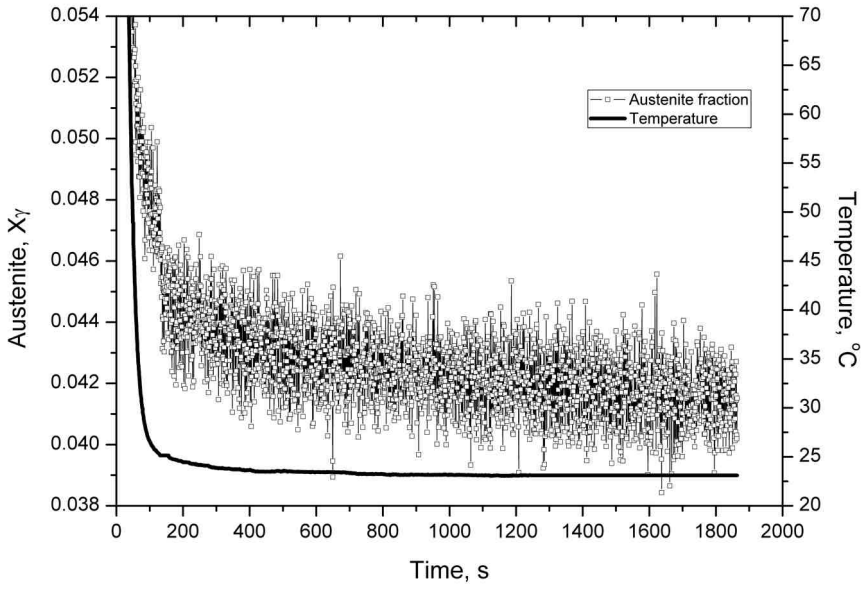

(b) *Austenite fraction with time after cooling from 1100 °C*

Figure 6.19: *The austenite content of High-Si steel after cooling from 1100 °C to room temperature and subsequent holding.*

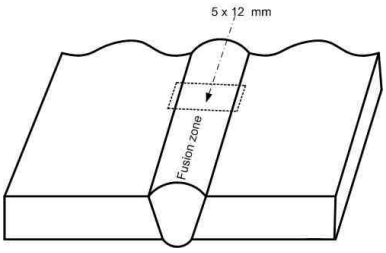

Figure 6.20: *Schematic view of the samples used for dilatometric studies on welded TRIP steel samples.*

same heating conditions. However, the difference in the expansion behaviour with time after welding confirms the time-dependant changes occurring in welded TRIP steel.

The dilatation behaviour of the samples, while holding at 100 ^{o}C, also shows difference with time after welding (figure 6.22). The sample taken 50 minutes after welding shows a continuous expansion with holding time at 100 ^{o}C whereas samples tested 2 days and 5 hours and, 6 days after welding initially contracts over the first 5000 s and then expands with time.

6.5 Discussions

The fast heating and cooling involved in a typical weld thermal cycle, demands characterisation techniques with high time-temperature resolution to study the phase transformation kinetics, such as synchrotron X-ray diffraction. A previous synchrotron X-ray diffraction study on the welded TRIP plates indicated a significant amount of austenite retained in the heat affected and fusion zones (figure 5.10). The retained austenite fraction in the heat affected zone varied along the welded plate depending on the peak temperatures reached during the weld thermal cycle (section 5.2.3). The thermal cycle examined in the *in-situ* diffraction studies simulated the heating and cooling cycles of a GTA weld thermal cycle. The peak temperature reached at a point 4.2 mm from weld centre line and 1.1 mm from the fusion boundary was about 1000 ^{o}C. At 3.8 mm from the weld centre line, a peak temperature of 1100 ^{o}C was achieved (figure 4.1). The 2D synchrotron diffraction patterns were recorded *in-situ* every 0.6 s and temperature recordings were carried out at 0.1 s intervals, while applying the thermal cycle. This resolution was found to be sufficient to calculate the fractions of co-existing phases and their lattice parameters with a better time-temperature resolution than conventional X-ray diffraction, dilatometry or magnetic saturation techniques.

Apart from the mechanical properties, the generation of residual stresses which determine the buckling and bending distortion of welded plates are greatly influenced by the kinetics of phase transformations [5]. In TRIP steels where transformation

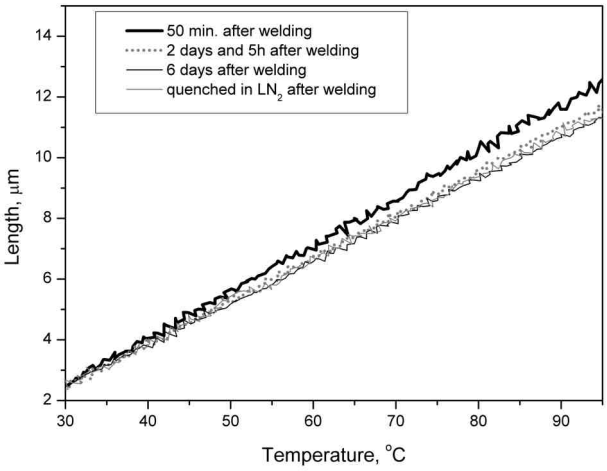

Figure 6.21: *Thermal expansion behaviour of the GTA welded High-Al steel samples while heating to 100 °C.*

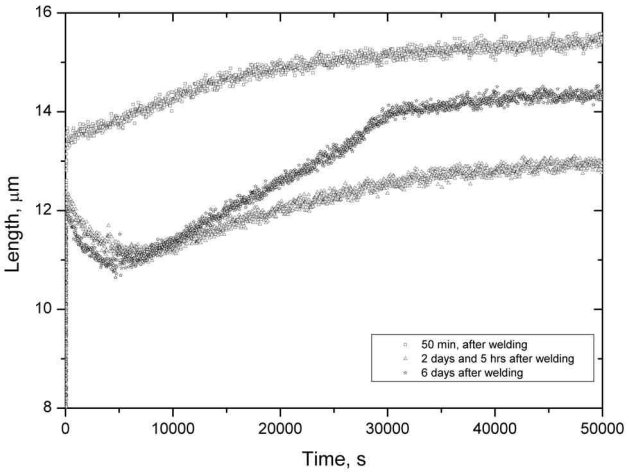

Figure 6.22: *The dilatation behaviour of the GTA welded High-Al TRIP steel sample while holding at 100 °C.*

plasticity controls the required mechanical properties, it is also important to study the thermal expansion/contraction behaviour of co-existing phases along with the phase transformation kinetics [6, 7]. Moreover, the measurement of lattice parameters and thereby the thermal expansion co-efficients of individual phases and quantification of microstructural phases as a function of temperature yields essential fundamental material data for the physical simulation of material behaviour during a weld thermal cycle [8].

In-situ synchrotron diffraction in the High-Al and High-Si TRIP steels was used to study the effect of composition and the austenisation temperature on the kinetics of phase transformation in a given thermal cycle. Although the effect of alloying elements on the transformation behaviour of austenite in TRIP steel is well documented [9, 10], recent studies indicate an effect of prior austenite grain size on the transformation kinetics and the onset of martensitic transformation in low alloyed steels [11, 12]. In this study, the effect of composition is shown in the first part of the results (see section 6.2) where High-Si and High-Al TRIP steel samples were heated to 1000 ^{o}C and the kinetics of retained austenite decomposition, austenite formation and transformation kinetics were presented along with the lattice parameters of austenite and ferrite with temperature. High-Si steel samples were also heated to 1100 ^{o}C and the results were compared with the experimental data on the same steel sample heated to 1000 ^{o}C to study the effect of austenisation temperature and in turn the prior austenite grain size on the transformation during cooling. Both results showed the transformation of austenite while holding at room temperature after continuously cooling from the austenisation temperatures. The time dependant changes that are happening in welded TRIP steels were also confirmed by the dilatometry analysis. In the following discussions section, these results are analysed and a possible explanation for the time-dependant changes occure in welded TRIP steels is given.

6.5.1 Effect of composition

The amount of retained austenite present in the base metal High-Al and High-Si samples (condition HT800/400 in figure 3.3) is 10.3 and 15.4 % respectively. This result is agreement with those obtained by magnetic measurements (section 5.1) and quantitative synchrotron diffraction analysis carried out on the welded plates (figure 5.10) with its experimental accuracy and measurement principle, close to the austenite content measured by the synchrotron measurements.

During heating to 1000 ^{o}C, the retained austenite present in both steels is stable only up to 290 ^{o}C. Above this temperature, the retained austenite fraction starts to decrease slowly, but when the temperature reaches 450 ^{o}C, the decomposition rate is as high as 2.5 % s^{-1} in High-Al steel. In a typical weld thermal cycle, as shown in figure 4.1, a peak temperature of 290 ^{o}C is achieved at about 9 mm from the weld centre line. Thus in comparison to conventional auto-body steels, welded TRIP steels ought to have an extended heat affected zone where the base metal microstructure is altered by the weld thermal cycle. In the conventional auto-body steels, a heat affected zone weld thermal cycle where the peak temperature reaches about 300 ^{o}C seldom

significantly alters the microstructure. However, in TRIP steels, decomposition of the retained austenite at low temperatures ($\geq$290 ^{o}C) eventually leads to inhomogeneous distribution of microstructure in a larger area, as seen in figure 5.10.

The decomposition of retained austenite during heating of a Fe-0.18C-1.8Si-1.5Mn (wt. %) TRIP steel was also observed earlier but that study reported that the decomposition started from 340 ^{o}C compared to 290 ^{o}C in the present study [2]. In the present study, the High-Si steel contains 0.4 wt. % less silicon and 0.01 wt. % higher carbon than the steel used in the previous study (table 3.1). Silicon is known suppress the precipitation of iron carbides from the austenite and as a result, despite containing slightly higher carbon, the decomposition of austenite is evident at a slightly lower temperature in the present study.

From this study, it is found that the rate of decomposition of retained austenite $\left(\frac{d(x_\gamma)}{d(t)}\right)$ is similar in both steels while heating from 290 to 440 ^{o}C. The High-Si steel showed a decomposition rate of 1.5 % s^{-1} at 400 ^{o}C whereas a maximum decomposition rate of 2.5 % s^{-1} was recorded for High-Al steel at 450 ^{o}C. A faster rate of decomposition is observed in High-Al because the base metal of High-Al steel contained a higher amount of retained austenite (15.4 %) compared to the High-Si steel which contained only 10.3 %. Moreover, the ability of aluminium to suppress iron carbide formation is also reported to be lower than that of silicon due to its slightly higher solubility in the iron carbides. The decomposition of retained austenite was also confirmed by the thermo-magnetic measurements carried out on a TRIP steel sample where the formation of ferro-magnetic ferrite and transient carbides were observed while heating above 295 ^{o}C (see section 5.1.3). During this synchrotron diffraction study, there were no diffraction spot/patterns of transient carbides observed possibly due to their limited size, volume and distribution. However, the formation of the transient carbides during the decomposition of retained austenite cannot be neglected as thermo-magnetic measurements and previous studies reported the possibilities of their formation [13, 14].

The austenite content in High-Al and High-Si samples reached a minimum when the temperatures reached 528 and 550 ^{o}C, respectively. Thus, during welding, when a heat affected zone thermal cycle reaches peak temperatures of about 525 to 550 ^{o}C, a minimum of austenite can be expected to be retained in the microstructure for this steels. This result is also reflected during the quantification of retained austenite in GTA welded TRIP steels where a distinctive low austenitic zone is found when the peak temperature reached between 500 to 600 ^{o}C (figure 5.10).

The new austenitic rings were observed during heating when the temperature reached 529 and 551 ^{o}C respectively in High-Al and High-Si samples. These A_{c_1} temperatures are far less than the equilibrium A_{e_1} temperatures (719 and 702 ^{o}C respectively in High-Al and High-Si steels) calculated from a thermodynamic database TCFE5 using Thermocalc^{TM} (figure 3.1). The nucleation of new austenite at low temperatures can occur due to the chemical heterogeneity and high carbon containing regions (where prior retained austenite grains were present) in the microstructure. The retained austenite contained 1.2 and 1.04 wt. % carbon respectively in High-

Si and High-Al samples (table 3.3). This high carbon containing retained austenite also becomes more enriched with carbon due to the formation of ferrite during its decomposition. The high carbon containing sites are known to facilitate the nucleation of austenite during heating [15]. In addition, the EPMA measurements of these steel base metal samples indicated a partitioning of manganese among the co-existing phases (figure 3.5). As a result, nucleation of austenite may start earlier than the equilibrium austenite nucleation temperature. Based on the peak temperature in the heat affected zone, several areas in this zone locally enter into the inter-critical ($\alpha + \gamma$) region at lower temperatures (from 529 and 551 ^{o}C respectively, in High-Al and High-Si steels).

The decomposition kinetics of retained austenite during heating is also reflected in its lattice parameter. The lattice parameter of the austenite was found to increase linearly with temperature up to a temperature of 290 ^{o}C during heating. The linear thermal expansion co-efficient of austenite (a_γ) during heating was determined to be 27.85_9x10^{-6} ^{o}C^{-1}, which is a more realistic value than the previously reported value of 24.53x10^{-6} ^{o}C^{-1}, extrapolated from a high temperature (1273 ^{o}C) [16]. Once the decomposition of retained austenite starts above 290 ^{o}C, the lattice parameter increases initially due to the possible enrichment of carbon in the remaining austenite. This deviation in linearity was also reported by Choi *et al.* [2] while heating a retained austenite containing steel. A further heating above 290 ^{o}C, the lattice parameter of austenite in both steels decreases at 430 ^{o}C possibly due to the depletion of carbon from the austenite matrix, driven by the formation of iron carbides.

Conversely, the lattice parameter of ferrite a_α shows only a linear variation with temperature up to A_{c_1}, indicating that compositional or structural changes during heating do not play any significant role. The calculated thermal expansion co-efficient of ferrite in both steels showed a difference of 1.16x10^{-6} ^{o}C^{-1} (table 6.1). Given that the solubility of carbon in ferrite is very low, the difference in the lattice parameters and in the a_α can be attributed to the variation of the substitutional alloying elements aluminium and silicon. The austenite thermal expansion co-efficient also showed a difference of 0.95x10^{-6} ^{o}C^{-1}. This difference is expected as the retained austenite in both steels contained different carbon concentrations (figure 3.9). Moreover, the presence of silicon in austenite is not known to affect the lattice parameter of austenite, while, a strong influence of aluminium on the lattice parameter of austenite is reported [17].

The results indicate the effect of composition on the lattice parameters and thermal expansion co-efficient of ferrite and austenite. These temperature and composition dependant lattice parameters and thermal expansion co-efficient measurements provide vital input parameters for the simulation of material response to welding, especially for the prediction and mitigation of residual stresses after welding where it is normally assumed that the thermal expansion varies linearly with temperature and the effect of composition is often neglected [8].

The formation of new austenite rings was observed once the sample temperature exceeded A_{c_1} and thereafter the lattice parameter of austenite was found to be affected by the combined effects of carbon in austenite (given by the lever rule) and

thermal expansion. The rate of transformation of ferrite to austenite above A_{c_1} varies significantly between the High-Si and High-Al steels. For the High-Si steel, a maximum austenite formation rate of 24 % s^{-1} was recorded whereas for the High-Al steel, the maximum rate of formation was only 18 % s^{-1} (figure 6.6). The difference in the rate is mainly due to the sluggishness in ferrite transformation provided by the presence of aluminium in the High-Al steel. In section 4.4.2, it was shown that strong partitioning of aluminium causes ferrite stabilisation on the fusion boundaries of welded High-Al TRIP steel. It can also be seen from this results that the decomposition of ferrite upon heating above A_{c1} is slower in the High-Al steel and even after heating to 1000 ^{o}C, only about 99 % of austenite was formed. Whereas in High-Si steel, a complete austenisation was achieved at 805 ^{o}C with a comparatively faster transformation rate than High-Al steel.

During cooling from 1000 ^{o}C, the rate of austenite transformation to ferrite in High-Al steel was always higher than High-Si steel down to a temperature of 484 ^{o}C, confirming the ferrite stabilisation with the presence of aluminium in steel (figure 6.10). Moreover, the first new ferrite diffraction spots were also observed in High-Al steel at 974 ^{o}C, which is much higher than for the High-Si steel, which showed new ferrite rings during cooling at 727 ^{o}C.

In High-Si steel, the transformation of austenite is sluggish down to 420 ^{o}C and upon cooling below this temperature a rapid transformation of austenite is observed with a maximum transformation rate of 22 % s^{-1} (figure 6.9). This kind of transformation behaviour has already been reported for austenite transformation to martensite during continuous cooling from a fully austenitic temperature, as in the present case [18]. However, in High-Al steel, the austenite transformation is continuous from 1000 ^{o}C to 480 ^{o}C. Upon cooling below 480 ^{o}C, there is an increase in transformation rate observed in this steel and at 405 ^{o}C, a maximum transformation rate of 14 % s^{-1} was measured, possibly due to the martensite formation from austenite during cooling. The calculated martensitic start (M_s) temperatures for High-Si and High-Al steels are 407 and 409 ^{o}C respectively (using the well known Andrews' euqation) [19]. The faster transformation rates of austenite were observed during cooling below 420 and 480 ^{o}C in High-Si and High-Al steels respectively, which can be due to the onset of martensite transformation. However, the start temperatures do not correlate with the calculated M_s temperature from Andrews' equation because the equation suggested by Andrews does not include the effect of silicon and aluminium.

The amount of austenite left untransformed after cooling to 40 ^{o}C is 6.5 and 7 % in High-Si and High-Al steel. This untransformed austenite fraction was not found to be constant during further cooling to room temperature ($\simeq$23 ^{o}C). In GTA welded High-Si and High-Al TRIP steel plates, at a point in HAZ where the peak temperature achieved was 1000 ^{o}C, about 8 to 9 % of retained austenite was obtained (figure 5.10). There is about 1 to 2 % difference between the real welded plate and the experimentally simulated condition described in this chapter. This is mainly because although the peak temperatures are similar, the heating and cooling rates achieved during welding are slightly different than the one is used in the simulation. Moreover, in actual welding, there is always a strong temperature gradient present across the

HAZ and the possibilities of diffusion of alloying elements in and around HAZ from the base metal to the fusion zone makes comparison difficult between a real weld thermal cycle with a peak temperature of 1000 ^{o}C and a simulated thermal cycle with the same peak temperature.

Although the kinetics of austenite transformation during cooling showed a possibility for martensite transformation in High-Si steel, in High-Al steel it does not explicitly show the nature of transformation such as formation of bainite or martensite from austenite. However, the variation in the lattice parameter with cooling temperature does show some qualitative information about the possible bainite and martensitic transformations in both steels. During cooling, the ferrite lattice parameter in High-Al steel showed two distinctive shifts in linearity, one at 613 ^{o}C and another at around 450 ^{o}C (figure 6.11b). The calculated bainitic start (B_s) for the High-Al steel is 630 ^{o}C (using Steven and Haynes empirical equation) [20]. This equation however does not include the effect of aluminium and silicon when calculating B_s. The change in the slope of the ferrite parameter at 613 ^{o}C most likely correlated to the formation of bainite from austenite during cooling. In the High-Si steel, the ferrite lattice parameter showed a distinctive jump at from 460 ^{o}C to 310 ^{o}C, possibly due to the formation of martensite from austenite. There are no distinctive changes in the slope of the ferrite lattice parameter at around 600 to 650 ^{o}C which can otherwise be correlated to bainite formation from austenite in this High-Si steel.

The results indicate that the variation of lattice parameters of ferrite and austenite with cooling are not linear with temperature and the effect composition and the transformation stresses are reflected when the transformation of austenite proceeds. Thus, while simulating the microstructural evolution during welding and calculating the residual stresses, it is important to incorporate the temperature dependant lattice parameters of individual phases to reflect the effect of composition and transformation stress associated with the phase transformation.

6.5.2 Effect of austenisation temperature

During welding, the HAZ is subjected to a weld thermal cycle where each point in HAZ reaches a different peak temperature. When the temperatures enter the intercritical (α+γ) or the fully austenitic region, the newly formed austenite grain sizes may vary based on the peak temperatures. In addition, the faster heating rates involved in a thermal cycle can also cause strong compositional gradients at the grain level, especially with respect to substitutional elements such as Mn, Si and Al. Thus, it is important to study the effect of peak temperatures on the transformation of austenite during cooling to room temperature. In this study, High-Si steel samples were heated to 1100 ^{o}C and cooled at the same rates as reported in section 6.2. After cooling from 1100 ^{o}C, the first ferrite diffraction spots were observed at 862 ^{o}C as compared to 727 ^{o}C for the steel cooled from 1000 ^{o}C. The equilibrium ferrite nucleation temperature (A_{c_3}) temperature for this steel is 885 ^{o}C (figure 3.1a). Apart from compositional homogenisation and austenite grain coarsening effects, the cooling rates from the peak temperature also dictate the formation of ferrite from austenite.

A maximum cooling rate of 90 ^{o}C s^{-1} is reached in between 1100 to 890 ^{o}C while cooling from 1100 ^{o}C, whereas while cooling from 1000 ^{o}C, this maximum was also achieved between 1000 to 900 ^{o}C. Below 890 ^{o}C, both samples were cooled at similar cooling rates (figure 6.15).

The transformation rate of austenite is higher on average when cooling from 1100 ^{o}C to 350 ^{o}C. In High-Si steel, heating to peak temperatures of 1000 or 1100 ^{o}C results in complete austenisation. Thus, in the sample heated to 1100 ^{o}C, apart from compositional homogenisation, the austenite grains are expected to grow. An increase in grain size should in general reduce the rate of transformation of austenite because of the reduction in grain boundary nucleation sites [21, 22]. However, the growth of acicular products such as bainite can be constrained by the grain size and thereby the growth can be retarded [22, 23]. During cooling from 1100 ^{o}C, when the temperature reaches 600 ^{o}C, the transformation rate of austenite increases suddenly (figure 6.17). Whereas while cooling from 1000 ^{o}C, there is no noticeable change in transformation rate observed around 600 ^{o}C. The lattice parameter of ferrite during cooling from 1100 ^{o}C clearly shows an steep increase when the temperature reaches 600 ^{o}C and a change in slope at 460 ^{o}C (figure 6.18b). Conversely, the ferrite lattice parameter during cooling from 1000 ^{o}C showed a clearly distinguishable increase only at 460 ^{o}C. Thus, from the growth rate curves and changes in the lattice parameters, it can be concluded that while cooling from 1100 ^{o}C, there is a strong possibility that both bainitic and martensitic transformations predominate while when cooling from 1000 ^{o}C, the austenite primarily transforms to martensite.

The amount of austenite left untransformed at 40 ^{o}C after cooling from 1100 ^{o}C is 5.3 % which is 1.2 % less than that in the sample cooled from 1000 ^{o}C. As in the latter case, the untransformed austenite is still found to transforming even after sample reached room temperature (figure 6.19).

The results indicate that based on the peak temperature reached in HAZ, the nature and kinetics of transformation will vary and the lattice parameters of co-existing phases will change based on the kinetics of the transformation. Moreover, the amount of austenite retained at room temperature will also change with peak temperature even after a complete austenisation prior to cooling.

6.5.3 Transformation of austenite at room temperature

In-situ synchrotron diffraction analysis in TRIP steel samples showed that a significant amount of austenite is left untransformed at room temperature after cooling from the austenisation temperatures. The High-Al steel contained 7 % of retained austenite at 25 ^{o}C after cooling from 1000 ^{o}C. After holding at room temperature (23 to 24 ^{o}C) for 2110 s, the retained austenite content reduced to 5.4 %. Thus about 1.6 % of retained austenite left in the sample transformed at room temperature holding (section 6.2.6). Similarly, in the High-Si steel, the retained austenite content reduced from 6 to 5 % and 4.8 to 3.9 % after cooling from 1000 and 1100 ^{o}C respectively. This is quite significant in TRIP steels where the mechanical properties are severely affected by the retained austenite content in the microstructure.

The dilatometric analysis carried out on the welded High-Al TRIP samples showed the change occurred at room temperature after welding. The thermal expansion behaviour can be a qualitative indication to the microstructural constituents present in the material, i.e. for a given microstructure, thermal expansion behaviour must be the same at a given heating rate. Figure 6.21 shows the thermal expansion behaviour of samples taken 50 minutes, 2 days and 5 hrs, 6 days and quenched in liquid nitrogen after the welding. A large variation in the thermal expansion behaviour of these samples can be seen with holding time after welding. It can be concluded from the difference in the thermal expansion behaviour that the microstructures of the samples are not exactly the same and that they are changing with time. The thermal expansion behaviour of the sample which was quenched in liquid nitrogen immediately after the welding is similar to the samples aged at room temperature for 6 days. It is known that quenching in liquid nitrogen transforms retained austenite into martensite [4]. The similarities in the dilatation of the sample quenched in liquid nitrogen and the sample aged for 6 days shows that there must be a significant amount of decomposition of retained austenite at room temperature. There is also a significant difference in dilatation behaviour of welded sampels observed while isothermal holding at 100 ^{o}C (figure 6.22). During isothermal holding at 100 ^{o}C, the sample which was taken 50 minutes after welding showed continuous expansion, whereas the samples which were taken after 2 and 6 days of ageing at room temperature contracted initially and then started expanding during prolonged holding. In steels, volume expansion during phase transformation is mainly due to either austenite to ferrite or martensite transformations and contraction in volume is attributed to the tempering of martensite [24]. Possible decomposition of retained austenite to low temperature bainite or martensite causes expansion in the dilatation when the sample was tested 50 min after welding. After ageing the samples at room temperature for 2 or more days, all the unstable austenite decomposes to bainite or martensite. When these samples were heated to 100 ^{o}C, the tempering kinetics of martensite dominates the decomposition of left over austenite, resulting in a net contraction. Waterschoot *et al.* reported a similar low temperature dilatation behaviour of multi-phase steels with 12 % retained austenite in the microstructure. It was reported that the samples contracted initially due to the tempering of martensite at 250 ^{o}C and started expanding once the kinetics of tempering becomes lower than the decomposition kinetics of austenite [24].

It was already reported that the properties of welded TRIP steels are not stable with time after the welding during commercial production [25]. Zhao *et al.* showed a time dependent strain development under constant stress due to the decomposition of retained austenite to martensite in TRIP steels [26]. It is possible to explain the decomposition of retained austenite at room temperature due to the build up of stored energy from the transformation stresses under fast cooling rates. Further experimental evidence should be sought to consolidate this finding. The mechanism driving room temperature phase transformation is, as yet, unknown. The measured data shows instability in the volume fraction, which is significantly greater than the measurement error. It is likely that the energy driving the transformation is derived

from stress relaxation, possibly initiated by hydrogen diffusion, although to date, no experimental evidence is available to support such a speculation.

In order to confirm the effect of room temperature transformation of austenite after applying the weld thermal cycle or as in this case, after continuous cooling from the austenisation temperature, mechanical properties of welded TRIP steels were evaluated with several time intervals after welding. These results will be presented in chapter 7 and the properties will be correlated with changes in the austenite content at room temperature.

6.6 Conclusions

The decomposition, formation and transformation kinetics of austenite in TRIP steel samples was studied by *in-situ* synchrotron X-ray diffraction. Using a purpose built high temperature furnace, with a high time-temperature resolution, phase transformation kinetics were studied under conditions simulating weld thermal cycle at points in the heat affected zone where peak temperatures reaches 1000 and 1100 ^{o}C. The results show that during heating, retained austenite present in the sample starts to decompose and the lattice parameter of the austenite increases linearly with temperature at temperatures up to 290 ^{o}C. Heating up to 500 ^{o}C resulted in the decomposition of almost half of the retained austenite present in the base metal. The presence of aluminium in TRIP steel showed a strong tendency for stabilisation during heating by retarding austenite formation. A fully austenitic structure was obtained after heating to 1000 and 1100 ^{o}C in the High-Si steel and the combined effect of carbon and thermal expansion resulted in changes in the lattice parameter of austenite. A linear variation in lattice parameter of ferrite was observed during heating in both steels.

During cooling from 1000 ^{o}C, the changes in ferrite lattice parameter and growth kinetics indicated that in High-Si steel, the transformation of austenite to martensite is dominant, whereas after cooling from 1100 ^{o}C in the same steel and also in the High-Al steel, there are possibilities for both bainite and martensitic transformation from austenite. Surprisingly, the austenite content was found to decrease with time during holding at room temperature, changing from 7.5 to 5.7 wt % over a period of 2110 s. The reduction in austenite content may explain the time dependant changes in mechanical properties observed in welded TRIP steels.

References

[1] H.Sharma, A.C.Wattjes, M.Amirthalingam, T.Zuidwijk, N.Geerlofs and S.E.Offerman, 'Multipurpose furnace for *in-situ* studies of polycrystalline materials using synchrotron radiation', *Review of scientific instruments*, 80, 123301–1 – 123301–7, 2009.

[2] S.D.Choi, H.S.Kim, J.H.Je and S.H.Park, 'Annealing behaviour of retained

austenite in low carbon steel: Real time synchrotron x-ray scattering study.', *Journal of Material Science Letters*, 21, 353 – 355, 2002.

[3] T.van der Veldt, 'Ageing in weded TRIP steels', 5th knowledge exchange meeting with SMI on joining, Corus R&D and T, 2007.

[4] N.H.van Dijk, A.M.Butt, L.Zhao, J.Sietsma, S.E.Offerman, J.P.Wright and S.van der Zwaag, 'Thermal stability of retained austenite in TRIP steels studied by synchrotron X-ray diffraction during cooling', *Acta Materialia*, 53, 5439–5447, 2005.

[5] P.J.Withers and H.K.D.H.Bhadesia, 'Overview: Residual stress, part 2 - nature and origin', *Materials Science and Technology*, April, 366 – 375, 2001.

[6] H.Murakawa, 'Theoretical prediction of residual stresses in welded structures', *Welding International*, 11(8), 599 – 604, 1997.

[7] P.Ferro, H.Porzner, A.Tiziani1 and F.Bonollo, 'The influence of phase transformations on residual stresses induced by the welding process - 3d and 2d numerical models', *Modelling and Simulations in Material Science and Engineering*, 14, 117 – 136, 2006.

[8] E.M.van der Aa, R.G.Thiessen, M.Amirthalingam, M.J.M.Hermans, J.Sietsma and I.M.Richardson, 'Influence of a trailing heat sink on the microstructure and stress distribution in DP600 welds', *Mathematical modelling of weld phenomena*, 8, 387 – 407, 2007.

[9] B.C.De Cooman, 'Structure-properties relationship in TRIP steels containing carbide-free bainite', *Current Opinion in Solid State and Material Science*, 8, 285–303, 2004.

[10] S.J.Kim, C.G.Lee, I.Choi and S.Lee, 'Effects of heat treatment and alloying elements on the microstructures and mechanical properties of 0.15 wt. % C transformation induced plasticity aided cold rolled steel sheets', *Metallurgical and Material Transactions A*, 32A, 505–514, 2001.

[11] S.J.Lee, J.S.Park and Y.K.Leeb, 'Effect of austenite grain size on the transformation kinetics of upper and lower bainite in a low-alloy steels', *Scripta Materialia*, 59, 87 – 90, 2008.

[12] H.S.Yang and H.K.D.H.Bhadesia, 'Austenite grain size and the martensite-start semperature', *Scripta Materialia*, 60, 493 – 295, 2009.

[13] B.K.Jha and N.S.Mishra, 'Microstructural evolution during tempering of a multiphase steel containing retained austenite', *Material Science and Engineering A*, A263, 42–55, 1999.

[14] M.Amirthalingam, M.J.M.Hermans, L.Zhao and I.M.Richardson, 'Quantitative analysis of microstructural constituents in welded trasformation induced plasticity steels', *Metallurgical and Materials Transactions A*, 41A, 431 – 439, 2010.

[15] V.I.Savran, S.E.Offerman and J.Sietsma, 'Austenite nucleation and growth observed on the level of individual grains by three-dimensional x-ray diffraction microscopy', *Metallurgical and Material Transactions A*, 41A, 583 – 591, 2010.

[16] M.Onink, C.M.Brakrnan, F.D.Tichelaar, E.J.Mittemeijer and S.van der Zwaag, 'The lattice parameters of austenite and ferrite in fe-c alloys as a function of carbon concentration and temperature', *Scripta Metallurgica et Materialia*, 29, 1011 – 1016, 1993.

[17] D.J.Dyson and B.Holmes, 'Effect of alloying additions on the lattice parameter of austenites', *Journal of the iron and steel institute*, May, 469 – 474, 1970.

[18] R.E.Reed-Hill and R.Abbaschian, Physical metallurgy principles, 3rd edn., PWS Publishing company, 1994.

[19] K.W.Andrews, 'Empirical formulas for the calculation of some transformation temperatures', *Journal of the Iron and Steel Institute*, 203, 721 – 727, 1965.

[20] W.Steven and A.J.Haynes, 'The temperature of formation of martensite and bainite in low-alloy steels', *Journal of Iron and steel Institute*, 183, 349–359, 1956.

[21] J.Barford and W.S.Owen, 'The effect of austenite grain size and temperature on the rate of the bainite transformation', *Journal of Iron and Steel Institute*, 197, 146, 1961.

[22] R.E.Reed-Hill and R.Abbaschian, Physical metallurgy principles, 3rd edn., PWS Publishing company, 1994.

[23] H.K.D.H.Bhadesia, Bainite in steels; Transformations, Microstructure and Properties, 2nd edn., IOM Commuication Ltd, 1 Carlton House terrace, SW1Y 3DB, London, 2001.

[24] T.Waterschoot, K.Verbeken and B.C.De Cooman, 'Tempering kinetics of the martensitic phase in dp steel', *ISIJ International*, 46, 138–146, 2006.

[25] Corus R&D and T, 'Internal communication', 2005-2009.

[26] L.Zhao, B.Mainfroy, M.Janssen, A.Bakker and J.Sietsma, 'Time-dependent strain development under constant stress in TRIP steels', *Scripta Materialia*, 55, 287 290, 2006.

Chapter 7

Mechanical properties of welded TRIP steels

Previous chapters described how a carefully designed microstructure of the TRIP steels is affected by a weld thermal cycle. Quantitative microstructural analysis also showed that, based on the peak temperatures of the weld thermal cycle, the presence of retained austenite in the heat affected and fusion zones (HAZ and FZ), an essential component which dictates the mechanical properties of TRIP steel, varies across the welded zone. *In-situ* synchrotron X-ray diffraction also indicated that a significant amount of austenite (about 1.5 to 2 %) transforms at room temperature after cooling from the fully austenitic region. During the commercial manufacturing of automobiles, where TRIP steel is largely applied, steel is subjected to various mechanical forming operations immediately after welding. Thus, the mechanical properties of the welded TRIP steels become very critical in order to improve the commercial applicability of these steels. Moreover, it is also important to evaluate the mechanical properties of welded TRIP steels with respect to post welding time in order to study effect of room temperature transformation of austenite after welding. In this chapter, the mechanical properties of welded TRIP steels are presented. The properties are evaluated using micro-hardness, tensile and Erichsen cupping tests and correlated with the weld zone microstructure. The tensile and Erichsen cupping tests were also carried out on welded TRIP steels with respect to welding time to study possible changes in properties of welded TRIP steels due to room temperature transformation of austenite after welding.

7.1 Micro-hardness variation in welded TRIP steels

In general, the mirco-hardness measurements provide first hand information about the variation in the mechanical properties of welded steels across the weld zones. Measurements are carried out transverse to the weld centre line towards the base

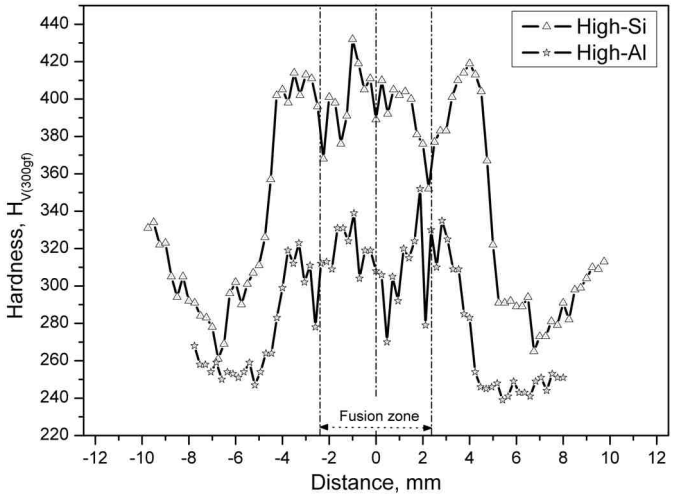

Figure 7.1: *The Hardness variation across the weld zone of GTA welded TRIP steel plates*

metal through the fusion and heat-affected zones and the hardness values obtained can be correlated with the microstructural constituents. Figure 4.19 showes one such measurement where hardness variation over the weld zone of GTA welded High - Al steel indicates a softer zone adjacent to an equi-axed grained weld centre line. Table 4.1 describes the welding parameters used for the welding. The samples from these plates were extensively characterised for elemental distribution (see chapter 4) and quantitative phase analyses were carried out using magnetic saturation and synchrotron X-ray diffraction (chapter 5). Quantitative analysis using synchrotron x-ray diffraction indicated that based on the peak temperatures reached during a weld thermal cycle, the amount of austenite retained across the HAZ varied (figure 5.10). In order to correlate the microstructure-properties relationship in welded TRIP steels, hardness measurements were carried out on GTA welded High-Si and High-Al TRIP steel plates.

The hardness variation across the fusion zones of GTA welded High-Si and High-Al TRIP steel plate is shown in figure 7.1. The hardness plots show that the overall hardness of welded High-Si steel is higher than welded High-Al steel. The hardness values decrease gradually in High-Si steel while moving from 10 mm to 7 mm from the weld centre line. This is quite significant since in this zone, the quantitative microstructural analysis indicated that the retained austenite content also decreases gradually and at about 8 mm from the weld centre line, the welded plate had a minimum retained austenite content of 1 % (figure 5.10b). The peak temperature reached at this zone is less than 600 ^{o}C, and as shown in previous chapters, when the temper-

ature does not exceed A_{c_1} (onset temperature of austenite formation during heating), the retained austenite present in the steel decomposes. The hardness measurement in the welded High-Si steel shows the effect of this retained austenite decomposition as hardness drops significantly from 340 to 260 $HV_{(300gf)}$. However, in the High-Al steel, there is no steep decrease in hardness found in this zone ($\pm$10 mm to $\pm$7 mm from the weld centre line). Quantitative microstructural analysis in High-Al steel has also shown that there is no significant reduction in retained austenite in this zone in contrast to the High-Si steel (figure 5.10a). In a similar area of the HAZ in welded dual phase (DP) steels, a reduction in hardness was observed due to the tempering of martensite present in the base metal microstructure [1], whereas in TRIP steels, the reduction in the hardness in the HAZ is mainly due to the decomposition of retained austenite.

The hardness gradually increases while moving from $\pm$7 mm towards the fusion boundaries. The peak temperatures reached in this zone are above A_{r1} due to which the newly formed austenite transforms to martensite during cooling after welding, resulting in an increased hardness. The hardness values drops again close to the fusion boundaries in both steels due to grain coarsening in the heat affected zone in High-Si steel and grain coarsening combined with the effects of the formation of polygonal ferrite in the High-Al steel (section 4.4.2). In the fusion zone, the heterogeneity in grain sizes and the presence of martensite and acicular products dictates the variation of hardness in the solidified microstructure.

7.2 Tensile testing of welded TRIP steels

The mechanical properties of the welded TRIP steels are always poorer than other commercially used advanced high strength steels such as dual phase (DP) steels [2]. Moreover, the mechanical properties of welded TRIP steels are reported to change after welding with time at room temperature [3, 4]. Changes in the properties of welded TRIP steels indicate that the welds become brittle with time. Since there is no literature in the public domain concerning the changes in properties of welded TRIP steel with time, an attempt was made to measure the mechanical properties of the welded TRIP steels with periodic intervals after welding. Tensile samples were prepared from as-received High-Al steel plates based on the ASTM-E8m-04 standard and the prepared samples were subjected to TRIP steel heat treatment HT800/400 (figure 3.3) using salt bath furnaces (see section 3.3.1 for the heat treatment procedure). The sample preparation was carried out before the TRIP heat treatment to avoid any possible stress-induced transformation of retained austenite during mechanical cutting and grinding. This procedure generated the base metal microstructure similar to the one used for quantitative synchrotron phase analysis (section 5.2) and *in-situ* synchrotron diffraction studies (section 6.1). Tensile testing was carried out in an electro-mechanical Zwick Z100 tensile testing machine with a load cell of 100 kN. Using an extensometer with a gauge length of 12.5 mm and an extension range of $\pm$ 2.5 mm, elongations were recorded for the applied load using the data acquisition

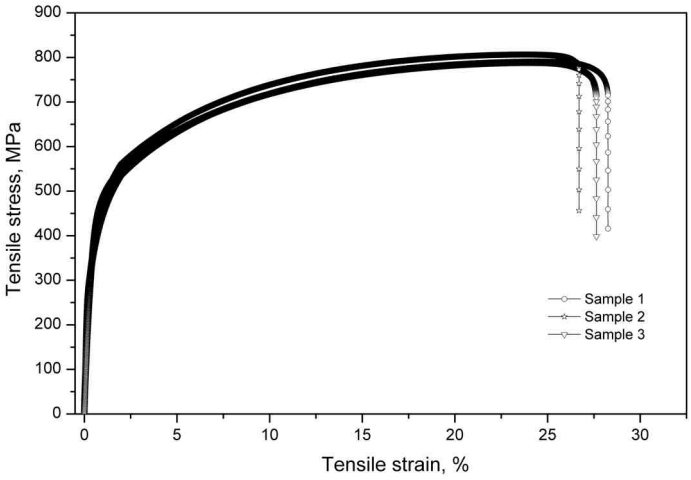

Figure 7.2: *The tensile stress with strain curves for HT800/400 High-Al TRIP steel base metal samples, showing a typical TRIP steel behaviour with continuous yielding*

software TestXpert®. Testing was carried out on 3 samples to ascertain the tensile properties of the base metal samples.

The tensile behaviour of HT800/400 heat treated High-Al TRIP steel samples showed a typical TRIP steel stress-strain curves with a continuous yielding and a completely ductile failure (figure 7.2). The results show that after the heat treatment, the average yield stress of the High-Al base metal at 0.2 % offset is 374 MPa. With an average ultimate tensile stress of 795 MPa, the heat treated base metal showed a maximum average elongation of 17.9 mm with a total tensile strain of 27.5 %. Table 7.1 summaries the mechanical properties of the heat treated High-Al TRIP steel base metal obtained by tensile testing.

In order to carry out tensile tests on welded TRIP steel samples, bead-on-plate laser welding was preformed on the HT800/400 heat treated High-Al TRIP tensile samples using a continuous wave (CW) Nd:YAG laser beam oriented perpendicular to the plate surface with the welding parameters described in section 4.2. The weld bead, with a width of about 5 mm was placed on the centre of the gauge length in the transverse direction. Figure 7.3 schematically shows the tensile sample with a bead-on-plate weld configuration used for the tensile testing. It can be seen from figure 7.3 that in the centre of the tensile sample, runner plates with dimensions of 25x25 mm^2 were attached at either sides to protect the backing plate of the weld set-up while passing the laser beam and to avoid the samples fusing to it. These runner plates were prepared from similar heat treated High-Al TRIP steel, placed at the sides without any pre-set gap and removed manually after welding by twisting them.

Table 7.1: *Tensile properties of HT800/400 heat treated High-Al TRIP steel base metal samples (UTS - Ultimate tensile stress and YS - Yield stress, in MPa)*

Sample	UTS, MPa	Tensile strain at UTS, %	YS at 0.2 % strain, MPa	Extension at break, mm	Tensile strain at break, %
1	789.7	23.8	425	18.1	27.6
2	805.9	23.7	340.3	17.6	26.6
3	791.2	24.1	357.8	18.1	28.2
Mean	795.6	23.9	374.3	17.9	27.5

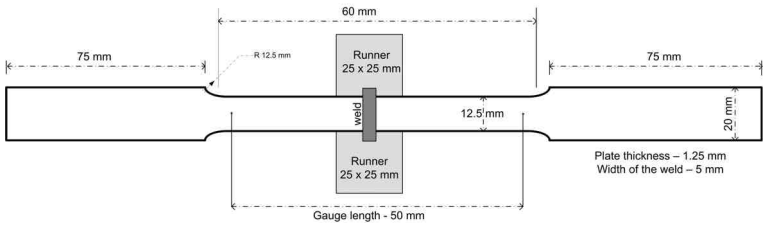

Figure 7.3: *Schematic view of the tensile sample with a bead-on-plate weld at the centre of its gauge length. Welding was done with a continuous wave (CW) Nd:YAG laser beam oriented perpendicular to the plate surface.*

This procedure has to be followed to minimise the influence of externally applied mechanical stresses from the sample preparation machining on the retained austenite in the microstructure, and to start the tensile test as soon as possible after welding.

The welded samples were quickly removed from the weld set-up and mounted on a tensile testing machine to start the loading. The tensile tests were started 90 s after the welding. In order to study the effect of possible room temperature transformation of austenite, the welded TRIP steel samples were kept at room temperature for 900 s (15 minutes) and testing was carried out. For both time steps, 3 samples were tested to ensure repeatability.

The results of the tensile tests indicated that the welded High-Al TRIP steel samples tested 90 s after welding showed a completely ductile failure far away from the weld centre line in the base metal region (18 mm from the weld centre line), as shown in figure 7.4. The stress-strain behaviour of the sample tested 90 s after welding was found to be similar to that of the base metal samples (figure 7.2). The presence of dimples in the fracture surface of the failure in the base metal also confirms a ductile failure (figure 7.5).

Conversely, the welded TRIP steel samples tested 900 s (15 minutes) after welding showed a completely brittle failure at the weld centre line. Figure 7.6 shows a sample tested 900 s after welding with a brittle failure at the centre of the weld. The fracture

Figure 7.4: *A welded High-Al TRIP sample tensile tested 90 s after welding showing a ductile failure in the base metal region, about 18 mm from weld centre line.*

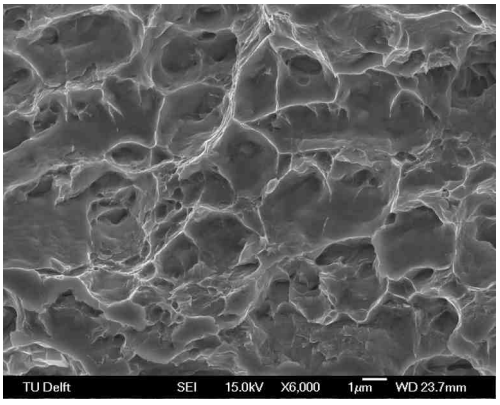

(a)

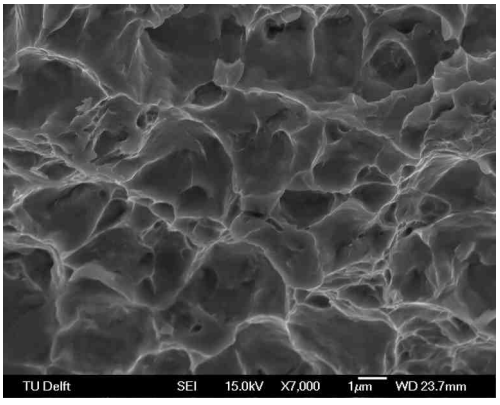

(b)

Figure 7.5: *The fracture surface of the welded High-Al TRIP steel sample, tensile tested 90 s after welding showing a ductile failure with the presence of dimples.*

Figure 7.6: *A welded High-Al TRIP sample tensile tested 900 s after welding showing a complete brittle failure at the centre of the weld.*

surface of samples tested 900 s after welding did not show the presence of dimples, indicating a complete brittle failure (figure 7.7).

The results of these tensile tests clearly indicate that within 900 s after welding, the failure behaviour of the samples changed from ductile to brittle. The samples tested 90 s after welding showed mechanical behaviour of a good weld, a failure at the base metal instead of at the centre of the weld line as in the samples tested 900 s after welding. In the previous chapter, it was shown that the austenite left untransformed after cooling from the austenisation temperatures to room temperature is unstable at room temperature, and decomposes in due course (see section 6.5.3). If the austenite retained in the microstructure transforms to martensite with time after welding, the weld metal becomes brittle, which results in brittle failure of the weld as in the case of samples tested 15 minutes after welding.

Studies were made by tensile testing the welded TRIP steels at various time intervals after welding, starting from 90 s to find out after what time the nature of the failure turns brittle from ductile, but the results were inconclusive and the failure modes could not be ascertained successfully due to various uncertainties involved in the tensile testing of welded TRIP steel samples immediately after welding namely,

1. The unstable austenite fraction in the fusion and heat affected zones of the welded TRIP steel,

2. Possibility of creating a uncontrolled "notch" while removing the runner plates attached to the tensile sample after welding,

3. Controlling the size, shape and compositional distribution of the non-metallic inclusion formation in the fusion zones.

In-situ synchrotron diffraction studies indicated that a significant amount of austenite (about 5.5 to 7 %) is retained based on the peak temperature reached in a continuously cooled thermal cycle. In actual welding conditions, the steel is subjected to a thermal cycle where the peak temperature in the heat affected zone is affected by the external conditions such as ambient temperature, humidity etc. The *in-situ*

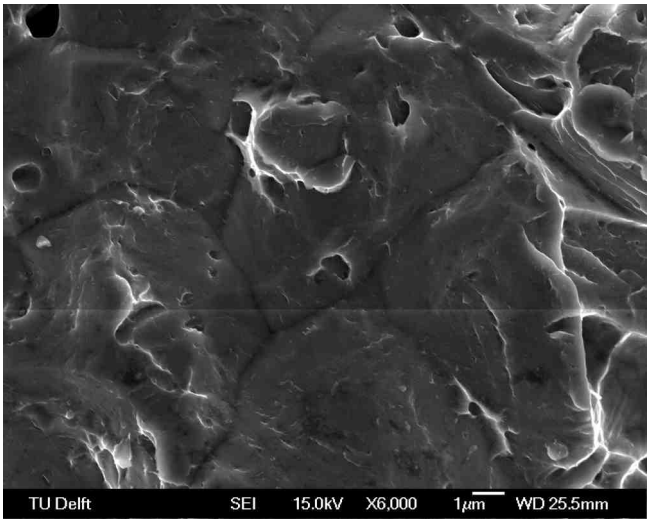

(a)

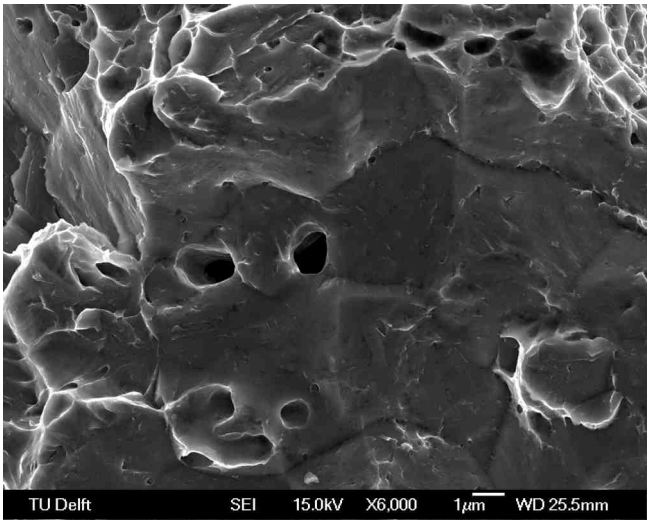

(b)

Figure 7.7: *The fracture surface of the welded High-Al TRIP steel sample, tensile tested 900 s after welding showing a complete brittle failure.*

synchrotron diffraction studies also showed that while cooling from as low as 40 ^{o}C to room temperature about 2 % of austenite was transformed in TRIP steels (figures 6.13, 6.19). Thus, tensile testing at identical ambient conditions is difficult and ascertaining the temperature of the heat affected zones for every test by attaching thermocouples at the weld metal delays the tensile testing. During the failure analysis of the fracture surface, it is found that improper removal of runner plates from the tensile sample after welding creates an uncontrolled notch at the edges of the sample at the centre of the weld. Figure 7.8 shows one such notch formed at the centre of the weld in a sample tested 2 minutes after welding which subsequently failed in a brittle manner. The formation of notches at the sides of the samples leads to stress concentration during tensile loading and to premature brittle failure at the centre of the weld. Added to these, the presence of non-metallic inclusions in the fusion zones also alters the crack initiation behaviour during loading. Fracture surfaces of the samples failed prematurely in brittle mode showed the presence of spherical inclusion cavities (figure 7.9). Although similar welding and base metal conditions were used for the experiments, due to the local variation in the fluid flow, the composition of the weld pool during solidification can vary the size and distribution of the non-metallic inclusions in each welded TRIP steel samples (see section 4.4.1).

Due to all these uncertainties in the tensile testing conditions, no reliable conclusions can be drawn from these tests to assess the mechanical properties of the welded TRIP steels or about the possible effect of room temperature transformation on the changes in mechanical properties with time after welding. This resulted in the use of another mechanical test, the Erichsen cupping test by which these uncertainties can be minimised and mechanical properties of welded TRIP steels can be determined soon after welding is completed.

7.3 Erichsen cupping testing

The Erichsen cupping test is widely employed as a ductility and formability test for sheet and strip metals used in automotive applications, where stretch forming is a major manufacturing step. The test consists of forming an indentation by pressing a punch with a spherical end against a test piece clamped between a blank holder and a die, until a through crack appears. The depth of the cup is measured and given as Erichsen cupping index *IE* after averaging at least three individual measurements. This test is also used to estimate the formability of the welded steel sheets to evaluate the strength of the welded zones compared with the base metal. Figure 7.10 schematically shows the experimental arrangement and table 7.2 describes the testing parameters used for the test [5].

The samples for the Erichsen cupping tests were prepared with a length of 250 mm and a width of 100 mm from HT800/400 heat treated High-Al TRIP steel plates (see section 3.3.1 for the heat treatment procedure). Sample plates with the same dimensions were also prepared from the commercially produced cold-rolled, annealed and galvanised plates to compare the results with heat treated plates. Bead-on-plate

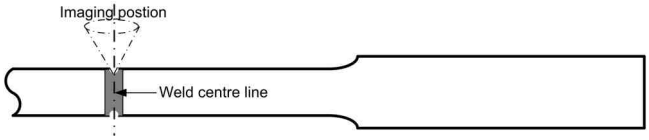

(a) *Schematic view of the notch in the weld centre line in the sample edge from where image (b) was taken.*

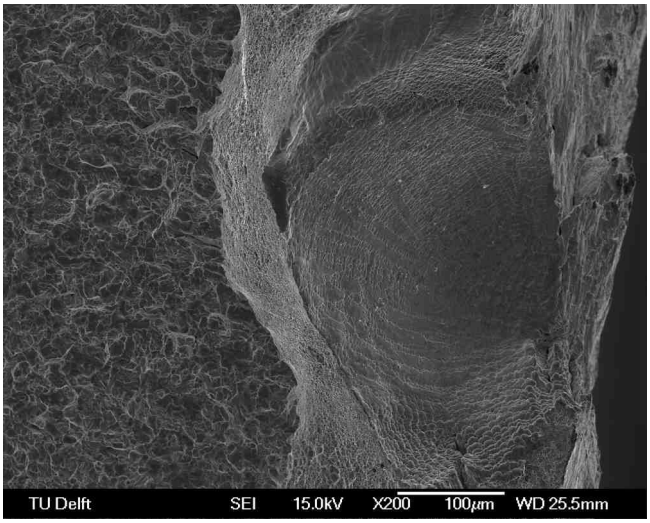

(b) *Fracture surface at the edge of the sample showing the presence of a notch*

Figure 7.8: *Fracture surface of a welded TRIP steel samples, tensile tested 2 minutes after welding showing a formation of notch at the edges due to improper removal of runner plates from the sample.*

laser welding was preformed on the High-Al TRIP tensile samples using a continuous wave (CW) Nd:YAG laser beam oriented perpendicular to the plate surface with the welding parameters given in section 4.2. The weld bead, with a width of about 3 mm, was placed on the centre of the plate in the longitudinal direction as shown in figure 5.8a.

A mechanised electro-mechanical Ericshen cupping tester was used for this study. Before starting the experiment, a graphite grease lubricant was applied to the punch and die areas that come into contact with the welded plate. After welding, the welded plates were placed in the die cavity in such a way that the longitudinal weld centre line is perpendicular to the cylindrical axis of the punch and to the plane of observation in figure 7.10. The welded plates were clamped in between the die and the punch with a blank holding force of 10 kN. The punch was loaded and brought into contact with the welded plate. The measurement of penetration of the punch was started at this point

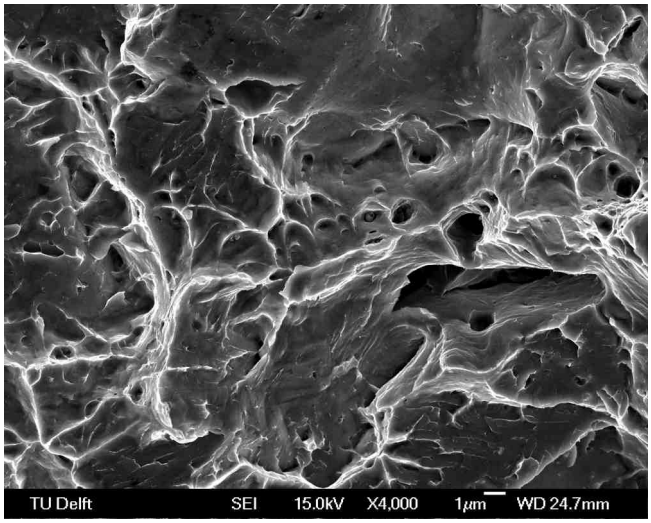

Figure 7.9: *Fracture surface of a welded TRIP steel samples, tensile tested 2 minutes after welding showing the presence of circular inclusion cavities and micro-cracks nucleating from them.*

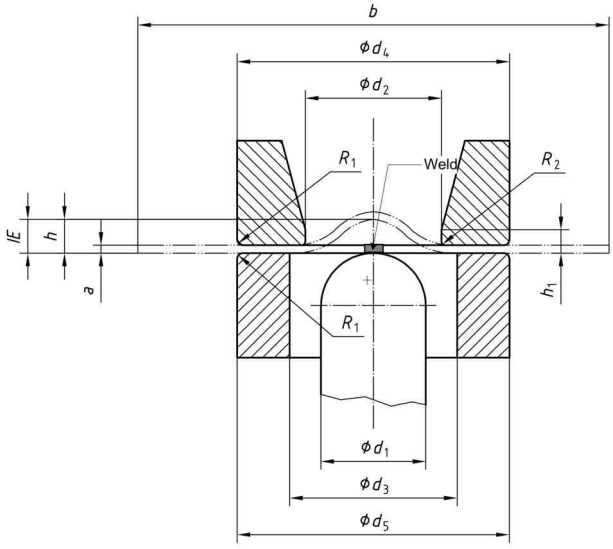

Figure 7.10: *Schmatic illustration of Erichsen cupping testing set-up [5]. The black area indicates the position of the fusion zone of the weld cross-sectioned in thickness direction.*

Table 7.2: *Erichsen cupping test parameters used for welded TRIP steel*

Symbol	Designation	Value, mm
a	Thickness of the test piece	1.25
b	Width of the test piece	100
d_1	Diameter of the spherical end of the punch	20±0.05
d_2	Bore diameter of the die	27±0.05
d_3	Bore diameter of the blank holder	33±0.1
d_4	Outside diameter of the die	55±0.1
d_5	Outside diameter of the blank holder	55±0.1
R_1	Outside corner radius of the die, outside corner radius of the blank holder	0.7±0.1
R_2	Inside corner radius of the die	0.75±0.05
h_1	Height of the inside rounded part of the die	3.0±0.1
h	Depth of the indentation during the test	variable
IE	Erichsen cupping index	variable

until the instant a crack appeared through the thickness of the welded plate. The depth of indentation was averaged from 8 measurement points under each condition to calculate the Erichsen cupping index (IE) which indicates the stretchability of the welded plates. The quality of the welds were assessed from the crack propagation modes. Based on the commercially acceptable weld quality assessments, if the crack appears perpendicular to the weld and propagates towards the base metal, the weld quality is acceptable. Conversely, if the crack appears at the weld centre line and propagates along the weld, the weld is brittle and not acceptable [5]. On each 250 mm welded plate, 3 indentations were made in the longitudinal direction. Total measurement time for each indentation is 45 s. In this way, measurements were carried out at time intervals of 60, 120, 300, 900, 1800, 3600, 7200, 10800 and 14400 s after welding.

The Erichsen cupping index IE of the HT800/400 heat treated High-Al TRIP base metal steel was 10.3 mm and commercially produced cold-rolled, annealed and galvanised High-Al TRIP steel showed an IE of 10.7 mm. However, after welding, the IE index reduced to 3.4 mm when the cupping test was carried out 60 s after welding (figure 7.13). The IE index slightly increases to 3.7 mm in the sample tested 120 s after welding, but the increase remains within the experimental scatter. In both cases, the crack was observed perpendicular to the weld centre line. When the test was conducted 300 s after welding, the IE reduced to 2.5 mm and a crack appeared to form at the centre of the weld and propagated along the weld centre line. Figure 7.11 shows an overview of rupture seen on the welded TRIP steel plates where the crack is seen at the centre of the weld in indentations made 300 s after welding. The failure analysis of the rupture surface of the welded plate, tested 300 s after welding clearly shows that crack appeared in the centre of the fusion zone (figure 7.12). The

IE and the cracking behaviour was similar in both HT800/400 heat treated and as received TRIP steel samples (figure 7.13).

The Erichsen cupping index *IE* further decreases with time and the samples tested 900 s after welding showed an *IE* of 1.9 mm. The rupture behaviour remains the same as the plates tested 300 s where the crack appeared at the centre of the weld line (figure 7.14). Interestingly however, after 900 s holding time after welding, the *IE* starts to increase steadily. At 1800 s, *IE* increased to 2.5 mm and further increases with time. Samples tested after 14400 s after welding showed an *IE* of 3.4 mm (figure 7.15).

Apart from the increase in *IE*, there is also a change in cracking pattern observed on the samples tested 1800 s to 14400 s after welding (figure 7.16). At 1800 s, out of three indentations, cracks were observed perpendicular to welds in two indentations, whilst one indentation produced a crack at the weld centre line. When the time after welding increases to more than 1800 s after welding (3600 to 14400 s), all the samples ruptured with cracks perpendicular to the weld centre line, similar to the cracking behaviour observed at 90 and 120 s after welding.

7.3.1 Discussion

The results of the Erichsen cupping test shows that the formability of the welded TRIP steel is inferior to that of TRIP steel base metals. The Erichsen cupping index *IE* of welded TRIP steels is about 1.9 to 3.7 mm which is significantly lower than the base metal index of 10.3 to 10.7 mm. Moreover, the properties of the welded TRIP steels were found to change with time at room temperature after welding. The tests conducted within 120 s after welding showed acceptable cracking behaviour whilst for the welds tested between 300 to 1800 s, brittle failures at the weld centreline were observed. The *IE* starts to decrease in the first 900 s after welding and remains low upon further holding at room temperature, but increases again after 1800 s. The cracking behaviour also starts to change from a brittle weld centre line failure to a more ductile-like failure after 1800 s.

During the *in-situ* synchrotron X-ray diffraction measurements, it was found that after continuously cooling from the austenisation temperatures to room temperature, the retained austenite in the microstructure was not stable and decomposed with time at room temperature (see section 6.5.3). In TRIP steels, the elongation and formability is strongly influenced by the amount of retained austenite present in the microstructure: generally, formability decreases with decreasing austenite content in steels [6]. In an actual welding condition, thermal gradients across the weld zone stabilise varying amounts of retained austenite in the microstructure as shown in figure 5.10. When the austenite content in the weld zone decreases with time after welding, the weld zone becomes brittle, as observed in Erichsen cupping testing of welded TRIP steels.

The change in formability behaviour of welded TRIP steel observed 1800 s after welding cannot be explained by the room temperature transformation behaviour of austenite as it shows a continuous decomposition behaviour with time after cooling to room temperature. In an unpublished work [3], a possible influence of weld metal

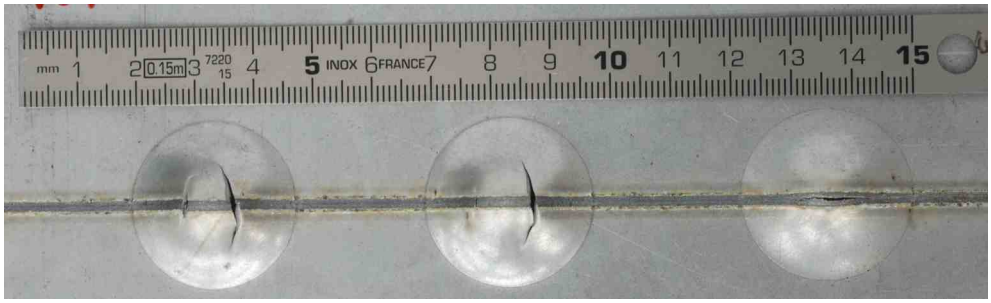

(a) *Sample plate 1, with the indentations of 60, 120 and 300 s after welding*

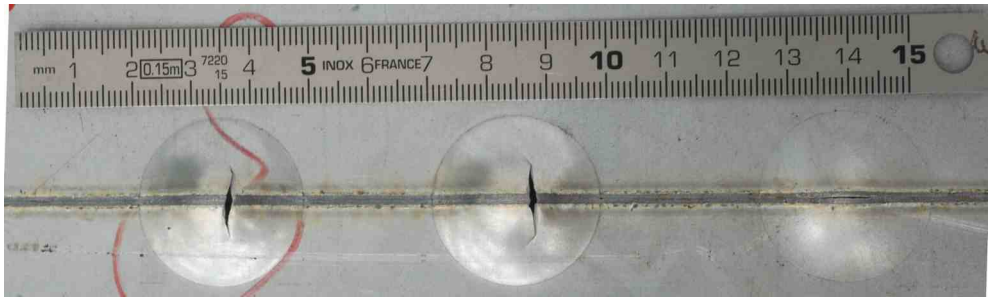

(b) *Sample plate 2, with the indentations of 60, 120 and 300 s after welding*

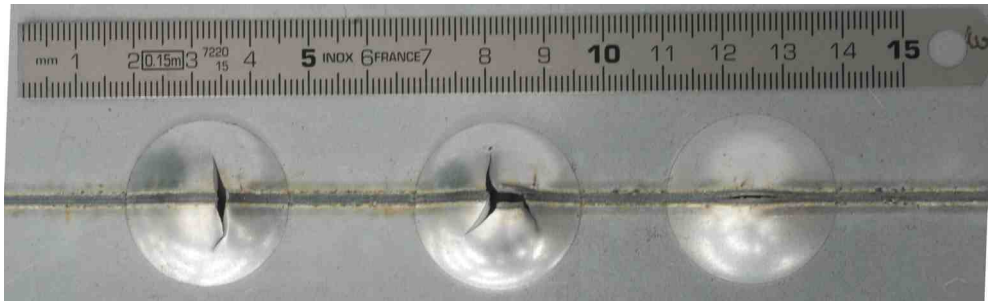

(c) *Sample plate 3, with the indentations of 60, 120 and 300 s after welding*

Figure 7.11: *Overview of the rupture seen after the Erichsen cupping test in welded as received High-Al TRIP steel plates, showing a brittle weld failure 300 s after welding.*

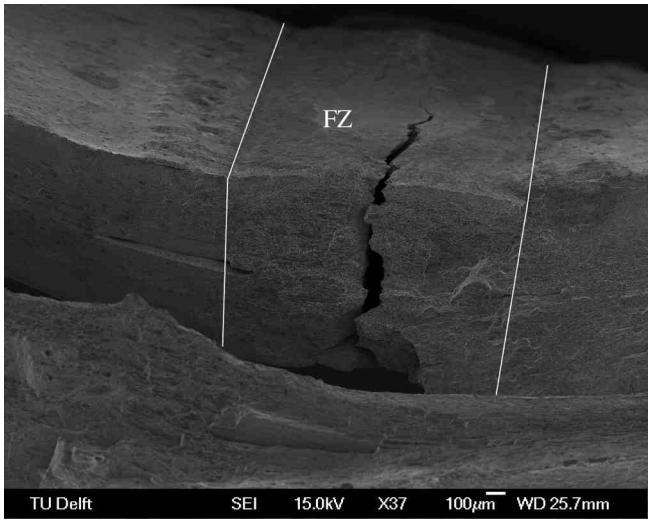

Figure 7.12: *A fracture surface of the welded plate tested 300 s after welding showing the crack at the centre of the fusion zone. The solid white lines indicate the fusion boundaries.*

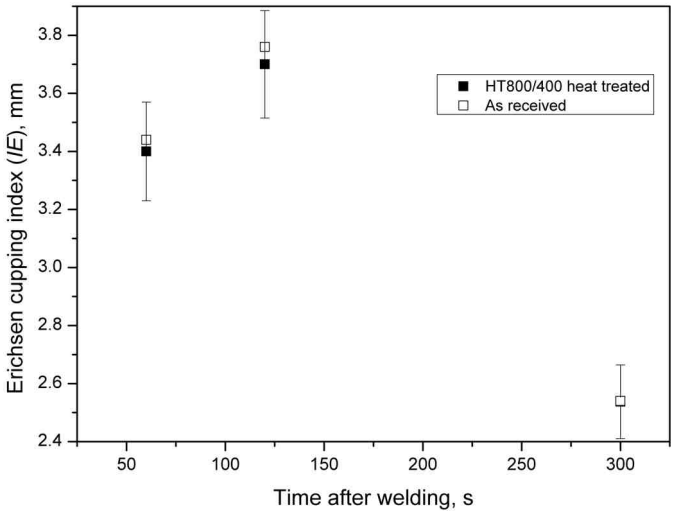

Figure 7.13: *The Erichsen cupping index (IE) of welded HT800/400 heat treated and as received High-Al TRIP steel plates.*

Figure 7.14: *The overview of the rupture of welded TRIP steel, tested 900 s after welding showing the cracks on the weld centre line.*

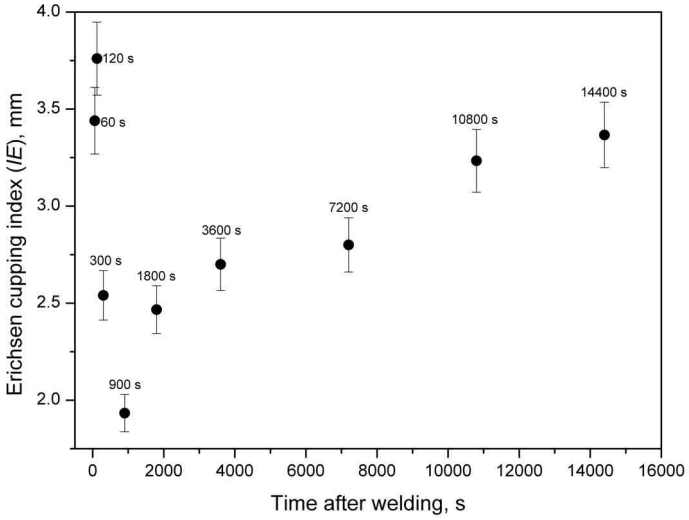

Figure 7.15: *The Erichsen cupping index (IE) of welded High-Al TRIP steel plates.*

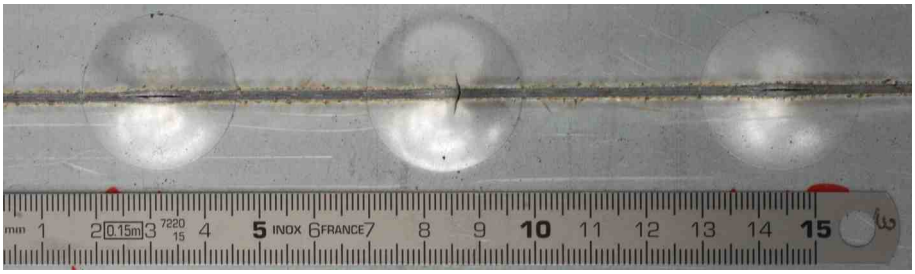

(a) *1800 s after welding*

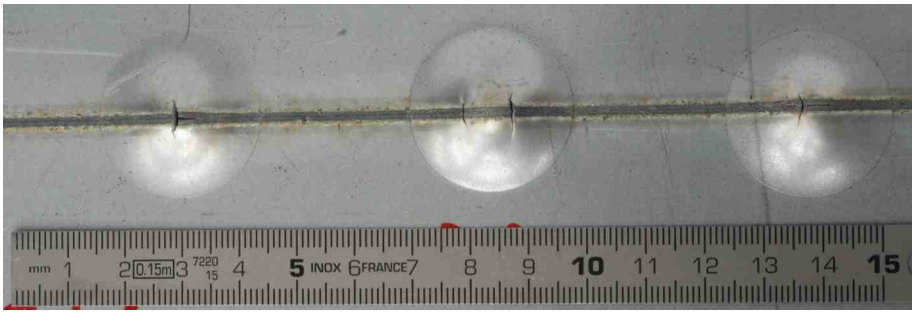

(b) *3600 s after welding*

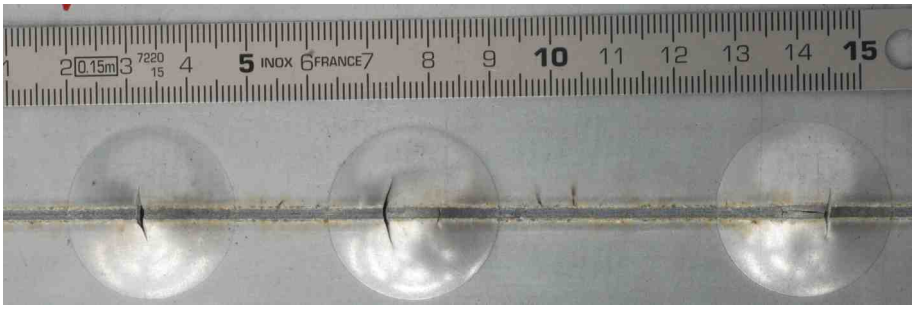

(c) *10800 s after welding*

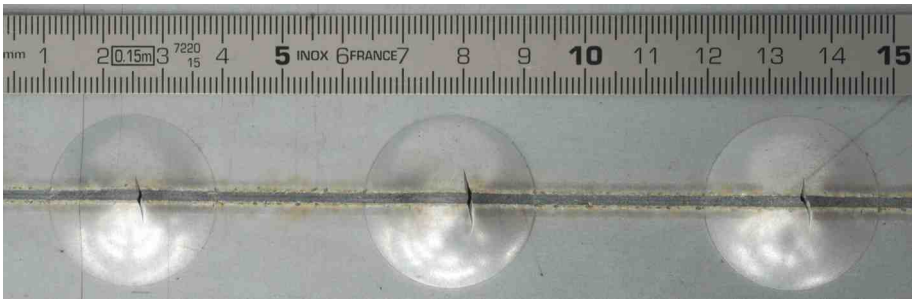

(d) *14400 s after welding*

Figure 7.16: *Overview of the rupture seen in welded High-Al TRIP steel plates, testing at 1800, 3600 10800 and 14400 s after welding.*

hydrogen on mechanical properties of the welded TRIP steels has been described. Hydrogen is a austenite stabiliser and is known to diffuse out of steel at room temperature [7]. The total charged hydrogen concentration in steel is reported to be linearly proportional to the volume fraction of retained austenite in the microstructure [8, 9]. Studies on TRIP steels containing retained austenite showed that the mechanical properties are affected by the hydrogen diffusion in the austenite and vice versa [9, 10]. Thus, the possible influence of hydrogen entrapment in retained austenite in the welded TRIP steel should to studied to understand the time-dependent changes in the mechanical behaviour of the TRIP steels.

In the following general discussion (chapter 8), the possible mechanisms for the time dependent changes in the mechanical properties of welded TRIP steels are analysed in detail.

7.4 Conclusions

The mechanical properties of welded TRIP steels are found to be strongly influenced by fusion welding. The hardness variation across the weld zone of TRIP steels was correlated to the retained austenite fraction in the weld microstructure. The tensile testing of welded TRIP steels showed time dependent changes in fracture mode after welding. During tensile testing, the samples tested 90 s after welding fractured in the base metal region, whereas after 900 s a brittle failure was observed at the centre of the weld. However, mechanical characterisation by tensile testing cannot be undertaken due to experimental uncertainties such as variation of ambient conditions, notch formation at the fusion zone and possible variations of non-metallic inclusions. Erichsen cupping tests showed that the formability of welded TRIP steel is poorer than un-welded TRIP steels. The Erichsen cupping index decreases in the first 900 s after welding and remains low with further holding at room temperature before starting to increase again from 1800 s. The fracture surfaces of the ruptured samples after Erichsen cupping indentations showed a crack formation perpendicular to the weld centre line initially after welding and change to brittle failure at 900 s. The failure mode changed again in Erichsen cupping tests 3600 s after welding.

References

[1] I.M.Richardson, M.Amirthalingam, M.J.M.Hermans and N.Den Uijl, 'The influence of welding on advanced high strength trip and dp steels', *Mathematical modelling of weld phenomena*, vol. 9, Technical University Graz, 2010.

[2] N.J.den Uijl, 'Post weld heat treatments of advanced high strength steel for automotive joining', *Mathematical modelling of weld phenomena*, 8, 217–223, 2007.

[3] T.van der Veldt, 'Ageing in weded TRIP steels', 5th knowledge exchange meeting with SMI on joining, Corus R&D and T, 2007.

[4] Corus R&D and T, 'Internal communication', 2005-2009.

[5] 'Metallic materials - sheet and strip - erichsen cupping test (iso 20482:2003)', .

[6] M.H.Saleh and R.Priestner, 'Retained austenite in dual-phase silicon steels and its effect on mechanical properties', *Journal of materials processing technology*, 113, 587–593, 2001.

[7] V.P.Ramunni, T.de Paiva Coelho and P.E.V.de Miranda, 'Interaction of hydrogen with the microstructure of low-carbon steel', *Materials Science and Engineering A*, 435436, 504514, 2006.

[8] T.Hojo, K.I.Sugimoto, Y.I.Mukai, H.Akamizu and S.Ikeda, 'Hydrogen embrittlement properties of ultra high-strength low alloy trip-aided steels with bainitic ferrite matrix', *Tetsu-To-Hagane/Journal of the Iron and Steel Institute of Japan*, 92, 83–89, 2006.

[9] T.Hojo, K.I.Sugimoto, Y.Mukai and S.Ikeda, 'Effects of aluminium on delayed fracture properties of ultra high strength low-alloy trip-aided steels', *ISIJ International*, 48, 824–829, 2008.

[10] B.C.De Cooman, 'Structure-properties relationship in TRIP steels containing carbide-free bainite', *Current Opinion in Solid State and Material Science*, 8, 285–303, 2004.

Chapter 8

General discussion and recommendations

8.1 Discussions

A thorough understanding of the evolution of microstructure during the welding of TRIP steels is necessary to improve their mechanical behaviour and thereby to increase the commercial applicability of these steels. Experimental investigations on the microstructural evolution during welding showed the influence of weld thermal cycles on the behaviour of alloying elements and the thermal stability of the retained austenite across the weld zone (chapters 4 and 5). The magnetic, dilatometric and *in-situ* synchrotron X-ray diffraction analyses described the phase transformation kinetics and lattice parameter behaviour during heating and cooling thermal cycles representative of typical welding conditions (chapters 5 and 6). Experiments also indicated ambient temperature transformation of austenite after cooling. The mechanical properties of the welded TRIP steels were affected by the distribution of retained austenite in the weld zone and its stability at room temperature after welding (chapter 7). In this chapter, the observations made from the experimental investigations described in previous chapters are discussed together, to analyse the various metallurgical effects induced in the TRIP steels by the weld thermal cycle. The metallurgical changes that were observed during the welding of TRIP steels are sequentially discussed starting from the base metal and addressing the heating, melting and cooling thermal cycles involved in the welding processes.

The High-Si and High-Al TRIP steel microstructures contain ferrite, bainite and retained austenite. These microstructures are generated by subjecting the material to a heat treatment consisting of inter-critical annealing and isothermal bainitic holding. By altering the temperature of inter-critical annealing and bainitic holding, the percentage of retained austenite in the base metal microstructure varied from 3.6 to 15 %. The results showed that, for TRIP steel compositions used in this study, the

use of a low inter-critical annealing temperature (800 ^{o}C in this case) and a high isothermal bainitic holding temperature (400 ^{o}C in this case) always leads to a higher retained austenite content in the microstructure (up to 15 %) (section 3.4.1).

During a typical weld thermal cycle, the TRIP steel containing retained austenite microstructure is heated to a peak temperature close to the melting point (about 1530 ^{o}C) at the fusion boundaries. The peak temperature reached during welding gradually decreases with distance from the fusion boundary. The results of the *in-situ* synchrotron X-ray diffraction studies, where the TRIP steel samples were subjected to simulated weld thermal cycles, showed the decomposition of retained austenite during heating above 290 ^{o}C (section 6.2.2). Thermo-magnetic measurements showed that the paramagnetic retained austenite transforms into ferromagnetic ferrite and carbides after heating to 290 ^{o}C (section 5.1.3). The decomposition of retained austenite was also evident in the welded TRIP steel plates where the quantitative microstructural analysis indicated that in the area where the peak temperature reached during welding was above about 300 ^{o}C, the retained austenite content was reduced (section 5.2). In gas tungsten arc welded TRIP steel plates, this peak temperature was reached at around 10 to 12 mm from the weld centre line. Thus, in welded TRIP steel plates, the heat affected zone extends to $\simeq$12 mm from the weld centre line, to the point where the retained austenite is not affected by the weld thermal cycle. Similar extensions of heat-affected zones are also found in laser beam and resistance spot welded TRIP steel plates. This makes the heat affected zone of welded TRIP steels wider than reported for other AHSS such as DP steels [1, 2]. Moreover, there are no metallograhically detectable changes that occurred in the base metal microstructure except for the decomposition of retained austenite in this low temperature zone (from 250 to 350 ^{o}C) (section 5.2). Thus, the heat affected zone in a welded TRIP steel needs to be defined from the position where the retained austenite is decomposed during welding, rather than from the position where microstructural changes observable in optical microscopy occur, as is generally accepted for heat affected zone boundary identification.

The *in-situ* synchrotron X-ray diffraction analysis shows that the lattice parameter of retained austenite (a_γ) in both High-Si and High-Al TRIP steels varied linearly with temperature up to 290 ^{o}C during heating. Once the austenite decomposition begins above this temperature, an increase in a_γ is observed due to the partitioning of carbon from the newly formed ferrite to the remaining austenite. The a_γ drops at 430 ^{o}C and continues to vary linearly until the temperature reaches A_{c1} (section 6.2.3). It is reported that when a retained-austenite containing microstructure is tempered, the retained austenite decomposes into ferrite and carbides in the following sequence [3];

$$\gamma_{RA} \longrightarrow \alpha + \epsilon \longrightarrow \alpha + \eta(\epsilon') \longrightarrow \alpha + \theta(Fe_3C)$$

Generally, this sequence of decomposition is reported for high carbon steels [4–6]. However, Jha *et al.* [3] found that the decomposition of retained austenite in low carbon (0.06C-1.0Mn-0.90Si-0.35Mo-0.4Cr wt. %) dual phase steels follows the same sequence. In TRIP steels, the formation of iron carbides is not generally foreseen due

to the high amounts of silicon and aluminium (1.47 and 1.1 wt. % respectively in the steels used in this work). However, during the thermo-magnetic measurement, it is found that the paramagnetic austenite transforms into ferro-magnetic ferrite upon heating to 290 ^{o}C (section 5.1.3). During further heating, in the range of 390 to 400 ^{o}C, a sudden decrease in saturation magnetisation was observed (see figure 5.4a). If the retained austenite decomposes only to ferro magnetic ferrite, it should only lead to an increase in saturation magnetisation. The cementite is paramagnetic above its curie temperature (210 ^{o}C) and ϵ carbide is ferromagnetic within the temperature range (290 to 600 ^{o}C) [7, 8]. Thus, a decrease in saturation magnetisation during the decomposition of retained austenite can only be explained by the formation of paramagnetic $\eta(\epsilon')$ carbide. From this result, it can be concluded that the initial increase in austenite lattice parameter a_γ after the start of austenite decomposition at 290 ^{o}C is due to the carbon enrichment from the newly formed ferrite. When the decomposition proceeds, the untransformed austenite is further enriched in carbon which subsequently leads to carbide precipitation, this causes a decrease in a_γ while heating above 430 ^{o}C (section 6.2.3).

In the heat-affected zone, positions where the peak temperature during the weld thermal cycle reached the inter-critical (α+γ) region, the amount of retained austenite was found to be higher than the area where the peak temperature reached the fully austenitic region. When the peak temperature remains in the inter-critical region, the newly formed austenite grains were enriched in carbon from co-exisiting ferrite, as given by the lever rule; this results in an increased retained austenite content after welding. Conversely, when the peak temperature during welding remains below A_{c_1}, the retained austenite decomposes and a reduction of austenite content in the HAZ is found. Similarly, when the peak temperature rises above A_{c_3}, the austenite formed attains the bulk carbon concentration, which is always less than the carbon content of the austenite in the inter-critical region, resulting in less retained austenite in the higher-temperature ($> A_{c_3}$) positions (section 5.2).

In the fusion zones, where the peak temperature during a weld thermal cycle is above the melting point of the steel, the presence of highly oxidising alloying elements, such as aluminium and silicon, leads to the formation of non-metallic inclusions. Aluminium and silicon are added in TRIP steel to suppress the formation of iron carbides and thereby increase the carbon concentration of austenite, which results in an increased austenite stability. However, these elements in liquid metal combine with oxygen and form complex oxide inclusions; as a result, the fusion zone is depleted in dissolved aluminium and silicon, which results in a reduced retained-austenite content in the fusion zone. The fusion zone in the High-Al TRIP steel contains a higher volume fraction of non-metallic inclusions that are coarser than those in the High-Si steel; the retained austenite content in the fusion zone of High-Al TRIP steel is lower than that of High-Si steel (sections 4.4.1 and 5.1.2).

During the solidification of the weld pool, the newly formed δ-ferrite in the fusion boundaries is enriched with aluminium due to partitioning from the solidifying liquid metal and also from the austenite in the heat affected zone in the High-Al TRIP steel. This enrichment results in a stabilisation of δ-ferrite in the fusion boundaries.

The stabilised δ-ferrite zone is wider in GTA welded steel (200 μm) than in LB (60 μm) and RS welded steels (20 μm) as the solidification and subsequent partitioning is defined by the cooling rate of the welding process. The stabilisation of ferrite at the fusion boundaries during welding of aluminium containing TRIP steel was also reported recently by Kaputska *et al.* [9] for an aluminium-rich plain carbon steel [10]. The formation of a soft ferritic zone at the fusion boundary leads to a reduction in hardness and heterogeneity in the microstructure of the heat affected zone in welded High-Al TRIP steel. The formation of a soft ferritic zone in the fusion zone is not found in welded High-Si TRIP and dual phase steels (section 4.4.2).

The fusion zone and the coarse- and fine-grained heat-affected zones contain primarily a martensitic structure in LB and RS welded High-Si and High-Al TRIP steels. However, in GTA welded steels, occasional grain boundary Widmanstätten ferrite, bainite and intragranular acicular ferrite was found. The *in-situ* synchrotron X-ray diffraction measurements showed that for the applied cooling rate, the nature and kinetics of transformation of austenite differed between the High-Si and High-Al TRIP steels. The variation in lattice parameter and the kinetics of austenite transformation indicated a possibility of a completely martensitic transformation in High-Si steel, whereas in High-Al steel, both martensite and bainite has been found. This result indicates that, despite the use of a similar thermal cycle, the nature of transformation and the final microstructure after a thermal treatment strongly depends on the composition of the steel. Thus, during welding in practice, it is important to choose the thermal cycle of the welding process based on the chemical composition of the TRIP steels, rather than by its strength levels as both High-Si and High-Al TRIP steel have a similar UTS of 800 MPa.

The *in-situ* synchrotron X-ray diffraction measurements indicate that about 5 to 7 % of austenite is retained at room temperature initially after continuously cooling from austenisation temperature in TRIP steels. The quantitative microstructural analysis on welded TRIP steel plates also indicates that about 5 to 8 % of the fusion zone microstructure is retained austenite. In heat affected zones, in some positions as much as 12 % retained austenite was found after a typical continuous heating and cooling weld thermal cycle. The amount of austenite retained varies in weld microstructure and is determined by the peak temperature and cooling rate for a given material chemistry. The retained austenite content found in the welded TRIP steel microstructures is also close to the amount found in the heat treated TRIP steel base metal (close to 4 to 15 %), despite the fact that standard TRIP steel base metal heat treatment involves a complex thermal cycle involving inter-critical ($\alpha+\gamma$) annealing and isothermal bainitic holding.

The austenite that is left untransformed at room temperature after cooling from the austenisation temperature, is found to be unstable at room temperature and further decomposes with time. The results of the *in-situ* synchrotron X-ray diffraction measurements show that about 1 to 1.5 % of the retained austenite decomposes within $\sim$2100 s at room temperature after continuously cooling from 1000 or 1100 ^{o}C (sections 6.2.6 and 6.3.4). The dilatation measurements on welded TRIP steels also indicate that changes occur with holding time at room temperature after weld-

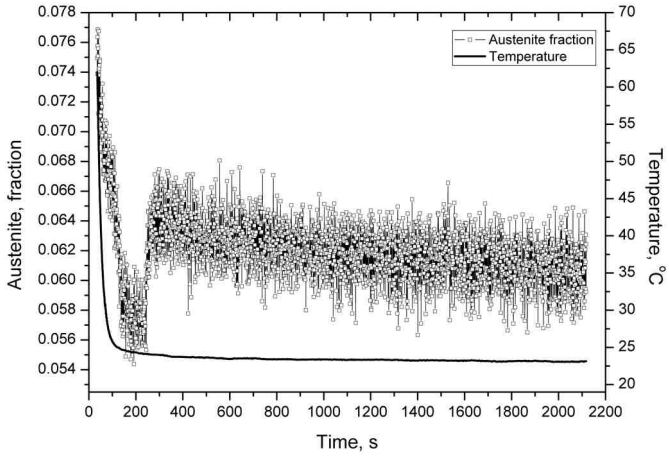

Figure 8.1: *An anomalous result in in-situ synchrotron X-ray diffraction measurement on a High-Al TRIP steel sample, showing a decrease and increase in austenite fraction at room temperature after cooling from 1000 °C.*

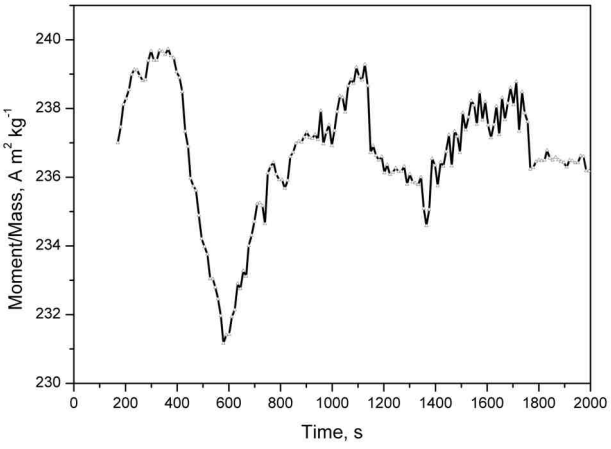

Figure 8.2: *The variation of saturation magnetisation with time in a laser spot welded High-Al TRIP steel.*

ing, and mechanical properties of the welded TRIP steels also show variations with time. Following a negligible increase within 120 s, the Erichsen cupping index of the welded High-Al TRIP steel started to decrease with time up to 900 s. The cracking behaviour of the welds also changed from ductile transverse cracks to brittle weld centre line cracks for the samples tested after 120 s and before 900 s, indicating that the weld becomes brittle. However, with upon further holding at room temperature, the Erichsen cupping index starts to increase after 1800 s and the cracking behaviour changed to ductile transverse cracking across the weld. When the retained austenite is not stable and decomposes continuously with time, it must ultimately result in a reduction in ductility and formability of the welds. However, the Erichsen cupping tests show that the weld is brittle between 120 and 900 s but with holding further, the ductility of the weld improves (section 7.3).

During the *in-situ* synchrotron X-ray diffraction measurements, when a High-Al steel sample is cooled from 1000 ^{o}C with the same cooling rate as shown in figure 6.3, an anomalous result was obtained where the austenite fraction decreased initially after cooling to room temperature (figure 8.1). Upon further holding, a sudden increase in austenite fraction was found. These phenomena appeared around 200 to 400 s after cooling from 1000 ^{o}C. In order to confirm this finding, a magnetisation measurement was carried out on a High-Al steel sample, after bead-on-plate laser spot welding. Using a laser power of 2000 W and a welding time of 5 s, a circular weld pool was created in a HT800/400 heat treated 10x5x1.25 mm^3 High-Al TRIP steel sample. After welding, the sample was immediately transferred to a magnetometer to measure the saturation magnetisation of the sample with respect to welding time.

Figure 8.2 shows the saturation magnetisation of the welded sample with time where an initial increase at 200 to 400 s and a dip in saturation magnetisation at around 400 to 500 s was found after welding, indicating a decrease followed by an increase in the paramagnetic component in the microstructure of the welded sample.

Whilst this transformation and magnetisation behaviour can be correlated with the time dependent changes that were observed during the Erichsen cupping test, no literature evidence has been found to support the austenite formation from martensite at room temperature in welded TRIP steels. The instability in austenite fractions at room temperature after a weld thermal cycle is possibly the result of the combined effects of carbon partitioning from martensite to austenite leading to a bi-directional movement of the martensite-austenite interface (related to the chemical driving pressure) with the association of transformation stresses (related to the mechanical driving pressure) and the evolution of hydrogen.

The chemical driving pressure for the movement of the martensite-austenite interface can be positive or negative depending on the relative difference between the equilibrium and actual carbon concentration in austenite and martensite at the interface. Few researchers attempted to study this interface behaviour while studying the transformation behaviour of martensite-austenite in quench and partitioning (Q&P) steels, whose chemical compositions are similar to the TRIP steels used here [11–17]. These quench and partitioning steels were subjected to isothermal annealing below the M_s temperature (between 220 to 400 ^{o}C). This annealing enriches the untrans-

formed austenite with carbon so that the chemical stability of austenite increases upon further cooling to room temperature. Although it is still not clear how the transfer of carbon atoms from supersaturated martensite to austenite takes place during isothermal annealing below the M_s temperature, it is generally assumed that the constrained carbon equilibrium (CCE) condition governs the transfer of carbon atoms between martensite and austenite [11, 12]. Under the *CCE* conditions, the iron and substitutional atoms are less mobile at lower temperatures at which carbon diffusion takes place and martensite-austenite interface is immobile or stationary. Therefore, only carbon equilibrates its chemical potential. However, in some cases it has been suggested that the interface could not be stable and could migrate during isothermal annealing of martensite and austenite containing microstructures [13–17].

Figure 8.3 schematically illustrates two situations where the actual carbon concentration of austenite at the interface is higher (figure 8.3a) or lower (figure 8.3b) than the equilibrium carbon concentration of austenite at a given temperature under the condition of equilibrium partitioning of carbon at the interface. If the interface is enriched in carbon relative to equilibrium, then the chemical potential of iron is higher in martensite than austenite and therefore the interface migrates from austenite to martensite. As a result, the austenite fraction increases at the expense of martensite (figure 8.3a). Conversely, the interface is promoted to move into austenite if the interface is depleted of carbon relative to equilibrium (figure 8.3b), resulting in the reduction of the austenite fraction.

Santofimia *et al.* developed a model to study the migration of the martensite-austenite interface and carbon diffusion during annealing of martensite-austenite microstructures at temperatures as low as 220 ^{o}C to 400 ^{o}C [13, 14]. In order to study the interface behaviour at room temperature, the model has been extended to express the welded High-Al TRIP steel microstructure which contains martensite and retained austenite after applying weld thermal cycle (see table 3.1 for the composition). The microstructure was assumed to contain 8 % retained austenite with a carbon concentration of 1.1 wt. % (table 3.3) and the rest of the microstructure was assumed to be bcc-martensite with a carbon concentration of 0.11 wt. %. The concentration of substitutional alloying elements was assumed to be the same as the bulk concentration in both phases (see table 3.1). The equilibrium carbon concentrations was calculated using ThermoCalc$^{\mathrm{TM}}$ and diffusion co-efficient of austenite and martensite were calculated using the procedure explained elsewhere [13]. When the interface carbon concentrations in martensite and austenite are different from the equilibrium concentrations, the phases experience a driving pressure ΔG for a transformation towards the equilibrium composition (figure 8.3). Under the assumption of equilibrium partitioning of carbon, $\Delta G = x_{Fe}\Delta\mu_{Fe}$, this local driving pressure is experienced at the interface and results in an interface velocity v according to,

$$v = M\Delta G \tag{8.1}$$

where $M_{fcc-bcc}$ is the interface mobility given by,

$$M_{fcc-bcc} = M_0 exp\left(-\frac{Q_M}{RT}\right) \tag{8.2}$$

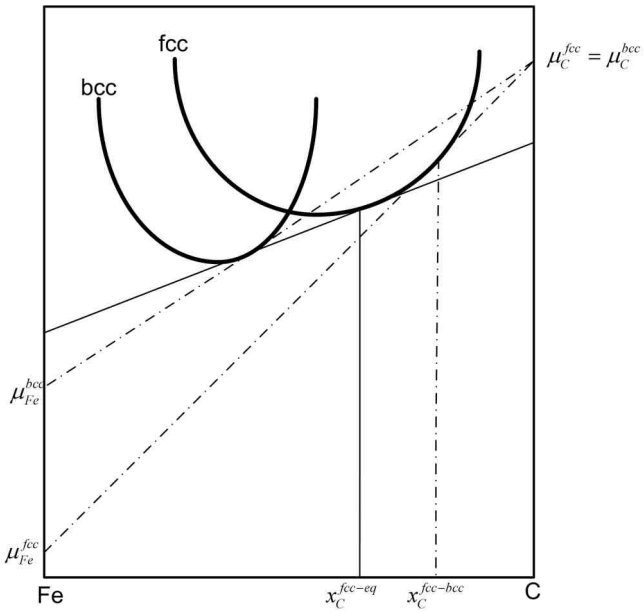

(a) *Carbon concentration of austenite at the interface* $x_C^{fcc-bcc}$ *is higher than the equilibrium concentration.*

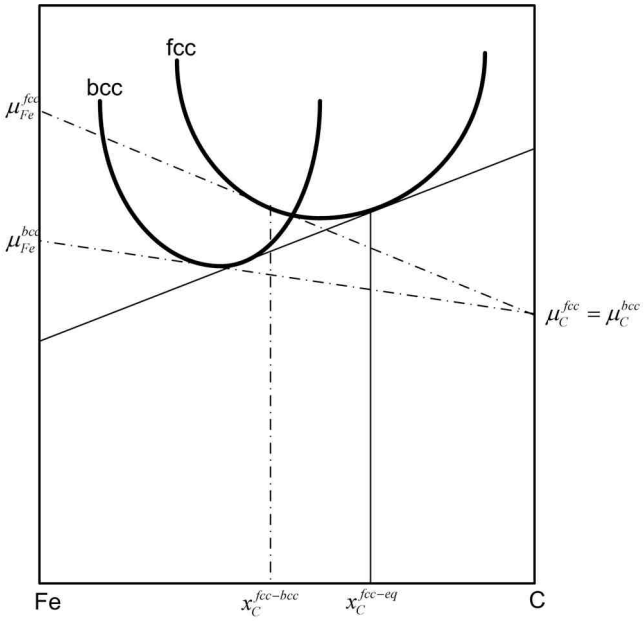

(b) *Carbon concentration of austenite at the interface* $x_C^{fcc-bcc}$ *is lower than the equilibrium concentration.*

Figure 8.3: *Schematic illustration of austenite interface composition under constrained carbon equilibrium condition (dashed lines) and under equilibrium (solid lines). Martensite is considered as bcc, supersaturated with carbon.*

where M_0 is a pre-exponential factor which is a function of atomic spacings, Debye frequency, Boltzmann constant and the temperature. Q_M is the activation energy for the movement of iron atoms at the interface. Several researchers assume 140 kJ mol^{-1} [18, 19] or 160 kJ mol^{-1} [20] as an activation energy for the atomic motion. However, the activation energy can be expected to be strongly dependent on the character of the interface, namely the degree of coherency. Therefore, in the original model proposed by Santofimia *et al.*, various activation energies were used to calculate the interface velocity. In the present calculations also three different activation energies were employed, namely 100, 140 and 180 kJ mol^{-1}. The diffusion of carbon in martensite and austenite was calculated as explained elsewhere [13, 14] and the evolution of microstructure was simulated while isothermally holding at 20 ^{o}C.

Figure 8.4 shows the variation in retained austenite fraction at 20 ^{o}C. At the starting time, the microstructure contains 8 % retained austenite. When Q_M is assumed to be 140 or 180 kJ mol^{-1}, the retained austenite fraction does not significantly change while holding for 60000 s at 20 ^{o}C. When the activation energy is reduced to 100 kJ mol^{-1}, the retained austenite fraction increases with holding time and after 60,000 s, the calculation shows that about 9.3 % of the retained austenite was present in the microstructure (an increase of 1.3 %).

The use of Q_M=140 kJ mol^{-1} by several researchers was based on an experimental prediction of activation energy for interface mobility in Fe-Mn systems by Krielaart *et al.* [18]. Although the present calculations on welded TRIP steel show a possibility of growth of retained austenite at around room temperature (20 ^{o}C) for a interface activation energy of 100 kJ mol^{-1}, this calculation must be validated with experimentally measured activation energies for interface mobility for appropriate TRIP steel compositions.

Provided the activation energy is not too high, it is possible for martensite-austenite interface to move at ambient temperatures, which can result in variations in retained austenite fraction in the microstructure. Deviation of interface carbon concentration from equilibrium can generate sufficient driving pressure for the movement of the martensite-austenite interface. This chemical driving pressure added with mechanical driving pressure available from the transformation stresses during the formation of martensite and type-III micro stresses that are generated due to rapid heating and cooling cycles involved in a weld thermal cycle can cause local variation in the activation energy for the interface movement and may result in the variations in the retained austenite content of a weld microstructure [21, 22]. The movement of hydrogen in welded steels, whose effect is well known to cause delayed fracture in TRIP steels may also cause variations in the mechanical properties of welded TRIP steels [23, 24]. However, the effect of dissolved hydrogen on the mechanical properties of welded TRIP steels should be studied further to determine whether hydrogen plays any significant role with respect to the stability of retained austenite in welded TRIP steels.

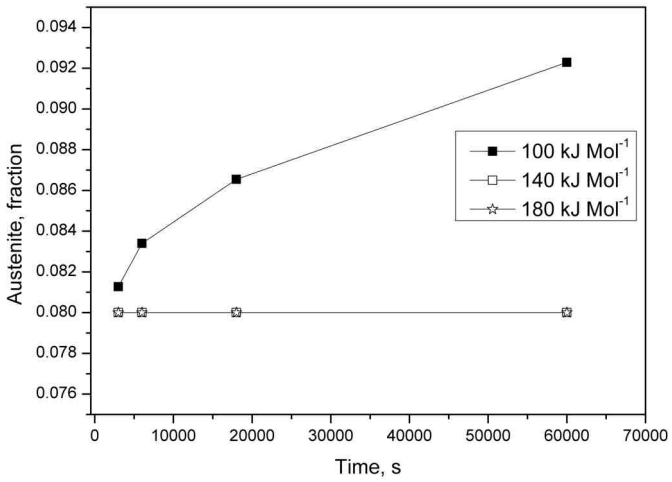

Figure 8.4: *Variation of retained austenite fraction with time at 20 °C, for three different activation energies for the interface mobility. Calculations were carried out using the model proposed in refs. [13, 14].*

8.2 Recommendations to the industry

From the experimental investigation on the microstructural development during welding of TRIP steels, the following welding procedures can be recommended to avoid inherent metallurgical problems that may arise during the welding of TRIP steels in practice;

- In the heat affected zone in positions where the peak temperature reaches the inter-critical $(\alpha + \gamma)$ region, the amount of retained austenite is found to be similar to that of the base metal retained austenite content. This is higher than at positions where the peak temperature was below A_{c_1} or above A_{c_3}. Thus, a post heating thermal cycle with a peak temperature in the inter-critical $\alpha + \gamma$ range can be applied to the heat affected zone in order to increase the retained austenite content.

- The formation of non-metallic inclusions is found in the fusion zones of High-Si and High-Al steels due to the presence of highly oxidising aluminium and silicon in the steel. In order to avoid oxide inclusion formation, the presence of oxygen in the welding atmosphere should be avoided. Production of TRIP steels with little or no dissolved oxygen and the use of high purity shielding gases during welding can avoid the formation of hard and brittle non-metallic inclusions in the fusion zone. As this may not be entirely feasible, a shorter welding time and faster cooling rate can reduce the size and volume fraction of inclusions that

form during welding. The addition of filler wires which contain elements with high affinity to oxygen can be added to the weld pool to increase the dissolved aluminium and silicon contents, thereby, the retained austenite content of the fusion zone can be increased.

- The partitioning of aluminium results in stabilisation of ferritic grains in the fusion boundaries of High-Al TRIP steels. Due to this stabilisation, a soft zone was produced in the heat affected zone and the distribution of retained austenite across the weld zone was affected. Thus, it is important to control the aluminium concentration in the TRIP steel. Aluminium can be replaced by silicon or other elements with an ability to suppress carbide formation.

- The compositional and temperature dependent thermal expansion co-efficient of austenite and ferrite measured in this study can be used for the simulation of material response to welding. The reported thermal expansion co-efficient of austenite generally extrapolated from higher temperatures for low carbon and low alloyed steels are less accurate. Moreover, the lattice expansion of austenite and ferrite is found to be strongly affected by the partitioning of alloying elements, especially carbon. For the prediction of residual stresses during welding, it is important to include the effect of composition on the dilatation behaviour of the steels.

- The retained austenite in the microstructure decomposes while heating at temperatures as low as 290 ^{o}C. This decomposition strongly affects the mechanical properties of the welded TRIP steels, which is also clearly reflected in the hardness measurements. However, the microstructural changes that appear at the positions where peak temperatures reached 290 ^{o}C cannot be studied by optical or scanning electron microscopy. Thus, the width of a heat affected zone of the TRIP steel should be defined from the position where the retained austenite decomposes, rather than from the position from where metallographically observable changes occur.

- The mechanical properties of the welded TRIP steels are found to vary with time after welding. It is important to ensure that welds exhibit adequate properties at the time when the weld is subjected to mechanical loading.

References

[1] M.K.Wibowo and I.M.Richardson, 'Investigation on the influence of welding processes on the microstructure and mechanical properties of DP 600 and DP 1000 steels', in '5th Asian Pacific IIW International Congress, Sydney', 2007.

[2] I.M.Richardson, M.Amirthalingam, M.J.M.Hermans and N.Den Uijl, 'The influence of welding on advanced high strength trip and dp steels', *Mathematical modelling of weld phenomena*, vol. 9, Technical University Graz, 2010.

[3] B.K.Jha and N.S.Mishra, 'Microstructural evolution during tempering of a multiphase steel containing retained austenite', *Material Science and Engineering A*, A263, 42–55, 1999.

[4] Y.Hirotsu and S.Nagakura, 'Crystal structure and morphology of the carbide precipitated from martensitic high carbon steel during the first stage of tempering', *Acta metallurgica*, 20, 645–655, 1972.

[5] Y.Hirotsu, Y.Itakura, K.Su and S.Nagakura, 'Electron microscopy and diffraction study of the carbide precipitation form martensitic low and high nickel steels at the first stage of tempering', *Transactions JIM*, 17, 503 – 513, 1976.

[6] E.J.Mittemeijer and I.A.Wierszyllowsky, 'The isothermal and non-isothermal kinetics of tempering iron-carbon and iron-nitrogen martensites and austenites', *Zeitschrift für Metallkunde*, 82, 419 – 429, 1991.

[7] L.Zhao, N.H.van Dijk, E.Bruck, J.Sietsma and S.van der Zwaag, 'Magnetic and X-ray diffraction measurements for the determination of retained austenite in TRIP stees', *Material Science and Engineering A*, A313, 145–152, 2001.

[8] N.Luzginova, L.Zhao and J.Sietsma, 'Evolution and thermal stability of retained austenite in SAE 52100 bainitic steel', *Material Science and Engineering A*, A448, 104–110, 2007.

[9] N.Kaputska, C.Conrardy, S.Babu and C.Albright, 'Effect of GMAW process and material conditions on DP780 and TRIP780 welds', *Welding Journal Supplement*, 135s – 148s, 2008.

[10] S.S.Babu, J.W.Elmer, S.A.David and M.Quintana, 'Nonequilibrium solidification in Fe-C-Al-Mn steel welds', in '6^{th} international trends in welding research conference proceedings', 169 – 173, ASM International, 2002.

[11] J.Speer, D.K.Matlock, B.C.De Cooman and J.G.Schroth, 'Carbon partitioning into austenite after martensite transformation', *Acta Materialia*, 51, 2611 – 2622, 2003.

[12] J.G.Speer, D.K.Matlock, De Cooman, B. and J.G.Schroth, 'Comments on "on the definitions of paraequilibrium and orthoequilibrium" by M.Hillert and J.Agren, scripta materialia, 50, 697-9, 2004', *Scripta Materialia*, 52, 83–85, 2005.

[13] M.J.Santofimia, L.Zhao and J.Sietsma, 'Model for the interaction between interface migration and carbon diffusion during annealing of martensite-austenite microstructures in steels', *Scripta Materialia*, 59, 159 – 162, 2008.

[14] M.J.Santofimia, J.G.Speer, A.J.Clarke, L.Zhao and J.Sietsma, 'Influence of interface mobility on the evolution of austenite-martensite grain assemblies during annealing', *Acta Materialia*, 57, 4548 – 4557, 2009.

[15] S.G.Kim, J.G.Speer, H.S.Kim and B.C.De Cooman, 'Internatinal conference on new developments in advanced high strength steels', 179 – 189, AIST, Orlando, Florida, USA, 2008.

[16] N.Zhong, X.Wang, Y.Rong and L.Wang, 'Interface migration between martensite and austenite during quenching and partitioning (Q&P) process', *Journal of material science and technology*, 22, 751 – 754, 2006.

[17] S.J.Kim, H.S.Kim and B.C.De Cooman, in 'Material Science and Technology', 73–83, MS&T, Detroit, MI, USA, 2007.

[18] G.P.Krielaart and S.van der Zwaag, 'Kinetics of γ to α phase transformation in Fe-Mn alloys containing low manganese', *Material Science and Technology*, 14, 10 – 18, 1998.

[19] M.G.Mecozzi, J.Sietsma and S.van der Zwaag, 'Analysis of $\gamma \rightarrow \alpha$ transformation in a Nb micro-alloyed C-Mn steel by phase field modelling', *Acta Materialia*, 54, 1431–1440, 2006.

[20] R.G.Thiessen and I.M.Richardson, 'A physically based model for microstructure development in a macroscopic heat-affected zone:Grain growth and recrystallisation', *Metallurgical and Materials Transactions B*, 37B, 655–663, August 2006.

[21] P.J.Withers and H.K.D.H.Bhadesia, 'Overview: Residual stress, part 2 - nature and origin', *Materials Science and Technology*, April, 366 – 375, 2001.

[22] E.M.van der Aa, R.G.Thiessen, M.Amirthalingam, M.J.M.Hermans, J.Sietsma and I.M.Richardson, 'Influence of a trailing heat sink on the microstructure and stress distribution in DP600 welds', *Mathematical modelling of weld phenomena*, 8, 387 – 407, 2007.

[23] T.Hojo, K.I.Sugimoto, Y.I.Mukai, H.Akamizu and S.Ikeda, 'Hydrogen embrittlement properties of ultra high-strength low alloy trip-aided steels with bainitic ferrite matrix', *Tetsu-To-Hagane/Journal of the Iron and Steel Institute of Japan*, 92, 83–89, 2006.

[24] T.Hojo, K.I.Sugimoto, Y.Mukai and S.Ikeda, 'Effects of aluminium on delayed fracture properties of ultra high strength low-alloy trip-aided steels', *ISIJ International*, 48, 824–829, 2008.

Chapter 9

Conclusions and recommendations

9.1 General conclusions

The experimental investigation of microstructural development during welding of TRIP steels was carried out in this work, and the following conclusions were derived;

1. For the TRIP steel compositions used in this study, it is possible to generate base metal microstructures with a retained austenite content varying from 4 to 15 % by altering inter-critical annealing and isothermal bainitic holding temperatures.

2. Despite the continuous heating and cooling thermal cycles involved in a welding processes, a significant amount of retained austenite (5 to 10 %) is found in the heat affected and fusion zones. The amount of retained austenite in the weld zone is entirely based on the thermal cycle of the welding process for a given material chemistry. For the steels and heat treatments studied here, while welding a base metal with a low retained austenite fraction, the retained austenite content increases in the weld zone, whereas, when welding a base metal which contained a higher amount of retained austenite, the austenite fraction in the weld zone was reduced after welding.

3. The regions in the heat affected zone which attain peak temperatures below A_{c_1} but above around 290 ^{o}C contain less than 1 % retained austenite. Regions in the heat affected zone where the peak temperatures during welding reach the inter-critical $(\alpha + \gamma)$ temperature region contain higher amounts of retained austenite after welding (up to 11 %) compared to other regions in the heat affected zone.

4. The retained austenite present in the base metal is stable up to 290 ^{o}C during heating. The thermo-magnetic measurements suggest the formation of ferrite

and transient carbides during the decomposition of retained austenite upon further heating. At the onset of retained austenite decomposition, an increase in the lattice parameter of austenite occurs due to the partitioning of carbon from the new ferrite formed from the decomposing austenite. Conversely, the ferrite lattice parameter shows a linear variation during heating up to A_{c_1}. When the heating temperature reaches the inter-critial region, the combined effect of thermal expansion and carbon partitioning between the co-existing α and γ phases, results in non-linear variation of the lattice parameters.

5. Significant amounts of austenite (5 to 7 %) are retained in High-Si and High-Al TRIP steel samples after continuous cooling from 1000 and 1100 ^{o}C to room temperature in a simulated thermal cycle.

6. Upon cooling from the austenisation temperature, the austenite retained at room temperature is not stable. The fraction of retained austenite can change while holding at room temperature after cooling. This behaviour was confirmed by *in-situ* synchrotron X-ray diffraction, dilatometry and magnetic saturation analysis.

7. Erichsen cupping test conducted on the welded TRIP steels show a time dependent change in the mechanical properties. Following a negligible increase within 120 s, the Erichsen cupping index of the welded High-Al TRIP steel decreases with time up to 900 s. The cracking behaviour of the welds also changes from ductile transverse cracks to brittle weld centre line cracks for samples tested after 120 s and before 900 s, indicating that the weld becomes brittle. Upon further holding at room temperature, the Erichsen cupping index starts to increase again after 1800 s and the cracking behaviour changes to a ductile transverse crack across the weld. These changes in the mechanical properties of TRIP steel welds at room temperature are attributed to room temperature decomposition of retained austenite after welding.

8. The hardness variation across the width of welded TRIP steels correlates to the retained austenite variation in the weld zone. A reduction in hardness is found at the positions where the retained austenite is decomposed due to the weld thermal cycle.

9. The presence of highly oxidising elements such as aluminium and silicon in TRIP steels form complex non-metallic inclusions in the fusion zones. These inclusions contain an aluminium and a silicon rich core in High-Al and High-Si TRIP steels respectively. The dissolved aluminium and silicon present in the weld pool combine with the available oxygen. Conversely, fusion zones of dual phase steel welds do not contain complex inclusions. The inclusions in the fusion zone of resistance spot welded TRIP steels were mainly oxide inclusions whereas in gas tungsten arc and laser beam welding, epitaxial enrichment of alloying elements were found on the surface of the oxide core.

10. In aluminium based High-Al TRIP welds, stabilisation of ferritic grains is observed at the fusion boundaries due to the partitioning of aluminium to the solidified δ-ferrite. The width of the ferrite varies based on the thermal cycle of the welding process from 20 to 200 μm.

11. The formation of non-metallic inclusions in the fusion zone and the partitioning of aluminium and subsequent stabilisation of δ-ferrite in the fusion boundaries influences the stabilisation behaviour of the retained austenite in the fusion and heat affected zone.

12. The temperature dependent thermal expansion coefficients of ferrite and austenite calculated from their lattice parameters show differences between High-Si and High-Al TRIP steels. The difference in the thermal expansion coefficient of austenite is mainly due to the variation in the dissolved carbon concentrations, whereas in ferrite, substitutional alloying elements are likely to cause the difference, as the solubility of carbon in ferrite is low.

13. The rate of formation of austenite upon heating above A_{c_1} significantly differs between the High-Al and High-Si steels. For the High-Si steel, a maximum of rate of 24 % s^{-1} occurs whereas in High-Al steel, the maximum rate is only 18 % s^{-1}. Conversely, the rate of ferrite formation from austenite during cooling is higher in High-Al steel than in High-Si steel. This difference is due to the sluggishness in ferrite transformation to austenite, resulting from the ferrite stabilisation by aluminium.

14. The rate of transformation of austenite and the variation of lattice parameters during cooling from the austenisation temperatures shows that for similar cooling rates, the High-Si exhibit a nearly complete martensitic transformation whereas in the High-Al steel, both bainitic and martensitic transformations occur.

15. For the High-Si steel, austenisation at 1000 and 1100 ^{o}C results in differences in the rate and nature of the transformation of austenite. While cooling from 1100 ^{o}C, the rate of transformation of austenite is on average higher than that of samples cooled from 1000 ^{o}C. Moreover, the lattice parameter variation indicated that while cooling from 1100 ^{o}C, austenite transformed to both bainite and martensite, whereas cooling from 1000 ^{o}C resulted in a complete martensitic transformation.

16. The consistency in the quantification of retained austenite using magnetic saturation and synchrotron X-ray diffraction measurements show that both techniques can be used for the measurement of retained austenite in TRIP steel microstructures, yielding comparable results with due consideration of their merits and drawbacks.

9.2 Recommendations for future work

Although, an extensive experimental research on the microstructural development during welding of TRIP steels was carried out in this work, the following possibilities for interesting scientific and industrial work have been generated which can be pursued on the basis of the present study.

(a) The effect of the oxygen concentration in the welding atmosphere on the size, shape, distribution and the nature of non-metallic inclusions in the fusion zone can be studied to improve the understanding of inclusion formation mechanisms in TRIP steels. This study can also be extended to the addition of filler wires, which contain elements with higher affinity for oxygen than aluminium and silicon.

(b) Although, the formation of a soft ferritic zone in welded TRIP steel is not favourable, in some steels where fusion boundary embrittlement is observed, the effect of adding aluminium rich filler wires in the weld pool can be foreseen to reduced the brittleness by forming soft ferritic grains.

(c) The effect of a post weld heating thermal cycle with a peak temperature in the inter-critical ($\alpha + \gamma$) temperature region on the redistribution of retained austenite in welded TRIP steel should be studied.

(d) Studies on the effect of room temperature retained austenite decomposition should be extended to understand the underlying metallurgical phenomena that drive the transformation of austenite. This study should be extended to include the influence of dissolved hydrogen and the effect of transformation stresses on the stability of austenite at room temperature.

Summary

Microstructural Development during Welding of TRIP Steels

The development of modern automotive vehicles with improved environmental, safety and vehicle performance has driven the development of new steel grades that are lighter, safer, greener and more cost effective. As a result, conventional low carbon, high strength and low alloyed steels are increasingly being replaced with advanced high strength steels (AHSS) due to their better combination of strength and ductility. Transformation Induced Plasticity (TRIP) steel is one of the steels which offers a high strength and toughness combination with excellent uniform elongation. This steel also has an ability to absorb more energy during a crash due to the delayed transformation of retained austenite to martensite upon deformation. The superior combination of strength, ductility and formability of the TRIP steels compared to conventional steels is achieved by carefully designing the microstructure. A typical microstructure of a TRIP steel consists of ferrite (α), bainite and retained austenite (γ_{RA}, usually about 5 to 10 %) distributed in the matrix. The size, shape, chemical composition and volume fraction of the microstructural constituents, especially retained austenite, are critical in tailoring the mechanical properties of the TRIP steels.

In an automotive vehicle manufacturing process, fusion welding is an important process for the joining of steel parts and components. However, the thermal cycle of a welding process destroys the carefully designed microstructure. The mechanical properties of a welded TRIP steel are therefore affected by weld thermal cycles, which limit their commercial applicability. Several attempts have been reported to improve the mechanical properties of welded TRIP steels, but these works lack understanding of the microstructural evolution during welding and correlation of weld microstructure with mechanical properties. In this work, a good understanding of the response of the material to welding has been achieved by studying the microstructural evolution in response to weld thermal cycles of specific joining processes generally employed in automotive manufacturing, the use of specific heat treatments and their influence on the final properties of the welded material.

The research work began with an assessment the effect of heat treatment parameters on the retained austenite content in the microstructure of aluminium (High-Al) and silicon (High-Si) based TRIP steels. Various microstructures with different retained austenite contents were generated by selecting appropriate heat treatment

parameters. After characterising the retained austenite containing microstructure with various techniques such as optical and scanning electron microscopy, magnetic saturation and synchrotron X-ray diffraction, the selected base metal microstructures were welded with gas tungsten arc (GTA), laser beam (LB) and resistance spot (RS) techniques to study the phase transformations during the thermal cycles imposed by these welding processes.

After welding, it was found that despite a continuous heating and cooling thermal cycle involved in a welding process, a significant amount of retained austenite (5 to 10 %) is found in the heat affected and fusion zones. The amount of retained austenite in the weld zone is entirely based on the thermal cycle of the welding process. While welding a base metal with less retained austenite, the retained austenite content increases in the weld zone. Conversely, while welding a base metal which contained a higher amount of retained austenite, the austenite fraction in the weld zone was reduced after welding. The regions in the heat affected zone which attain peak temperatures below A_{c_1} but above around 300 ^{o}C contain less retained austenite ($\leq$1 %). Regions in the heat affected zone where the peak temperatures during welding reach the inter-critical ($\alpha + \gamma$) temperature region contain higher amounts of retained austenite after welding compared to other regions in the heat affected zone. The hardness variation across the width of welded TRIP steels correlates to the retained austenite variation in the weld zone. A reduction in hardness was found in the positions where the retained austenite is decomposed due to the weld thermal cycle.

The presence of highly oxidising elements such as aluminium and silicon in TRIP steels form complex non-metallic inclusions in the fusion zones. These inclusions contain an aluminium and a silicon rich core in High-Al and High-Si TRIP steels, respectively. The dissolved aluminium and silicon present in the weld pool combined with the available oxygen. The inclusions in the fusion zone of resistance spot welded TRIP steels were mainly oxide inclusions whereas in gas tungsten arc and laser beam welding, epitaxial enrichment of alloying elements were found on the surface of the oxide core. In aluminium based High-Al TRIP welds, stabilisation of ferritic grains was observed at the fusion boundaries due to the partitioning of aluminium to the solidified δ-ferrite. The width of the ferrite varies based on the thermal cycle of the welding process from 20 to 200 μm. The formation of non-metallic inclusions in the fusion zone and the stabilisation of ferrite at the fusion boundaries affects the retained austenite stabilisation in the fusion and heat affected zone.

The *in-situ* synchrotron X-ray diffraction and thermo-magnetic measurements showed that the retained austenite present in the base metal is stable up to 290 ^{o}C during heating and a formation of ferrite and transient carbides during the decomposition of retained austenite upon further heating. At the onset of retained austenite decomposition, an increase in the lattice parameter of austenite occurs due to the partitioning of carbon from the new ferrite formed from the decomposing austenite. Conversely, the ferrite lattice parameter shows a linear variation during heating. When the heating temperature reaches the inter-critial region, the combined effect of thermal expansion and carbon partitioning between the co-existing α and γ phases affects the variation of lattice parameters. The calculated temperature dependent

thermal expansion co-efficient of ferrite and austenite from their lattice parameters show differences between High-Si and High-Al TRIP steels. The difference in the thermal expansion coefficient of austenite is mainly due to the variation in the dissolved carbon concentrations, whereas in ferrite, substitutional alloying elements are likely to cause the difference, as the solubility of carbon in ferrite is low.

The rate of formation of austenite upon heating above A_{c_1} significantly differs between the High-Al and High-Si steels. For the High-Si steel, a maximum of rate of 24 % s^{-1} occurs whereas in High-Al steel, the maximum rate is only 18 % s^{-1}. Conversely, the rate of ferrite formation from austenite during cooling is higher in High-Al steel than in High-Si steel. This differences is due to the sluggishness in ferrite transformation to austenite resulting from the ferrite stabilisation by aluminium. The rate of transformation of austenite and the variation of lattice parameters during cooling from the austenisation temperatures shows that for similar cooling rates, the High-Si steel exhibits a nearly complete martensitic transformation whereas in High-Al steel, both the bainitic and the martensitic transformations occur. For High-Si steel, austenisation at 1000 and 1100 ^{o}C results in differences in the rate and nature of the transformation of austenite. While cooling from 1100 ^{o}C, the rate of transformation of austenite is on average higher than that of samples are cooled from a peak temperature of 1000 ^{o}C. Moreover, the lattice parameter variation indicated that while cooling from 1100 ^{o}C, austenite transformed to both bainite and martensite, whereas cooling from a peak of temperature of 1000 ^{o}C resulted in a complete martensitic transformation.

Significant amounts of austenite (5 to 7 %) are retained in High-Si and High-Al TRIP steel samples after continuous cooling from 1000 and 1100 ^{o}C to room temperature in a simulated thermal cycle. Upon cooling from the austenisation temperature, the austenite retained at room temperature is not stable. The fraction of retained austenite can change while holding at room temperature after cooling. This behaviour was confirmed by *in-situ* synchrotron X-ray diffraction, dilatometry and magnetic saturation analysis during simulated GTA, LB and RS weld thermal cycling. Erichsen cupping tests conducted on the welded TRIP steels show a time dependent change in the mechanical properties. Following a negligible increase within 120 s, the Erichsen cupping index of the welded High-Al TRIP steel decreases with time up to 900 s. The cracking behaviour of the welds also changes from ductile transverse cracks to brittle weld centre line cracks for samples tested after 120 s and before 900 s, indicating that the weld becomes brittle. Upon further holding at room temperature, the Erichsen cupping index starts to increase again after 1800 s and the cracking behaviour changes to a ductile transverse crack across the weld. These changes in the mechanical properties of TRIP steel welds at room temperature are attributed to room temperature decomposition of retained austenite after welding. The instability in austenite fractions at room temperature after a weld thermal cycle is possibly the result of the combined effects of carbon partitioning from martensite to austenite leading to a bidirectional movements of martensite-austenite interface with the association of transformation stresses and the evolution of hydrogen.

Samenvatting

Microstructurele ontwikkeling tijdens het lassen van TRIP staal

De ontwikkeling van moderne, milieuvriendelijkere, veiligere auto's met een verhoogde prestatie, heeft de ontwikkeling van nieuwe lichtere, veiligere, 'groenere' en meer kosteneffectief te produceren staalsoorten gestimuleerd. De combinatie van verbeterde sterkte en ductiliteit heeft ertoe geleid dat laag koolstof staal en hoge sterkte, laag gelegeerde (HSLA) staalsoorten meer en meer worden vervangen door geavanceerde hoge sterkte staalsoorten. Transformatie Geïnduceerde Plasticiteit (TRIP) staal is één van de staalsoorten die de gewenste unieke combinatie van hoge sterkte en ductiliteit bezitten en tevens een excelente uniforme rek hebben. Dit type staal kan tevens meer energie absorberen bij een botsing, ten gevolge van de vertraagde transformatie van restausteniet naar martensiet. De superieure combinatie van sterkte, ductiliteit en vervormbaarheid van TRIP staal in vergelijking tot andere staalsoorten wordt bereikt door een zorgvuldig ontworpen microstructuur. De typische microstructuur van een TRIP staal bestaat uit ferriet (α), bainiet en restausteniet (γ_{RA}, normaal circa 5 tot 10 %). De grootte, vorm, chemische samenstelling en volumefractie van de microstructuurbestanddelen, met name van het restausteniet, zijn van groot belang in het afstemmen van de mechanische eigenschappen van TRIP staalsoorten.

Bij de vervaardiging van auto's zijn smeltlasprocessen belangrijke processen voor het verbinden van stalen onderdelen. De thermische cyclus van het lasproces vernietigt de zorgvuldig ontworpen microstructuur. De mechanische eigenschappen van gelast TRIP staal zullen derhalve beïnvloed worden door de thermische cyclus, hetgeen de commerciële toepasbaarheid beperkt. In de literatuur wordt melding gemaakt van pogingen de mechanische eigenschappen te verbeteren, maar deze onderzoeken missen het begrip van de ontwikkeling van de microstructuur ten gevolge van het lassen en de correlatie tussen microstructuur en mechanische eigenschappen. In dit onderzoek is een goed begrip van de respons van het te lassen staal verkregen door het bestuderen van de ontwikkeling van de microstructuur door thermische lascycli van specifieke lasprocessen die worden toegepast in de automobielfabricage. De effecten van specifieke warmtebehandelingen op de microstructuur zijn eveneens onderzocht. Tenslotte, zijn de verkregen microstructuren, door zowel de lascyclus als de thermische cyclus van warmtebehandelingen, gerelateerd aan de uiteindelijke eigenschappen van

het gelaste materiaal.

Het onderzoek is gestart met de evaluatie van de effecten van warmtebehandelingsparameters op het restaustenietgehalte in de microstructuur van aluminium (High-Al) en silicium (High-Si) bevattende TRIP staalsoorten. Met geselecteerde warmtebehandelingsparameters zijn microstructuren met verschillend restaustenietgehalte vervaardigd. Verschillende technieken, zoals optische en elektronenmicroscopie, magnetische verzadiging en synchrotron Röntgendiffractie, zijn gebruikt om de restausteniet bevattende microstructuren te karakteriseren. Vervolgens zijn geselecteerde microstructuren gelast om het fasetransformatiegedrag tijdens de thermische cyclus van de lasprocessen te bestuderen. Voor het lassen is gebruik gemaakt van het Gas Tungsten Arc (GTA) lasproces, het laserbundellasproces en het weerstandspuntlasproces.

Ondanks de warmteïnbreng (thermische cyclus) van het lassen, werden na het lassen significante hoeveelheden restausteniet (5 tot 10 %) in de warmtebeïnvloede zone en het lasmetaal aangetroffen. De hoeveelheid restausteniet die in de laszone wordt aangetroffen wordt volledig bepaald door de thermische cyclus van het lasproces. Als het basismateriaal weinig restausteniet bevat zal de hoeveelheid restausteniet toenemen, terwijl in het geval dat het basismateriaal een hoog gehalte restausteniet bevat dit gehalte in de laszone na het lassen zal afnemen. De gebieden van de warmtebeïnvloede zone, die een piektemperatuur bereiken tussen de A_{c_1} en circa 300 ^{o}C, bevatten minder restausteniet ($\leq$1 %). In het gebied waar de temperatuur de inter-kritische temperatuur ($\alpha + \gamma$) bereikt wordt meer restausteniet aangetroffen in vergelijking tot de overige gebieden van de warmtebeïnvloede zone. De variatie in hardheid over de breedte van het gelaste TRIP staal correleert aan de variatie in het restaustenietgehalte. Een verlaging van de hardheid is waargenomen op de plaatsen waar de restausteniet is ontmengt ten gevolge van de thermische cyclus.

De aanwezigheid van oxiderende elementen zoals aluminium en silicium in TRIP staal resulteert in de vorming van niet-metallische insluitsels in het lasmetaal. Deze insluitsels bevatten een aluminiumrijke en een siliciumrijke kern in respectievelijk High-Al en High-Si TRIP staal. Het opgeloste aluminium en silicium in het lasmetaal reageert met de altijd aanwezige zuurstof. De insluitsels in de smeltzone bij weerstandspuntlassen zijn hoofdzakelijk oxidische insluitsels terwijl bij booglassen en laserbundellassen, epitaxiale verrijking van legeringselementen op het oppervlak van de oxidekern plaatsvindt. In High-Al TRIP stalen is de vorming van ferrietkorrels waargenomen aan de smeltlijn door de uitscheiding van aluminium naar het gevormde δ-ferriet. De breedte van de ferritische zone is afhankelijk van de thermische cyclus van het lasproces en varieert van 20 tot 200 μm. De vorming van niet-metallische insluitsels in het lasmetaal en de vorming van de ferritische zone aan de smeltlijn beïnvloeden de stabiliteit van restausteniet in het lasmetaal en de warmtebeïnvloede zone.

De *in-situ* synchrotron Röntgendiffractie en thermo-magnetische metingen toonden aan dat de restausteniet, die aanwezig is in het basismateriaal, bij opwarming stabiel is tot een temperatuur van 290 ^{o}C en dat de vorming van ferriet en overgangscarbiden optreedt tijdens de ontmenging van de restausteniet bij verdere opwarming. Wanneer restausteniet ontmengt, wordt er een toename in de roosterparameter van austeniet

waargenomen, door de uitscheiding van koolstof van de zojuist gevormde ferrietkorrels. Daarentegen laat de roosterparameter van ferriet een lineair verloop zien tijdens verhitting. Als de temperatuur het inter-kritische gebied bereikt zal het gecombineerde effect van thermische uitzetting en herrangschikking van de koolstof tussen de α en γ fasen, invloed hebben op de roosterparameters. De met de roosterparameters berekende temperatuurafhankelijke thermische uitzettingscoëfficiënten van ferriet en austeniet laten een verschil zien tussen High-Si en High-Al TRIP staal. Het verschil in thermische uitzettingscoëfficiënt van austeniet is hoofdzakelijk het gevolg van een verschil in de concentratie van opgelost koolstof, terwijl in ferriet substitutioneel opgeloste elementen de oorzaak zijn van het verschil, omdat de oplosbaarheid van koolstof in ferriet laag is.

De vormingssnelheid van austeniet na verhitting boven A_{c_1} verschilt wezenlijk tussen High-Al en High-Si TRIP staal. Bij het High-Si staal treedt een maximale vormingssnelheid op van 24 % s^{-1}, terwijl bij het High-Al staal de maximale snelheid slechts 18 % s^{-1} bedraagt. Daarentegen is de vormingssnelheid van ferriet uit austeniet tijdens afkoeling hoger in High-Al staal dan in High-Si staal. Dit verschil is te wijten aan de traagheid van de ferriet naar austeniet transformatie ten gevolge van de stabilisatie van ferriet door het aluminium. De transformatiesnelheid van austeniet en de variatie in roosterparameters tijdens afkoelen vanaf de gekozen austeniteertemperaturen tonen aan dat voor gelijke afkoelsnelheden, het High-Si staal een bijna complete martensitische transformatie laat zien, terwijl in High-Al staal zowel bainitische als martensitische transformaties optreden. In High-Si staal resulteert austeniteren op 1000 en 1100 ^{o}C in verschillen in transformatiesnelheid en de aard van de austeniettransformatie. Afkoeling vanaf 1100 ^{o}C geeft een hogere gemiddelde transformatiesnelheid in vergelijking tot preparaten die vanaf een piektemperatuur van 1000 ^{o}C worden afgekoeld. Voorts geeft de variatie in roosterparameter aan dat afkoeling vanaf 1100 ^{o}C resulteert in een transformatie van austeniet naar bainiet en martensiet, terwijl afkoeling vanaf 1000 ^{o}C een volledige martensitische transformatie oplevert.

Significante hoeveelheden austeniet (5 tot 7 %) worden gevonden in High-Si en High-Al TRIP staal na afkoeling vanaf 1000 ^{o}C en 1100 ^{o}C naar kamertemperatuur bij gesimuleerde thermische cycli. Na afkoeling vanaf de austeniteertemperatuur, is de restausteniet bij kamertemperatuur niet stabiel. De fractie restausteniet kan na afkoeling, bij kamertemperatuur verder veranderen. Dit gedrag is bevestigd door *in-situ* synchrotron Röntgendiffractiemetingen, dilatatiemetingen en magnetische verzadigingsmetingen bij gesimuleerde TIG-lassen, laserbundellassen en weerstandspuntlassen. De resulaten van de Erichsen cupping test op gelast TRIP staal laten een tijdsafhankelijke verandering in mechanische eigenschappen zien. Na een verwaarloosbare toename in de Erichsen upping index van gelast High-Al TRIP staal tot 120 s, volgt een afname van de index tot een tijdsduur van 900 s, hetgeen inhoud dat de las bros wordt. Het scheurgedrag van de las verandert na deze 120 s van een ductiele transversale scheur naar een brosse longitudinale scheur in het midden van de las. Na een tijdsduur van 1800 s op kamertemperatuur begint de index weer toe te nemen en verandert het scheurgedrag weer naar een ductiele transversale scheur. Deze

veranderingen in mechanische eigenschappen van de las in TRIP staal bij kamertemperatuur worden toegeschreven aan ontmenging van de restausteniet na het lassen. De instabiliteit van de fractie restausteniet bij kamertemperatuur na een thermische lascyclus is mogelijk het gevolg van het gecombineerde effect van de herverdeling van koolstof van martensiet naar austeniet, wat aanleiding geeft tot bidirectionele verplaatsingen van het martensiet-austenietgrensvlak, transformatiespanningen en de ontwikkeling van waterstof.

Acknowledgements

At the outset, I would like to thank all of those who supported me in every aspect during the completion of this thesis work as,

"A help rendered in the time of need, though it may be small (in itself), is (in value) much larger than the earth"

- Thiruvalluvar in Thirukkural, 1^{st} century BC.

This work might have not reached this stage without the support, constant encouragement, wishes and ideas of my daily supervisor Dr. Marcel Hermans. Marcel was always there whenever I needed him and it was due to our conversation on this thesis subject and also over various topics made my PhD period one of the best time in my life. I thank him for his time, guidance, patient and care he rendered during my stay in Delft.

I would like to extend my thanks to promoter Professor Ian.M. Richardson for his guidance and vision on this work which were invaluable to fulfil the objectives of my PhD work. I always enjoyed discussing metallurgy with him which had broaden my perspectives in physical metallurgy. I am grateful to him for providing me an opportunity to persue PhD in his group and now, a chance to extend my research work in Delft by the postdoctoral research. It was also wonderful to have a promoter with whom I can always discuss about the wonderful game of cricket.

My thanks are due to Professor J. Sietsma of microstrucutral control in metals group for his advice and guidance with his knowledge of phase transformation on the microstructural evolution during welding and, interpretation of synchrotron X-ray diffraction results. His comments and ideas were important to design the experiments and analyse the results.

I sincerely thank my synchrotron x-ray diffraction measurements team with whom I spent days and nights conducting experiments under the tunnel of ESRF - Grenoble, France. Starting from Ellen van der Aa who introduced the world of synchrotron to me, the year 2006 team; Ellen van der Aa, Marcel Hermans and Rob Delhez, the year 2007 team; Marcel Hermans, Hiske Landheer, Erik Offerman, Masoud Pazooki and Chuangxin Zhao, the year 2008 team; Richard Huizenga, Hemant Sharma, Erik Offerman and Joop van Heekere and finally, the year 2009 team; Richard Huizenga, Hemant Sharma and Erik Offerman and Gözde Dere, I thank you all for your support while conducting the experiments and later during the data analysis part.

I would like to thank joining and mechanical behaviour group members; Martin for his wonderful company during my PhD, Anneke for her secretarial work and wishes, Lucia for the conversation and discussions over the lunch table, Yu Pan for his help in laser welding, Masoud and Chuangxin for their help in conducting experiments in-house and also in France. I extend my thanks to the former members of the group, Richard Thiessen who broaden my view on microstructural modelling, Niels, Heather, Yudi and Menas for their support, wishes and encouragement. I would also like to thank Richard Huizenga for his valuable help in diffraction data analysis, Lie Zhao for helping me to carry out magnetic measurements, Maria Santofimia for her timely help in simulating the interface migration and Michael Janssen for his inputs on mechanical characterisation.

My sincere thanks are again due to laboratory staffs; Frans Bosman and Jurriaan van Slingerland for their help in conducting welding experiments in the welding laboratory and while fabricating a furnace for high temperature synchrotron x-ray diffraction experiments. I extend my thanks to Ton Riemslag, Kees Kwakernaak, Hans Hofman, Nico Geerlofs, Thim Zuidwijk and Erik Peekstok for their help while carrying out heat treatments, mechanical testing, optical and electron microscopy analysis. I am grateful to the timely contributions made by the people at DEMO and electrical services, mainly Alix Wattjes and Ben Schelen for their help in preparing the furnace and samples for the synchrotron measurements. I thank the welding research group of Tata Steel - Corus RD&T in IJmuiden for their interest in this work and providing me their experimental facilities. My sincere thanks to Sullivan Smith, Nick den Uijl and Tony van der Veldt for their time and valuable input in carrying out this work.

I extend my thanks to my desi friends Suresh, Kanagaraj, Chaitanya, Ragu, Guna, Poornima, Mrityunjay, Navin, Ram, Joe, Prem, Sampi, Saravanan, Vinoth for the fun and happiness provided by them during my stay in Delft.

A single word “thanks” is not enough for the care, support and happiness provided my family back in India who brought me up to this stage of my life. I really miss my grandfather who is unfortunately no more to bless me in person on this occasion. It is his guidance, love, support and advice along with the care of my Grandma, Appa, Amma, Bhari, Thangamani and Singh Sithaps, Rathna and Sagunthala Sithis, Shovi and Karl have made me what I am today. I also extend my thanks to my in-laws, relatives and well-wishes who helped me during my PhD study.

Finally, No words are enough to thank my wife Then and our newborn little angle Shruthi whose smile, love and care make my everyday of life more joy and happiness. It was due to Then’s encouragement I started doing my PhD and it was Then who was always there to support and advice whenever I faced a difficulty during my PhD.

List of publications

1. M. Amirthalingam, M.J.M. Hermans and I.M. Richardson, *Quantitative analysis of microstructural constituents in welded Transformation Induced Plasticity (TRIP) steels*, **Mat. Met. Trans. A**, 41A, 2010, 431 - 439.

2. M. Amirthalingam, M.J.M.Hermans, I.M.Richardson, *Microstructural development during welding of Silicon and Aluminium based Transformation Induced Plasticity (TRIP) steels - Inclusion and elemental partitioning analysis*, **Mat. Met. Trans. A**, 40A, 4, 2009, 901 - 909.

3. M. Amirthalingam, M.J.M. Hermans and I.M. Richardson, *Microstructural evolution during gas tungsten arc, laser and resistance spot welding of Al- containing transformation induced plasticity (TRIP) steel*, **Adv. Mat. Res.**, 89-91, 2010, 23-28.

4. M.Amirthalingam, M.J.M.Hermans, R.M.Huizenga, S.E.Offerman, J.Sietsma and I.M.Richardson, *In-situ phase transformation studies on a transformation induced plasticity steel under simulated weld thermal cycles using synchrotron diffraction*, **Chapter - 9 in *In-situ* studies with photons, neutrons and electrons scattering**, T.Kannengiesser *et al.*(eds), Springer-Verlag Berlin Heidelberg, 2011, 133 - 148.

5. H.Sharma, A.C. Wattjes, M. Amirthalingam, T.Zuidwijk, N. Geerlofs and S.E. Offerman, *Multipurpose furnace for in-situ studies of polycrystalline materials using synchrotron radiation*, **Rev. Sci. Instruments**, 80, 2009, 123301-1 - 7.

6. I.M. Richardson, M. Amirthalingam, M.J.M. Hermans N.J. den Uijl and M.K. Wibowo, *The influence of welding in advanced high strength TRIP and DP steels*, **Mathematical Modelling of Weld Phenomena**, 9, ed. H. Cerjak et al. (*in press*).

7. M. Amirthalingam, M.J.M. Hermans and I.M. Richardson *Het laserlassen van TRIP-Staal: Experiment voor optimale microstructuur*, **Lastechniek**, July/August 2008, (in Dutch).

8. E.M. van der Aa, R.G. Thiessen, M. Amirthalingam, M.J.M. Hermans, J. Sietsma, I.M. Richardson,*Influence of a trailing heat sink on the microstructure*

and stress distribution in DP600 welds, **Mathematical modelling of weld phenomena**, ed. H. Cerjak et al., 8, 2007, 387 - 408.

9. M. Amirthalingam, M.J.M. Hermans and I.M. Richardson *"Microstructural development during welding of silicon and aluminium based transformation induced plasticity (TRIP) steels".* In IIW / IWS TU Graz (Ed.), **IIW Doc.** IX-2291-08 and IX-L-1029-08. Proceedings of the 61st Annual Assembly and International Conference of the IIW (International Institute of Welding), Graz, Austria, 6-11 July, 2008 (pp. 1-26). Graz, Austria: IIW / IWS TU Graz.

10. M. Amirthalingam, M.J.M. Hermans and I.M.Richardson, *Microstructural development during Gas Tungsten Arc welding (GTAW) of silicon and aluminum based Transformation Induced Plasticity (TRIP) steels*, **TMS-2007 Annual meeting and Exhibition**, Orlando, Florida, February-March 2007.

11. M. Amirthalingam, M.J.M. Hermans and I.M. Richardson. *Microstructural evolution during gas tungsten arc, laser and resistance spot welding of Al- containing transformation induced plasticity (TRIP) steel*, **Thermec-2009**, Berlin, Germany.

In preparation

1. M. Amirthalingam, M.J.M. Hermans, R.M. Huizenga, S.E. Offerman, J. Sietsma and I.M. Richardson *In-situ formation and transformation kinetics of austenite in transformation induced plasticity steels (TRIP) under simulated weld thermal cycles.*

2. M. Amirthalingam, M.J.M. Hermans, R.M. Huizenga, S.E. Offerman, J. Sietsma and I.M. Richardson, *Synchrotron diffraction analysis of transformation induced plasticity (TRIP) steels under simulated weld thermal cycles.*

3. M. Amirthalingam, M.J.M. Hermans, R.M. Huizenga, S.E. Offerman, J. Si etsma and I.M. Richardson, *Synchrotron diffraction analysis of microstructural constituents in welded transformation induced plasticity (TRIP) steels.*

Curriculum Vitae

MURUGAIYAN AMIRTHALINGAM

born on 23^{rd} July, 1978 in Erode, TN, India

Present	Postdoctoral Researcher, Materials innovation institute (M2i), Delft, The Netherlands.
2005 - 2009	Technische Universiteit Delft, PhD in Materials Science, Delft, The Netherlands.
2005 - 2009	PhD Researcher, Materials innovation institute (M2i), Delft, The Netherlands.
2002 - 2005	Researcher, R&D, Tata Steel, Jamshedpur, JH, India.
2000 - 2002	Indian Institute of Technology - Madras, Master of Science in Metallurgical and Materials Engineering, Chennai, TN, India.
1995 - 1999	Government College of Engineering, Bachelor of Engineering in Metallurgical Engineering, Salem, TN, India.
1993 - 1995	Arulneri Thiruppani Mantram Higher Secondary School, Erode, TN, India.
1989 - 1993	Government Boys High School, Pallipalayam, Erode, TN, India.